

NANOCOMPOSITE NAFION AND HETEROPOLYACID INCORPORATED  
MESOPOROUS CATALYSTS FOR DIMETHYL ETHER SYNTHESIS FROM  
METHANOL

A THESIS SUBMITTED TO  
THE GRADUATE SCHOOL OF NATURAL AND APPLIED SCIENCES  
OF  
MIDDLE EAST TECHNICAL UNIVERSITY

BY

AYŞEGÜL ÇİFTÇİ

IN PARTIAL FULFILLMENT OF THE REQUIREMENTS  
FOR  
THE DEGREE OF MASTER OF SCIENCE  
IN  
CHEMICAL ENGINEERING

AUGUST 2009

Approval of the thesis:

**NANOCOMPOSITE NAFION AND HETEROPOLYACID INCORPORATED  
MESOPOROUS CATALYSTS FOR DIMETHYL ETHER SYNTHESIS  
FROM METHANOL**

submitted by **AYŞEGÜL ÇİFTÇİ** in partial fulfillment of the requirements for the degree of Master of Science in **Chemical Engineering Department, Middle East Technical University** by,

Prof. Dr. Canan Özgen \_\_\_\_\_  
Dean, Graduate School of **Natural and Applied Sciences**

Prof. Dr. Gürkan Karakaş \_\_\_\_\_  
Head of Department, **Chemical Engineering**

Prof. Dr. Timur Doğu \_\_\_\_\_  
Supervisor, **Chemical Engineering Dept., METU**

Assoc. Prof. Dr. Naime A. Sezgi \_\_\_\_\_  
Co-Supervisor, **Chemical Engineering Dept., METU**

**Examining Committee Members:**

Prof. Dr. H. Önder Özbelge \_\_\_\_\_  
Chemical Engineering Dept., METU

Prof. Dr. Timur Doğu \_\_\_\_\_  
Chemical Engineering Dept., METU

Prof. Dr. Gürkan Karakaş \_\_\_\_\_  
Chemical Engineering Dept., METU

Prof. Dr. Güzide Çalık \_\_\_\_\_  
Chemical Engineering Dept., Ankara University

Assoc. Prof. Dr. Nuray Oktar \_\_\_\_\_  
Chemical Engineering Dept., Gazi University

**Date:** **21.08.2009**

**I hereby declare that all information in this document has been obtained and presented in accordance with academic rules and ethical conduct. I also declare that, as required by these rules and conduct, I have fully cited and referenced all material and results that are not original to this work.**

Name, Last name: Ayşegül ÇİFTÇİ

Signature :

## ABSTRACT

### NANOCOMPOSITE NAFION AND HETEROPOLYACID INCORPORATED MESOPOROUS CATALYSTS FOR DIMETHYL ETHER SYNTHESIS FROM METHANOL

Çiftçi, Ayşegül

M.Sc., Department of Chemical Engineering

Supervisor: Prof. Dr. Timur Doğu

Co-Supervisor: Assoc. Prof. Dr. Naime A. Sezgi

August 2009, 135 pages

The need for alternative transportation fuels is rising with the rapid depletion of oil reserves and the simultaneous growth of the world's population. Production of dimethyl ether, a non-petroleum derived attractive fuel-alternate for the future, is a challenging research area. Different routes and various solid-acid catalysts are being developed in order to achieve the most efficient way of synthesizing this potential diesel alternative fuel. The focus of heterogeneous catalysis is to convert renewable feed stocks to valuable chemicals. Nafion resin and heteropolyacid compounds are active acidic catalysts with significantly low surface areas, which act as a strong barrier limiting their catalytic activity. Synthesizing solid-acid catalysts by incorporation of nonporous active compounds into mesoporous silicate structured materials opens a door to producing valuable chemicals by heterogeneous catalysis.

The objective of this work was to synthesize and characterize nafion and heteropolyacid incorporated nanocomposite catalysts and to catalyze DME synthesis

by dehydration of methanol at different temperatures. The interactions of methanol and DME with these catalysts were also investigated by in situ FT-IR.

Silicotungstic acid (STA)/Silica and Tungstophosphoric acid (TPA)/Silica catalysts were synthesized by following a one-pot hydrothermal route. These mesoporous catalysts had surface area values of 143-252 m<sup>2</sup>/g. The STA/SiO<sub>2</sub> nanocomposite catalyst having a W/Si atomic ratio of 0.33 showed the highest activity, with a DME selectivity approaching to 100% and a methanol conversion of 60% at 250°C at a space time of 0.27 s.g.cm<sup>-3</sup>. Effects of W/Si atomic ratio and the synthesis procedure on the performance of these novel materials were investigated.

Nanocomposite Nafion/SiO<sub>2</sub> solid-acid catalysts having high surface area values (595-792 m<sup>2</sup>/g) and narrow pore size distributions (4.3 nm) were successfully synthesized by a one-pot hydrothermal procedure. Effects of the modifications in the synthesis procedure concerning the surfactant removal, nafion loading, etc. were investigated based on the characterization results and activity tests. Nafion was observed to be uniformly distributed within these mesoporous catalysts. Nafion resin was also impregnated into aluminosilicate and  $\alpha$ -alumina, but one-pot synthesis was concluded to be better for obtaining well dispersed, nafion incorporated active catalysts. The Nafion/Silica catalyst synthesized by a nafion/silica weight ratio of 0.15 and washed with 2M sulfuric acid-ethanol solution exhibited the highest activity due to its highest Brønsted, as well as Lewis acidity. A methanol conversion of 40% at 300°C, 0.27 s.g.cm<sup>-3</sup> and DME selectivity values approaching to 100% over 180°C were very promising for the synthesis of this green fuel alternate over the new catalysts synthesized.

Keywords: Dimethyl ether, methanol dehydration, heteropolyacid, nafion, mesoporous catalyst

## ÖZ

### METANOLDEN DİMETİL ETER SENTEZİ İÇİN NANOKOMPOZİT YAPIDA MEZOGÖZENEKLİ NAFYON VE HETEROPOLİASİT İÇEREN KATALİZÖRLER

Çiftçi, Ayşegül

Yüksek Lisans, Kimya Mühendisliği

Tez Yöneticisi: Prof. Dr. Timur Doğu

Ortak Tez Yöneticisi: Doç. Dr. Naime A. Sezgi

Ağustos 2009, 135 sayfa

Petrol kaynaklarının hızla tükenmesi ve dünya nüfusunun eş zamanlı artışı sebebiyle alternatif ulaşım yakıtlarına olan ihtiyaç artmaktadır. Hammaddesi petrol olmayan ve geleceğin cazip alternatif yakıtı olarak kabul edilen dimetil eterin üretimi çok ilgi çeken bir araştırma alanıdır. Bu potansiyel dizel yakıt alternatifini en verimli şekilde sentezlemek için farklı yollar ve çeşitli katı asit katalizörler geliştirilmektedir. Heterojen katalizin amacı yenilenebilir kaynakları değerli kimyasallara dönüştürmektir. Nafyon reçinesi ve heteropoliasit bileşikleri önemli ölçüde düşük yüzey alanına sahip etkin asidik katalizörlerdir. Düşük yüzey alanları bu katalizörlerin katalitik etkinliğini büyük ölçüde sınırlamaktadır. Gözeneksiz etkin bileşikler mezogözenekli silika içerikli malzemelerin yapısına katarak katı-asit katalizörler sentezlemek heterojen kataliz ile değerli kimyasallar üretmeye olanak vermektedir.

Bu çalışmanın amacı nafyon ve heteropoliasit içerikli nanokompozit katalizörler sentezlemek, karakterize etmek ve bu malzemeleri kullanarak metanol

dehidrasyonu ile dimetil eter sentezini farklı sıcaklıklarda katalizlemektir. Ayrıca, metanol ve DME'nin bu katalizörlerle etkileşimi olduğu yerde FT-IR çalışmaları ile incelenmiştir.

Silikotungstik asit (STA)/Silika ve Tungstofosforik asit (TPA)/Silika katalizörleri doğrudan hidrotermal sentez yöntemi takip edilerek sentezlenmiştir. Bu mezogözenekli katalizlerin yüzey alanları 143-252 m<sup>2</sup>/g olarak bulunmuştur. Yapısındaki W/Si oranı 0.33 olan STA/SiO<sub>2</sub> nanokompozit katalizörü 250°C'de, 0.27 s.g.cm<sup>-3</sup> alıkonma süresinde, %100'e varan DME seçiciliği ve %60 metanol dönüşümü vererek en yüksek etkinliği göstermiştir. W/Si atomik oranının ve sentez prosedürünün bu yeni geliştirilen malzemelerin performansına etkileri incelenmiştir.

Geniş yüzey alanına (595-792 m<sup>2</sup>/g) ve dar gözenek büyüklüğü dağılımına (4.3 nm) sahip nanokompozit katı-asit Nafyon/Silika katalizörleri doğrudan hidrotermal sentez yöntemi ile başarıyla sentezlenmiştir. Sentez prosedüründe yapılan yüzey aktif malzemeyi uzaklaştırma yöntemi, nafyon yüklemesi, vs. gibi başlıklardaki değişikliklerin etkileri karakterizasyon sonuçları ve aktivite deneylerine dayalı olarak araştırılmıştır. Nafyonun bu mezogözenekli katalizörlerin yapısında muntazam bir şekilde dağıldığı gözlenmiştir. Bunlara ek olarak, nafyon reçinesi alüminyum silikat ve α-alümina'ya emdirilmiştir. Ancak doğrudan hidrotermal sentez yönteminin düzgün dağılımlı, nafyon içerikli etkin katalizörler elde etmek için daha iyi bir yöntem olduğu sonucuna varılmıştır. Nafyon/Silika ağırlık oranını 0.15 olarak sentezlenen ve 2M sülfürik asit-etanol çözeltisi ile yıkanan Nafyon/Silika katalizörü en yüksek Brönsted ve aynı zamanda da Lewis asitliğine sahip olması sebebiyle en yüksek etkinliği göstermiştir. 0.27 s.g.cm<sup>-3</sup> alıkonma süresinde, 300°C'de %40 metanol dönüşümü ve 180°C'nin üzerinde %100'e yaklaşan DME seçiciliği elde edilmesi, bu yeşil alternatif yakıtın sentezlenen yeni katalizörler kullanılarak üretilmesi konusunda oldukça ümit vericidir.

Anahtar Sözcükler: Dimetil eter, metanol dehidrasyonu, heteropoliasit, nafyon, mezogözenekli katalizör

*To my parents Nejla & Mustafa iftçi*

## ACKNOWLEDGEMENTS

I owe my deepest gratitude to my supervisor Prof. Dr. Timur Doğu who supported and guided me throughout my studies. He inspired me in a number of ways including not only my thesis work but also my future career as a chemical engineer. I cannot thank him enough for his encouragement, his kindly attitude in every aspect and for these enlightening two years during which I had the chance to work with him.

I would like to express my sincere thanks to Prof. Dr. Gülşen Doğu and her research group in Gazi University Chemical Engineering Department for their support in this work.

I would like to thank my co-supervisor Assoc. Prof. Dr. Naime A. Sezgi for her positive attitude and help in this study. I am thankful to Assist. Prof. Dr. Dilek Varışlı for her invaluable guidance and friendly manner throughout my thesis.

I would like to offer my sincere thanks to Prof. Dr. Emiel Hensen from Eindhoven University of Technology for providing research opportunities in his laboratory. His help, advice, supervision and the research experience I had in the Netherlands were priceless. Thanks are not enough to Dr. Volkan Değirmenci for providing me with all kinds of technical assistance, always sparing time for discussions and of course his friendship.

I would like to thank Assist. Prof. Dr. Emrah Özensoy and Seda Şentürk from Bilkent University Chemistry Department for the EDX analyses.

Concerning the characterization analyses, technical assistance of METU Central Laboratory, Metallurgical and Materials Engineering and Chemical Engineering staff are greatly appreciated.

Thanks are also due to my friends in Kinetic Lab; Zeynep Obalı, Canan Martı, Kenan Cem Tokay, Ayça Arınan, Buğçe Aydemir, Sultan Orman and Seval Gündüz who helped me in many ways. My special thanks go to Zeynep Obalı for always being so helpful in every technical issue and being so patient in answering all

my questions. I am grateful to Canan Martı and Kenan Cem Tokay for their help and assistance. I would like to thank Ayça Arınan for her help, friendship and all the nice memories we had in these two years.

I am grateful to my sister, Emel iftçi, who has always been supportive and encouraging in all stages of my life. My aunt, Sema iftçi, deserves a special thanks as she always gave moral support to keep me motivated. I am also thankful to my parents for their perpetual love and for being understanding and supportive all the time. I dedicate my thesis to them.

I would like to thank all my friends for always standing by me. Finally, words alone cannot express the thanks I owe to Seluk Sandıkçı, who has been my greatest motivation all the way through my masters studies, for his endless support and faith in me.

The support received from TÜBİTAK through BİDEB scholarship programme is gratefully acknowledged.

## TABLE OF CONTENTS

ABSTRACT .....	iv
ÖZ .....	vi
ACKNOWLEDGEMENTS .....	ix
TABLE OF CONTENTS .....	xi
LIST OF TABLES .....	xv
LIST OF FIGURES .....	xvii
NOMENCLATURE.....	xxi
CHAPTERS	
1. INTRODUCTION .....	1
2. DIMETHYL ETHER (DME) AS A DIESEL ALTERNATE FUEL .....	3
3. DME SYNTHESIS BY DEHYDRATION OF METHANOL .....	9
4. MESOPOROUS MATERIALS .....	12
5. HETEROPOLYACID (HPA) CATALYSTS .....	18
5.1. GENERAL PROPERTIES AND CLASSIFICATION OF HPA'S .....	18
5.2. CATALYTIC APPLICATIONS OF PURE HPA'S .....	21
5.3. SALTS OF HPA'S AND THEIR CATALYTIC APPLICATIONS .....	22
5.4. SUPPORTED HPA'S AND THEIR APPLICATIONS IN ALCOHOL DEHYDRATION .....	23
6. NAFION RESIN AS A CATALYST .....	25
6.1. GENERAL PROPERTIES OF NAFION RESIN .....	25
6.2. SUPPORTED NAFION CATALYSTS .....	27
6.3. CATALYTIC APPLICATIONS OF NAFION BASED CATALYSTS .....	29
7. THERMODYNAMIC ANALYSIS .....	31
8. EXPERIMENTAL .....	36
8.1. SYNTHESIS OF STA/SILICA MESOPOROUS CATALYSTS .....	36
8.2. SYNTHESIS OF TPA/SILICA MESOPOROUS CATALYSTS .....	39
8.3. SYNTHESIS OF NAFION/SILICA MESOPOROUS CATALYSTS .....	40

8.4. SYNTHESIS OF NAFION IMPREGNATED CATALYSTS .....	44
8.5. MATERIAL CHARACTERIZATION .....	45
8.5.1. X-Ray Diffraction (XRD) .....	45
8.5.2. N <sub>2</sub> Physisorption .....	46
8.5.3. Scanning Electron Microscopy (SEM) .....	46
8.5.4. Energy Dispersive X-Ray Spectroscopy (EDS-EDX) .....	47
8.5.5. X-Ray Photoelectron Spectroscopy (XPS) .....	48
8.5.6. Fourier Transform Infrared Spectroscopy (FTIR) .....	48
8.5.7. Thermal Analyses (TGA-DTA) .....	49
8.5.8. Diffuse Reflectance Infrared Fourier Transform Spectroscopy (DRIFTS) of Pyridine Adsorption .....	49
8.6. EXPERIMENTAL SET-UP OF THE METHANOL DEHYDRATION REACTION SYSTEM .....	50
9. RESULTS AND DISCUSSION .....	53
9.1. CHARACTERIZATION OF STA/SILICA CATALYSTS .....	53
9.1.1. X-Ray Diffraction (XRD) .....	53
9.1.2. Energy Dispersive Spectroscopy (EDS) .....	54
9.1.3. Scanning Electron Microscopy (SEM) .....	55
9.1.4. Energy Dispersive X-Ray Spectroscopy (EDX) .....	56
9.1.5. Nitrogen Physisorption .....	57
9.1.6. Fourier Transform Infrared Spectroscopy (FTIR) .....	60
9.1.7. DRIFTS of Pyridine Adsorbed Samples .....	60
9.2. CHARACTERIZATION OF TPA/SILICA CATALYSTS .....	61
9.2.1. Thermal Analyses (TGA-DTA) .....	61
9.2.2. X-Ray Diffraction (XRD) .....	62
9.2.3. Energy Dispersive Spectroscopy (EDS) .....	63
9.2.4. Scanning Electron Microscopy (SEM) .....	63
9.2.5. Nitrogen Physisorption .....	64
9.2.6. Fourier Transform Infrared Spectroscopy (FTIR) .....	66
9.2.7. DRIFTS of Pyridine Adsorbed Samples .....	66
9.3. CHARACTERIZATION OF NAFION/SILICA CATALYSTS .....	67
9.3.1. Thermal Analyses (TGA-DTA) .....	67
9.3.2. X-Ray Diffraction (XRD) .....	69

9.3.3. Energy Dispersive Spectroscopy (EDS) .....	69
9.3.4. Scanning Electron Microscopy (SEM) .....	70
9.3.5. Energy Dispersive X-Ray Spectroscopy (EDX).....	71
9.3.6. X-Ray Photoelectron Spectroscopy (XPS) .....	72
9.3.7. Nitrogen Physisorption .....	75
9.3.8. DRIFTS of Pyridine Adsorbed Samples .....	78
9.4. CHARACTERIZATION OF NAFION IMPREGNATED CATALYSTS ..	79
9.5. ACTIVITY RESULTS OF STA/SILICA CATALYSTS .....	81
9.5.1. The effect of the W/Si ratio.....	81
9.5.2. The effect of the surfactant removal step.....	83
9.5.3. The effect of space time .....	84
9.6. ACTIVITY RESULTS OF TPA/SILICA CATALYSTS .....	86
9.7. ACTIVITY RESULTS OF AN STA/ALUMINOSILICATE CATALYST	88
9.8. ACTIVITY RESULTS OF NAFION/SILICA CATALYSTS.....	90
9.8.1. The comparison of calcination and washing with SAE solution .....	90
9.8.2. The effect of different washing conditions .....	92
9.8.3. The effect of nafion loading.....	93
9.9. ACTIVITY RESULTS OF NAFION IMPREGNATED CATALYSTS ....	97
9.9.1. Activity Results of Nafion/Aluminosilicate Catalysts .....	97
9.9.2. Activity Results of Nafion/ $\alpha$ -Alumina Catalysts .....	98
9.10. IN-SITU INFRARED STUDIES : METHANOL AND DME	
ADSORPTION AND DESORPTION ON THE CATALYSTS SYNTHESIZED	
.....	99
9.10.1. Methanol Adsorption on Nafion/Silica Catalysts .....	100
9.10.2. Methanol Adsorption on Nafion/Aluminosilicate Catalyst .....	105
9.10.3. Methanol Adsorption on STA/Silica Catalyst .....	106
9.10.4. Methanol Adsorption on STA/Aluminosilicate Catalyst.....	108
9.10.5. DME Adsorption on the Nafion/Silica Catalyst.....	110
9.10.6. DME Adsorption on the STA/Silica Catalyst.....	111
10. CONCLUSIONS AND RECOMMENDATIONS .....	113
REFERENCES.....	117
APPENDICES	
A. PARAMETERS FOR THE REACTION SYSTEM.....	125

A.1. GC CALIBRATION FACTORS AND RETENTION TIMES OF THE SPECIES.....	125
A.2. CALCULATION OF FLOW RATES.....	125
A.3. EQUATIONS FOR METHANOL CONVERSION, DME YIELD AND DME SELECTIVITY.....	126
B. SEM IMAGES OF THE MATERIALS.....	128
C. CALCULATION OF THE EXPECTED F/Si RATIOS FOR NAFION/SILICA CATALYSTS.....	132
D. SINGLE POINT SURFACE AREAS OF THE CATALYSTS.....	133
E. FT-IR SPECTRA OF DEHYDRATED CATALYSTS.....	134

## LIST OF TABLES

### TABLES

<b>Table 1.</b> Physical properties of dimethyl ether [6] .....	4
<b>Table 2.</b> Properties of dimethyl ether in comparison with diesel oil, methanol and some other transportation fuel alternates [10].....	6
<b>Table 3.</b> The reactions occurring in DME synthesis [7].....	8
<b>Table 4.</b> The molar heat capacity coefficients of species in the $C_p = a + bT + cT^2$ , where $C_p$ is in J/mol.K .....	32
<b>Table 5.</b> Standard Enthalpies and Gibbs Energies of Formation at 298.15 K for one mole of Each Substance from its Elements.....	32
<b>Table 6.</b> Critical temperature (K) and critical pressure (MPa) values for methanol, DME and water vapor. ....	33
<b>Table 7.</b> Flow rates and molar compositions of the species at equilibrium conversion .....	34
<b>Table 8.</b> Denotation of the synthesized STA/Silica catalysts.....	38
<b>Table 9.</b> The nafion sources, starting Nafion/Silica weight ratios and pH of the synthesis mixtures .....	43
<b>Table 10.</b> Applied treatments and the denotation of the samples.....	43
<b>Table 11.</b> The nafion impregnated catalysts and their nafion/support starting ratios	45
<b>Table 12.</b> The catalysts and the conditions used in the activity tests .....	52
<b>Table 13.</b> EDS results of the STA/Silica catalysts .....	55
<b>Table 14.</b> Physical properties of the STA/Silica catalysts.....	58
<b>Table 15.</b> The comparison of the EDS results of TPA-75(L) and TRC-75(L).....	63
<b>Table 16.</b> Physical properties of TPA-75(L) and TRC-75(L).....	65
<b>Table 17.</b> Starting nafion/silica ratios of the catalysts and their nafion contents .....	68
<b>Table 18.</b> EDS analysis of NS1 .....	70
<b>Table 19.</b> XPS results of the as-synthesized catalysts.....	74
<b>Table 20.</b> XPS results of the final form of the catalysts (after surfactant removal) ..	74
<b>Table 21.</b> Physical properties of the as-synthesized catalysts .....	76

<b>Table 22.</b> Physical properties of the final form of the catalysts (after surfactant removal) .....	76
<b>Table 23.</b> Physical properties of the nafion impregnated catalysts .....	80
<b>Table 24.</b> Results of the stability tests and regeneration experiments over TRC-75(L) at 0.27 s.g.cm <sup>-3</sup> .....	86
<b>Table 25.</b> GC calibration factors and retention times.....	125
<b>Table 26.</b> Single point surface areas of some of the catalysts.....	133

## LIST OF FIGURES

### FIGURES

<b>Figure 1.</b> The chemical structure of dimethyl ether [6].....	4
<b>Figure 2.</b> Multiple uses of dimethyl ether [8].....	5
<b>Figure 3.</b> DME synthesis by methanol dehydration (conventional process) [13].....	7
<b>Figure 4.</b> Direct synthesis of DME (Haldor Topsoe or JFE Holdings) [13].....	8
<b>Figure 5.</b> Formation pathway of ordered mesoporous materials [22].....	13
<b>Figure 6.</b> TEM micrograph of MCM-41 [23] .....	14
<b>Figure 7.</b> Powder X-Ray diffraction pattern of MCM-41 [24] .....	15
<b>Figure 8.</b> Nitrogen adsorption/desorption isotherm of MCM-41 [25] .....	16
<b>Figure 9.</b> The primary structure of Keggin HPA's. [31].....	19
<b>Figure 10.</b> Keggin structure [30].....	19
<b>Figure 11.</b> The primary structure of Wells-Dawson HPA's. [31].....	19
<b>Figure 12.</b> Structure of nafion resin [50].....	25
<b>Figure 13.</b> The equilibrium curves for methanol dehydration at 1 bar and 30 bars..	35
<b>Figure 14.</b> Synthesis procedure of STA/Silica catalysts .....	38
<b>Figure 15.</b> Synthesis procedure of TPA/Silica catalysts .....	39
<b>Figure 16.</b> Synthesis procedure of the Nafion/Silica catalysts.....	42
<b>Figure 17.</b> Synthesis procedure of nafion impregnated catalysts.....	44
<b>Figure 18.</b> Experimental set-up of the methanol dehydration reaction system.....	51
<b>Figure 19.</b> XRD patterns of STA/Silica catalysts .....	54
<b>Figure 20.</b> SEM image of TRC-75(L).....	55
<b>Figure 21.</b> SEM image of TRC-75(L).....	56
<b>Figure 22.</b> SEM image of TRC-75-400.....	56
<b>Figure 23.</b> EDX elemental mapping analysis of TRC-75(L) .....	57
<b>Figure 24.</b> EDX elemental mapping analysis of TRC-75-400 .....	57
<b>Figure 25.</b> Nitrogen adsorption-desorption isotherm of TRC-75(L).....	59
<b>Figure 26.</b> Pore size distributions of the STA/Silica catalysts .....	59
<b>Figure 27.</b> FTIR spectra of STA/Silica catalysts and pure STA .....	60

<b>Figure 28.</b> DRIFTS spectra of the STA/Silica catalysts.....	61
<b>Figure 29.</b> TGA-DTA analysis of TPA-75(L) .....	62
<b>Figure 30.</b> X-ray diffraction pattern of TPA-75(L).....	62
<b>Figure 31.</b> SEM image of TPA-75(L) .....	64
<b>Figure 32.</b> SEM image of TPA-75(L) .....	64
<b>Figure 33.</b> Nitrogen adsorption-desorption isotherm of TPA-75(L).....	65
<b>Figure 34.</b> Pore size distribution of TPA-75(L) .....	65
<b>Figure 35.</b> FTIR spectra of pure TPA and TPA-75(L).....	66
<b>Figure 36.</b> DRIFTS spectra of TPA-75(L).....	67
<b>Figure 37.</b> TGA-DTA analysis of NS3 .....	68
<b>Figure 38.</b> XRD patterns of NS1, NS1R and NS1350 catalysts .....	69
<b>Figure 39.</b> SEM image of NS3R1 .....	70
<b>Figure 40.</b> SEM image of NS4R2 .....	71
<b>Figure 41.</b> SEM image of NS4R2 .....	71
<b>Figure 42.</b> EDX elemental mapping of Nafion/Silica nanocomposite (NS1R) .....	72
<b>Figure 43.</b> XPS spectrum of NS4R2 .....	73
<b>Figure 44.</b> Nitrogen adsorption-desorption isotherm of NS3R2.....	77
<b>Figure 45.</b> Nitrogen adsorption-desorption isotherm of NS4R2.....	77
<b>Figure 46.</b> Pore size distributions of Nafion/Silica catalysts .....	78
<b>Figure 47.</b> DRIFTS spectra of the Nafion/Silica catalysts .....	79
<b>Figure 48.</b> MeOH conversion over TRC-62(L), TRC-75(L), TRC-82(L) and TRC-92(L) at 0.27 s.g/cm <sup>3</sup> between 180-350°C.....	82
<b>Figure 49.</b> DME selectivities over TRC-62(L), TRC-75(L), TRC-82(L) and TRC-92(L) at 0.27 s.g/cm <sup>3</sup> between 180-350°C.....	82
<b>Figure 50.</b> MeOH conversion over TRC-75(L), TRC-75(L)-CO <sub>2</sub> and TRC-75-400 at 0.27 s.g/cm <sup>3</sup> between 180-350°C.....	83
<b>Figure 51.</b> DME selectivities over TRC-75(L), TRC-75(L)-CO <sub>2</sub> and TRC-75-400 at 0.27 s.g/cm <sup>3</sup> between 180-350°C.....	84
<b>Figure 52.</b> MeOH conversion over TRC-75(L) at different space times between 180-350°C .....	85
<b>Figure 53.</b> DME selectivities over TRC-75(L) at different space times between 180-350°C .....	85

<b>Figure 54.</b> MeOH conversion over TPA-75(L) and TRC-75(L) at 0.27 s.g/cm <sup>3</sup> between 180-250°C.....	87
<b>Figure 55.</b> DME selectivities over TPA-75(L) and TRC-75(L) at 0.27 s.g/cm <sup>3</sup> between 180-250°C.....	87
<b>Figure 56.</b> Methanol conversion over STAMAS at 0.27 s.g/cm <sup>3</sup> between 180-350°C .....	88
<b>Figure 57.</b> DME selectivities over STAMAS at 0.27 s.g/cm <sup>3</sup> between 180-350°C..	89
<b>Figure 58.</b> Stability test over STAMAS at 250°C at 0.27 s.g.cm <sup>-3</sup> .....	89
<b>Figure 59.</b> MeOH conversion over NS1R, NS1250, NS1350 and NS1 at 0.27 s.g/cm <sup>3</sup> between 120-300°C.....	91
<b>Figure 60.</b> DME selectivities over NS1R, NS1250, NS1350 and NS1 at 0.27 s.g/cm <sup>3</sup> between 120-300°C.....	91
<b>Figure 61.</b> MeOH conversion over NS3R2, NS3R1 and NS3A at 0.27 s.g/cm <sup>3</sup> between 120-300°C.....	92
<b>Figure 62.</b> DME selectivities over NS3R2, NS3R1 and NS3A at 0.27 s.g/cm <sup>3</sup> between 120-300°C.....	92
<b>Figure 63.</b> MeOH conversion over NS5R2, NS4R2, NS3R2 and NS1R at 0.27 s.g/cm <sup>3</sup> between 120-300°C.....	94
<b>Figure 64.</b> DME selectivities over NS5R2, NS4R2, NS3R2 and NS1R at 0.27 s.g/cm <sup>3</sup> between 120-300°C.....	94
<b>Figure 65.</b> Stability test over NS4R2 at 300°C at 0.27 s.g.cm <sup>-3</sup> .....	95
<b>Figure 66.</b> Reproducibility check over NS4R2 at 0.27 s.g.cm <sup>-3</sup> .....	96
<b>Figure 67.</b> DME yield over nafion/aluminosilicate catalysts at 0.27 s.g/cm <sup>3</sup> between 120-300°C .....	97
<b>Figure 68.</b> DME yield over nafion/aluminosilicate catalysts at 0.27 s.g/cm <sup>3</sup> between 120-400°C .....	98
<b>Figure 69.</b> DME yield over nafion/ $\alpha$ -alumina and pure $\alpha$ -alumina at 0.27 s.g/cm <sup>3</sup> between 180-400°C.....	99
<b>Figure 70.</b> Hydrate structures in Nafion membrane swollen with water [73].....	100
<b>Figure 71.</b> FT-IR spectra for methanol adsorption and desorption on NS4R2 catalyst .....	102

<b>Figure 72.</b> FT-IR spectra for methanol adsorption and desorption on NS3R1 catalyst at different temperatures : RT, 120°C, 150°C, 200°C, 250°C, 300°C, 350°C, 400°C, 500°C .....	104
<b>Figure 73.</b> Proposed reaction mechanism for methanol dehydration.....	105
<b>Figure 74.</b> FT-IR spectra for methanol adsorption and desorption on NFMAS3 catalyst at different temperatures : RT, 120°C, 150°C, 200°C, 250°C, 300°C, 350°C, 400°C .....	106
<b>Figure 75.</b> FT-IR spectra for methanol adsorption and desorption on TRC-75-400 catalyst at different temperatures : RT, 100°C, 200°C, 250°C, 300°C, 350°C, 400°C, 500°C .....	108
<b>Figure 76.</b> FT-IR spectra for methanol adsorption and desorption on STAMAS catalyst at different temperatures : RT, 100°C, 200°C, 250°C, 300°C, 350°C, 500°C .....	109
<b>Figure 77.</b> FT-IR spectra for DME adsorption and desorption on catalyst at NS4R2 different temperatures : RT, 5 min. after evacuation (RT-2), 120°C, 150°C, 200°C .....	110
<b>Figure 78.</b> FT-IR spectra for DME adsorption and desorption on TRC-75-400 catalyst at different temperatures : RT, 100°C, 200°C, 250°C, 300°C, 350°C, 400°C, 500°C .....	112
<b>Figure 79.</b> SEM images of the nafion/silica catalyst (NS1R).....	128
<b>Figure 80.</b> SEM images of the nafion/silica catalyst (NS3A).....	128
<b>Figure 81.</b> SEM images of the nafion/silica catalyst (NS3R2).....	129
<b>Figure 82.</b> SEM images of the nafion/silica catalyst (NS1).....	129
<b>Figure 83.</b> SEM images of the nafion/aluminosilicate catalyst (NFMAS2) .....	130
<b>Figure 84.</b> SEM image of the nafion/aluminosilicate catalyst (NFMAS3).....	130
<b>Figure 85.</b> SEM images of the nafion/ $\alpha$ -alumina catalyst (NFALFA1).....	131
<b>Figure 86.</b> SEM image of the STA/Silica catalyst (TRC-75-400) .....	131
<b>Figure 87.</b> FT-IR spectra of dehydrated Nafion incorporated catalysts.....	134
<b>Figure 88.</b> FT-IR spectra of dehydrated STA incorporated catalysts .....	135

## NOMENCLATURE

C<sub>p</sub>: Heat Capacity (J/mol.K)

DME: Dimethyl Ether

DTA: Differential Thermal Analysis

DRIFTS: Diffuse Reflectance Infrared Fourier Transform Spectroscopy

EDS-EDX: Energy Dispersive X-Ray Spectroscopy

f: Fugacity (bar)

F: Molar flow rate (mol/hr)

FA: Formaldehyde

FT-IR: Fourier Transform Infrared Spectroscopy

G: Gibbs Free Energy (kJ/mol)

H: Enthalpy (kJ/mol)

IUPAC: International Union of Pure and Applied Chemistry

K: Equilibrium Constant

MW: Molecular weight (g/mol)

MCM: Mobil Composition of Matter

MeOH: Methanol

n: Mole

P: Pressure (bar)

Q: Volumetric flow rate (ml/min)

R: Gas constant (8.314 J/mol.K)

S: Selectivity

SEM: Scanning Electron Microscopy

T: Temperature (°C)

TGA: Thermogravimetric Analysis

X: Conversion

XPS: X-Ray Photoelectron Spectroscopy

XRD: X-Ray Diffraction

y: Molar composition

Y: Yield

$\rho$ : Density ( $\text{g}/\text{cm}^3$ )

# CHAPTER 1

## INTRODUCTION

Due to the fast depletion of oil reserves and increasing rate of global warming, researchers have been seeking for environmentally friendly non-petroleum derived fuel alternatives. Alcohols and ethers are considered as alternative fuels due to their good burning characteristics and environmentally friendly aspects. Among them, dimethyl ether (DME) is considered as a clean alternative transportation fuel having excellent qualities as a diesel fuel alternate with very low NO<sub>x</sub> emissions, no black smoke formation and with a significantly high cetane number (55-60) [1]. Presently, the commercial method for DME synthesis is by dehydration of methanol. This reaction is carried out in the presence of solid acid catalysts like H-ZSM-5 [2],  $\gamma$ -Al<sub>2</sub>O<sub>3</sub> [3], Amberlyst-35 [4], etc. at atmospheric pressure.

Heteropolyacids and nafion are two types of acidic catalysts which are known to catalyze alcohol dehydration reactions. However, both of them have low surface areas; hence their catalytic activity in vapor phase dehydration of methanol is limited. High surface area silicate structured mesoporous molecular sieves with narrow pore size distributions are considered to be excellent support materials. By incorporation of metals and metal oxides into their structures following one-pot or impregnation procedures, novel heterogeneous catalysts with high surface areas and active acidic sites are obtained.

In this study, nafion and heteropolyacids incorporated silicate structured mesoporous catalysts having high surface areas were synthesized, characterized and their catalytic activities in methanol dehydration reaction to synthesize DME were tested in a fixed bed flow reactor system.

In the Chapters 2, 3, 4, 5 and 6 a detailed literature survey is provided. In Chapter 2, general information on dimethyl ether is given. Green aspects of DME are

explained and its advantages as a diesel-alternate fuel are presented by comparison with other fuels based on various physical properties of DME. Moreover, information on the chemistry of different DME synthesis routes is given. Chapter 3 summarizes the related work in literature concerning the different types of solid acid catalysts and reaction conditions used in methanol dehydration reaction. Chapter 4 focuses on mesoporous materials. Catalytic aspects, synthesis and characterization of the M41S family are discussed in detail. In Chapter 5, heteropolyacids are explained in all aspects. Supported forms and salts of HPA's are presented. The use of them in catalytic reactions is explained by giving examples from the previous studies. Chapter 6 focuses on the nafion resin as an acidic catalyst in heterogeneous catalysis. Information on the catalytic properties of nafion resin is given. Furthermore, details about the synthesis of supported nafion catalysts and their use in catalytic reactions, although very few, are discussed.

In Chapter 7, thermodynamic analysis of the reaction system is done. The equilibrium curve for the methanol dehydration reaction is given as a function of temperature at different pressures.

Chapter 8 presents experimental procedures concerning the synthesis of the novel catalytic materials produced in this work. The different characterization techniques applied to the synthesized catalysts are explained and the instruments used are presented. The experimental set-up of the methanol dehydration reaction system is explained in detail.

In Chapter 9, the results related to the characterization analyses of the catalysts and the activity tests in DME synthesis from methanol are given. The catalysts are compared based on their characteristics and catalytic activities. The effect of temperature on methanol conversion and DME selectivities are investigated. Also, results of the in situ infrared studies of methanol and DME adsorption and desorption on the synthesized catalysts are presented and the obtained FT-IR spectra are discussed. Finally, conclusions and recommendations on the work done are given in Chapter 10.

## CHAPTER 2

### DIMETHYL ETHER (DME) AS A DIESEL ALTERNATE FUEL

The two conventional transportation fuels in use today are gasoline and diesel oil. Gasoline is a petroleum-derived mixture consisting mostly of aliphatic hydrocarbons enhanced with aromatic hydrocarbons. Similarly diesel oil is known as a hydrocarbon mixture produced from petroleum. It contains more carbon atoms in longer chains than gasoline. It is heavier, evaporates more slowly and has a higher energy density than gasoline. Thus, the efficiency of diesel oil as a fuel is higher than gasoline. Diesel engines are different from gasoline engines. In conventional gasoline engines sparkplugs are used to ignite the fuel/air mixture in the engine's cylinders, whereas in diesel engines ignition is achieved by the self-ignition properties of the fuel under specific high-temperature and high-pressure conditions. The compression ratio of a gasoline engine is generally around 8-9 to 1, whereas the compression ratio of a diesel engine is about 17 to 1. In the early 1970s, diesel engines were started to be used to power personal automobiles due to their better fuel economy when compared to gasoline engines. However, with the use of diesel fuel high amounts of nitrogen compounds and particulate matter are released to the atmosphere, which lead to acid rain and poor health conditions. Also, emissions due to the combustion of fossil fuels such as carbon dioxide, sulfur oxides and nitrogen oxides, etc. contribute to global warming. Therefore, a clean alternative fuel is desired and dimethyl ether (DME) is considered as an environmentally benign transportation fuel alternate due to its characteristics as a high quality fuel [5].

The chemical structure of dimethyl ether, also known as methyl ether, methyl oxide and wood ether is given in Figure 1.

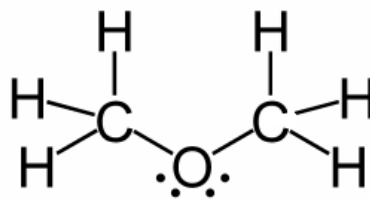


**Figure 1.** The chemical structure of dimethyl ether [6]

Dimethyl ether (DME) is colorless, non-toxic, non-corrosive and non-carcinogenic gaseous ether with a boiling point of  $-25^{\circ}\text{C}$  under ambient conditions [5]. The physical properties of DME are listed in Table 1.

**Table 1.** Physical properties of dimethyl ether [6]

Molecular Formula	$\text{C}_2\text{H}_6\text{O}$ , $\text{CH}_3\text{OCH}_3$
Molar Mass	46.07 g/mol
Melting Point	$-138.5^{\circ}\text{C}$
Boiling Point	$-25.1^{\circ}\text{C}$
Solubility in Water	328 g/100 mL ( $20^{\circ}\text{C}$ )

Dimethyl ether has multiple uses in many areas. It has been used as a propellant in consumer applications, namely personal care (hair spray, shaving creams, foams and antiperspirants), automotive, paints and finishes, food products, insect control, animal products, etc. replacing banned CFC gases [5,7]. Some examples to the usage areas of DME are given in Figure 2. As illustrated, it can also be used in power generation, in industry, as a transportation fuel or as a household gas.

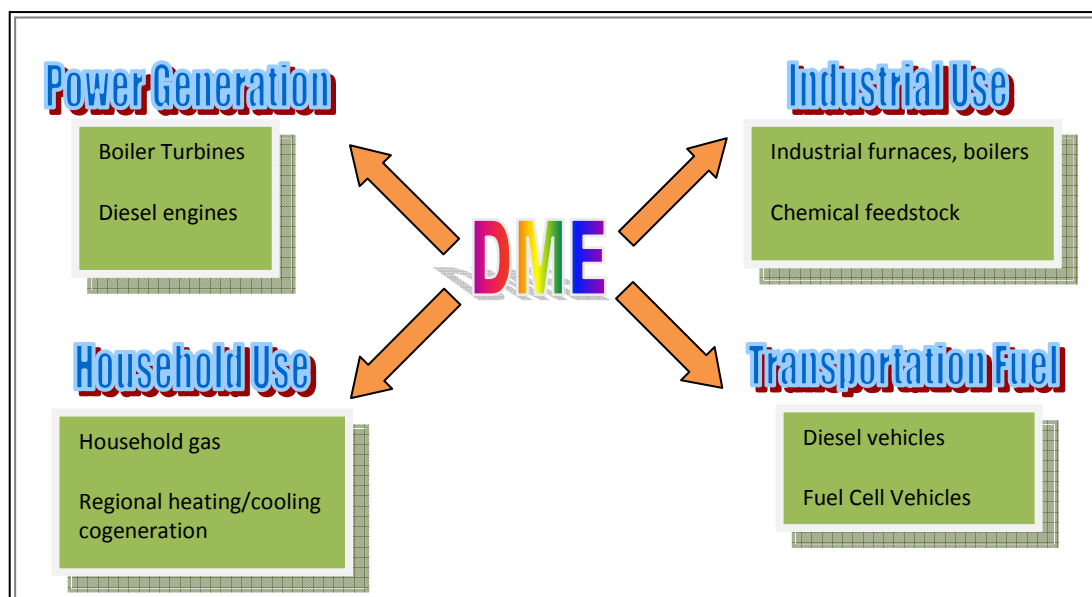


**Figure 2.** Multiple uses of dimethyl ether [8]

Dimethyl ether is considered as a green diesel-alternate fuel with excellent clean burning properties. It is compared with other fuel alternatives in Table 2. Cetane number of a fuel is the indication of its auto-ignition property under high heat and pressure and it is the key parameter for a diesel fuel. The cetane number of the conventional diesel fuel is about 40-55. As can be seen in Table 2, the cetane number of DME is greater than 55, which is higher than the cetane number of conventional diesel oil. This is the main reason why DME is considered as an excellent substitute for diesel fuel. Also, ignition point of DME is very close to the ignition point of diesel fuel.

In addition to these, DME is a clean-burning fuel and has no negative effects on health and on ozone layer depletion. Different from petroleum derived diesel fuel, DME produces no soot, black smoke or particulate matter emission. It causes no  $\text{SO}_x$  emissions, low amounts of  $\text{CO}_2$  emissions, very low  $\text{NO}_x$  emissions and other emissions even without exhaust gas after-treatment [5]. Also, use of dimethyl ether in diesel engines leads to low engine noise. Moreover, DME as a transportation fuel is highly economical when compared to the other alternative fuels. In terms of fuel distribution, since it can easily be liquefied and can be stored and transported in pressurized tanks like LPG, distribution of DME is rather easy [9].

**Table 2.** Properties of dimethyl ether in comparison with diesel oil, methanol and some other transportation fuel alternates [10]

Property	DME	Diesel	Methane	Methanol	Ethanol	LPG
Formula	CH <sub>3</sub> OCH <sub>3</sub>		CH <sub>4</sub>	CH <sub>3</sub> OH	CH <sub>3</sub> CH <sub>2</sub> OH	C <sub>3</sub> H <sub>8</sub>
Boiling Point, °C	-25	180-370	-162	65	78	-42
Liquid Density, g/cm <sup>3</sup>	0.66	0.84	0.42	0.79	0.81	0.49
Cetane Number	55-60	40-55	-	5	8	5
Explosion Limits, %	3.4-18	0.6-6.5	5-15	5.5-26	3.5-15	2.1-9.4
Auto Ignition temperature, °C	235	250	650	450	420	
Heat of evaporation, kJ/kg	460 at -20°C and 410 at +20°C	250	-	1110	904	

As new regulations are being implemented in most industrialized countries, new energy research and development is required to reduce the conventional exhaust emission levels in diesel engines. It is evident that expensive engine/fuel injection equipment modifications will be needed if compression ignition (CI) engines continue operating on diesel fuel. The use of DME, as a promising alternative fuel, in compression ignition engines proved that fueling CI engines with DME instead of diesel fuel enables meeting the 1998 California Ultra Low Emission Vehicle emissions standard without the addition of expensive emission systems [11]. Comparable efficiency and emission levels were obtained with the use of dimethyl ether in diesel engines with exhaust gas recirculation (EGR). DME was reported to be a fuel having similar physical properties with propane but with excellent compression ignitibility [12].

DME can be used in an ordinary diesel engine equipped with a new fuel injection system and can produce the same performance as the conventional diesel fuel by reducing the emissions to a great extent [5]. In order to show the low emission capabilities and high efficiency of DME in a diesel engine, the world's first DME fuelled heavy vehicle was developed by Volvo Truck Corporation and Volvo

Bus Corporation in 1996-1998. DME was seen to have unique auto-ignition capabilities due to its high cetane number with much less amount of pollution produced as a result of combustion when compared to diesel fuel. The European Union, Japan and China have buses which can technically run on DME. Based on Nissan's DME technology, Japan has introduced the DME technology for trucks into US for pilot trials [10].

Dimethyl ether production requires minimum two steps. First step is the conversion of hydrocarbons into synthesis gas, which consists of a combination of carbon monoxide and hydrogen. The synthesis gas is then converted to DME by following two possible routes. Conventional method is by methanol dehydration as shown in Figure 3. In this route, syngas (containing carbon monoxide and hydrogen) is converted to methanol. Then methanol is converted to DME by methanol dehydration reaction. Currently, DME production is achieved by methanol dehydration.

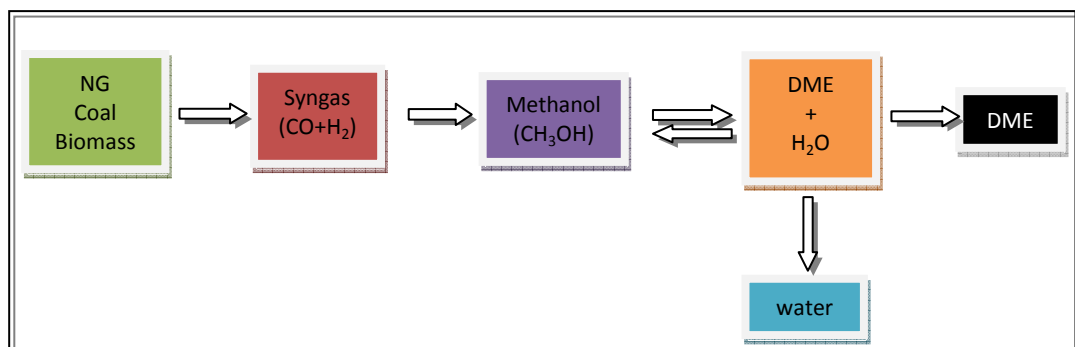


**Figure 3.** DME synthesis by methanol dehydration (conventional process) [13]

Second method is the direct synthesis of DME from synthesis gas (Figure 4). In this route, methanol dehydration step is eliminated and syngas is directly converted to DME. DME production by combining the methanol synthesis and dehydration steps in a single process (direct synthesis procedure) is under development.

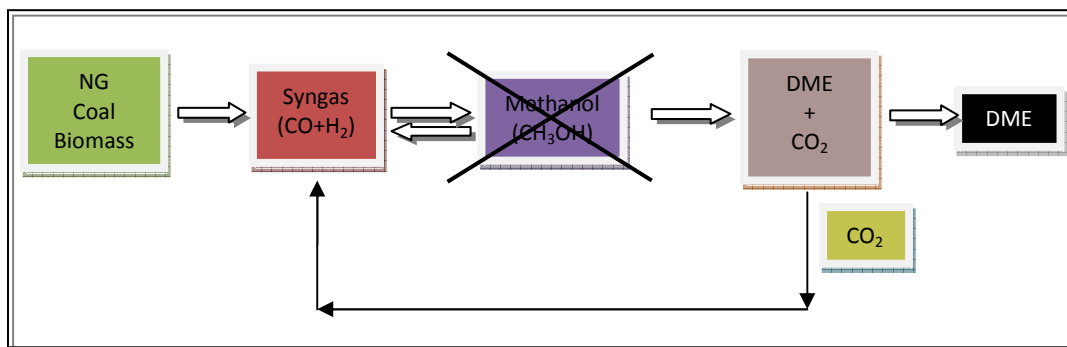


**Figure 4.** Direct synthesis of DME (Haldor Topsoe or JFE Holdings) [13]

The reactions involved in DME synthesis are given in Table 3. Being directly derived from methanol, a variety of feedstocks can be used in DME production such as coal, natural gas, biomass, etc. or reductive CO<sub>2</sub> recycling. The widely used feedstock for DME production is natural gas. The global demand for DME was given as 150000 tons per year by Olah et al. (2006) [5]. However, it was stated that if large quantities of DME was to be used as fuels the demand would be much higher.

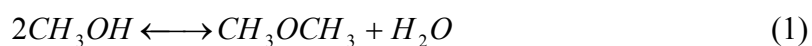
**Table 3.** The reactions occurring in DME synthesis [7]

Reaction	Chemistry	$\Delta H^{\circ}_{298K}$ (kJ/mol)
Partial oxidation reforming	$CH_4 + \frac{1}{2} O_2 \longrightarrow CO + 2 H_2$	-36.0
Steam reforming	$CH_4 + H_2O \longrightarrow CO + 3 H_2$	206.0
Gas/water shift reaction	$CO + H_2O \rightleftharpoons CO_2 + H_2$	-40.9
Methanol synthesis	$CO + 2 H_2 \longrightarrow CH_3OH$	-50.1
	$CO_2 + 3H_2 \longrightarrow CH_3OH + H_2O$	-50.1
Methanol dehydration	$2 CH_3OH \longrightarrow CH_3-O-CH_3 + H_2O$	-23.3
DME direct synthesis	$2 CO + 4 H_2 \longrightarrow CH_3-O-CH_3 + H_2O$	-205.0
	$3 CO + 3 H_2 \longrightarrow CH_3-O-CH_3 + CO_2$	-246.2
Overall DME synthesis	$2 CH_4 + O_2 \longrightarrow CH_3-O-CH_3 + H_2O$	

## CHAPTER 3

### DME SYNTHESIS BY DEHYDRATION OF METHANOL

Dimethyl ether (DME) synthesis by methanol dehydration is a heterogeneous catalytic reaction. The gas phase reaction is exothermic ( $\Delta H_R \sim -23$  kJ/mol) and reversible. It takes place in the presence of solid acid catalysts at atmospheric pressure and in a wide temperature range (up to 400°C) depending on the type of the solid acid catalyst used. The reaction is shown below.



Up to now, many different types of catalysts have been tested in DME synthesis by methanol dehydration.

Fu et al. [2] studied the activity of H-ZSM-5 and SDY catalysts in methanol dehydration. Also the activity of  $\gamma$ -alumina ( $\gamma$ -Al<sub>2</sub>O<sub>3</sub>) and Ti(SO<sub>4</sub>)<sub>2</sub> modified  $\gamma$ -Al<sub>2</sub>O<sub>3</sub> were tested between 127°C-327°C at atmospheric pressure in a stainless steel fixed bed reactor. They concluded that H-ZSM-5 showed the highest activity in methanol dehydration. However, it was reported that H-ZSM-5, due to its high acidity also caused conversion of methanol to hydrocarbons and resulted in coking on the catalyst surface. Coking is the formation of hydrocarbons on the strong acid sites on the surface of the catalyst which appears to be a serious problem since it inhibits the catalytic activity of the catalysts by causing deactivation. It was found that the addition of Ti(SO<sub>4</sub>)<sub>2</sub> increased the catalytic activity of  $\gamma$ -Al<sub>2</sub>O<sub>3</sub> by increasing the number and strength of Brönsted acid sites in the catalyst structure. A methanol conversion of 0.85 could be obtained 227°C. Another conclusion reached in this study was that Brönsted acid sites might be more active than Lewis acid sites in methanol dehydration reaction.

In another study by Vishwanathan et al. [14], highly acidic H-ZSM-5 catalysts were modified by Na at different loadings (up to 80 mol%) and tested in reaction in a fixed-bed micro-reactor between 230-340°C. It was concluded that increasing the Na loading of the catalysts led to a decrease in the strength of the acid sites and increased the resistance of the catalyst against hydrocarbon formation.

Yaripour et al. [3] prepared solid-acid catalysts by sol-gel method. Specifically, they worked on  $\gamma$ -Al<sub>2</sub>O<sub>3</sub> and silica modified  $\gamma$ -Al<sub>2</sub>O<sub>3</sub> (at 1,3,6,9,15 wt% loading). Methanol dehydration reactions were carried out at 300°C in a quartz fixed bed reactor at atmospheric pressure. As for the catalytic activity, silica modified  $\gamma$ -Al<sub>2</sub>O<sub>3</sub> showed better results than untreated  $\gamma$ -Al<sub>2</sub>O<sub>3</sub>. With increasing silica loading surface areas and surface acidity values of the catalysts increased. Catalysts with surface areas higher than 250 m<sup>2</sup>/g were synthesized and the one with 6 wt% silica loading showed the best conversion (85%) without leading to formation of any side product during the reaction. According to this study, DME synthesis takes place on sites with weak and medium acidity. Again, the dependence of methanol dehydration on Brønsted acid sites is emphasized here.

In another study of Yaripour et al. [15], aluminum phosphates with Al/P molar ratio of 1,2,3 and silica-titania (SiO<sub>2</sub>-TiO<sub>2</sub>) catalysts with 25,50,75 wt% silica loading were synthesized. Catalytic activities of phosphorus modified  $\gamma$ -Al<sub>2</sub>O<sub>3</sub> catalysts were found to be higher than the untreated  $\gamma$ -Al<sub>2</sub>O<sub>3</sub>. AlPO<sub>4</sub> (with Al/P=2) showed 83.3% conversion without leading to formation of any side products. An increase in surface area values and a decrease in the surface acidities of the catalysts were observed with increasing Al/P molar ratio. Silica-titania catalysts showed low activity and it was attributed to their low surface areas (below 60 m<sup>2</sup>/g) and low concentration of the acid sites on their surface. An important conclusion reached in this study concerning the aluminosilicate type catalysts was that the strength of the acid sites of  $\gamma$ -Al<sub>2</sub>O<sub>3</sub> should be reduced in order to prevent coke formation. In phosphorus modified alumina catalysts reduction in coking, hence decrease in the amount of by-products was achieved.

Fei et al. [16] studied HY zeolite and modified forms of HY zeolite in methanol dehydration. Reaction was carried out at 245°C in a stainless-steel fixed bed reactor. Fe, Co, Ni, Cr and Zr modified HY zeolites were prepared and it was found that all the catalysts except the Fe modified zeolite exhibited high initial

activity (86% conversion). Zr-HY and Ni-HY catalysts were observed to be more stable than the rest of the samples. This advantage resulted from the lower concentration of acid sites on their surface. On the other hand, Fe-HY, Co-HY, Cr-HY and HY itself were observed to deactivate during methanol dehydration reaction.

Xu et al. [17] used  $\gamma$ -Al<sub>2</sub>O<sub>3</sub>, H-ZSM-5, amorphous silica-alumina and titania modified zirconia. The reactions were carried out in a plug flow reactor made of fused quartz. It was observed that all the catalysts were active and selective towards dimethyl ether formation. Silica-alumina catalysts were tested in a temperature range of 140-190°C. As the silica content increased the activity of the catalysts decreased. Among the catalysts tested at 280°C, the highest activity was achieved with the amorphous silica-alumina catalyst with 20 wt% silica content.

In the study of Khom-in et al. [18], methanol dehydration to synthesize dimethyl ether was carried out in the presence of nanocrystalline alumina with mixed  $\gamma$  and  $\chi$  phases. The catalysts were synthesized by solvothermal method. The  $\gamma$ -Al<sub>2</sub>O<sub>3</sub> catalyst containing 20 wt%  $\chi$ -phase showed the highest catalytic activity when compared to pure  $\gamma$  and  $\chi$  phases. The DME yield obtained with this catalyst was 86%.

## CHAPTER 4

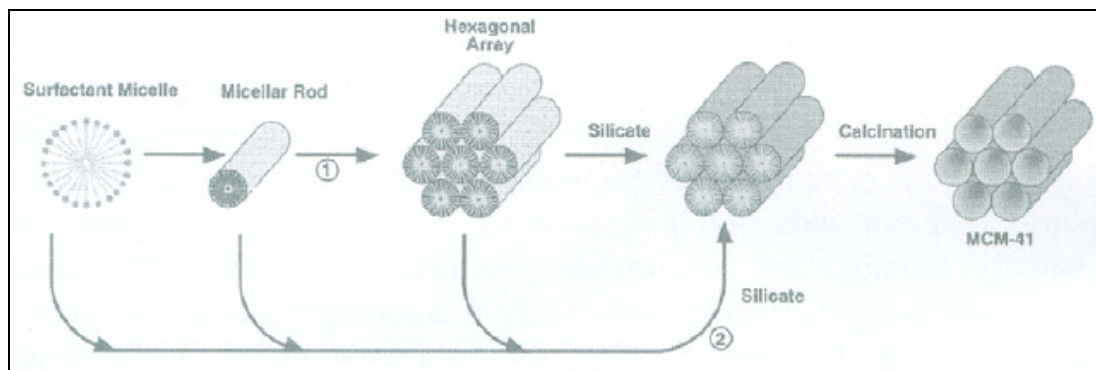
### MESOPOROUS MATERIALS

Heterogeneous catalysis has a very important role in the development and application of green processes. In order to eliminate toxic wastes produced as a result of harmful, environmentally hazardous processes, solid materials can be utilized instead of liquid acid catalysts. Porous materials received great attention in the past years owing to their useful applications as catalysts and catalyst supports.

Based on the IUPAC definition, porous materials can be classified as microporous (pore size less than 2 nm), mesoporous (pore size between 2-50 nm) and macroporous (pore size higher than 50 nm) materials. Zeolites are the most well-known member of the microporous materials family. They have very narrow and uniform micropore size distribution. Although it is possible to synthesize very stable zeolites, they have a serious disadvantage which limits their applications in catalytic reactions. Since their pore diameters are very narrow, they lose their efficiency when large reactant molecules with pore diameters larger than theirs are present in the reaction medium. Mass transfer limitations are dominant in such cases. For this reason, it was aimed to synthesize crystalline materials with increased pore sizes.

The discovery of ordered mesoporous materials is considered as the beginning of a new era in catalysis. In 1992, Mobil Research and Development Corporation used the surfactant templating method to synthesize a new family of ordered mesoporous silicates called as M41S. This new type of mesoporous structures have large surface areas and very narrow pore size distributions. The pore diameters can be tuned from 15 to 100 Å. Changing the synthesis conditions, different materials can be obtained. The class consisting of a hexagonal phase is known as MCM-41. Another class which is formed of a cubic phase is referred to as

MCM-48. An unstable lamellar phase which can be stabilized by post-synthesis treatment with tetraethylorthosilicate (TEOS) is called as MCM-50 [19,20,21].



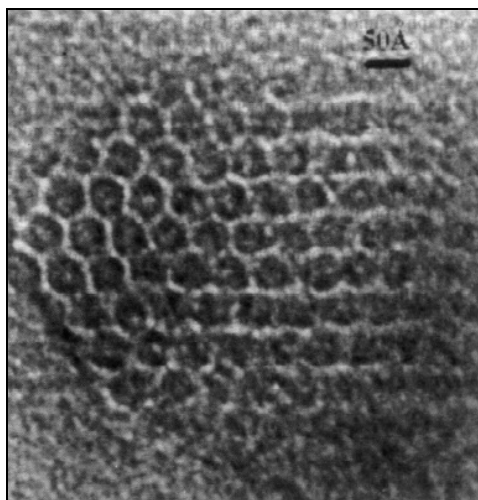
**Figure 5.** Formation pathway of ordered mesoporous materials [22]

Figure 5 shows the formation of MCM-41, a highly ordered hexagonal array of unidimensional pores with a very narrow pore size distribution. The Mobile group has two proposals for the formation mechanism of M41S silicates. In the first pathway, it is proposed that by self organization of the surfactant molecules a liquid crystalline phase is formed which acts as the template. The silicates polymerize to form a rigid shell around the hydrophilic parts of the aggregated surfactant. The second pathway suggests that silicate species in solution direct the formation of the organic-inorganic mesophase with the help of the charge balance with the surfactant ions [20].

Basically, four components are used in the synthesis of M41S type materials. Structure directing surfactants, a source of silica, a solvent and an acidic or basic catalyst. Researchers at Mobile R&D group used alkyl trimethyl ammonium halides as the surfactant. As the source of silica sodium silicate, tetraethoxy silicate (TEOS), fumed silica and Ludox were used. Sodium hydroxide and tetraethyl ammonium hydroxide were also added to the solution. When it was aimed to synthesize aluminosilicate materials, an aluminum source was also used. The aqueous synthesis solutions were kept at temperatures of 100-150°C for 24-144 hours. After filtering,

washing and drying the solid products, the materials were calcined at 540°C under the flow of air or nitrogen. Porous structures were obtained as final products [19].

In order to observe the ordered mesoporous structures of the materials, Transmission Electron Microscopy (TEM) is used. The ordered hexagonal pore shape of MCM-41 can be clearly observed by TEM in Figure 6.



**Figure 6.** TEM micrograph of MCM-41 [23]

The powder X-ray diffraction (XRD) pattern of MCM-41 is shown in Figure 7. It is assigned to a hexagonal unit cell. In the typical XRD pattern of MCM-41, three to five reflections at  $2\theta$  values between 2-5° are observed. The X-Ray diffraction patterns of mesoporous materials have reflection peaks only in the low-angle range, at  $2\theta$  less than 10. Thus, it is concluded that their pore walls are mainly amorphous [19]. The sharp peak at 2° and the reflections are indexed as (100), (110), (200) and (210), respectively.

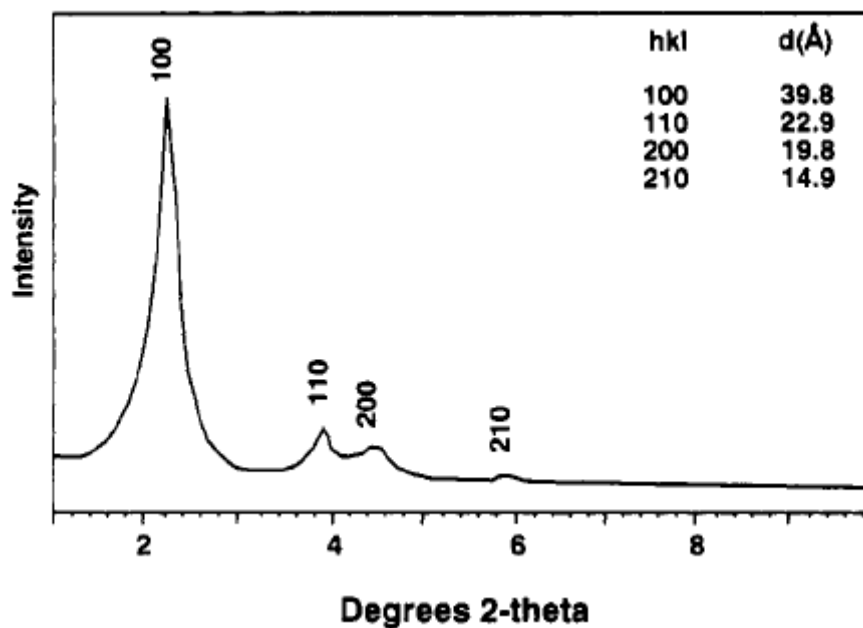


**Figure 7.** Powder X-Ray diffraction pattern of MCM-41 [24]

The nitrogen adsorption-desorption isotherms of an ordered mesoporous material is presented in Figure 8. According to the IUPAC definition, mesoporous materials show Type IV adsorption-desorption isotherm. At low relative pressures ( $P/P_0$ ), nitrogen is adsorbed only as a thin layer on the walls, called monolayer coverage [19].

Depending on the pore size, the isotherm for the mesoporous molecular sieve shows a sharp inflection at relative pressures 0.25 to 0.50, which is characteristic of capillary condensation of nitrogen within the uniform mesopores, where the  $P/P_0$  position of the inflection point is related to the diameter of the pore. The sharpness of the inflection is a measure of the uniformity of pore sizes and its height is related to the amount of pore volume. A hysteresis effect is observed for nitrogen adsorption-desorption isotherms when the pore diameter is larger than  $\sim 40 \text{ \AA}$  [19].

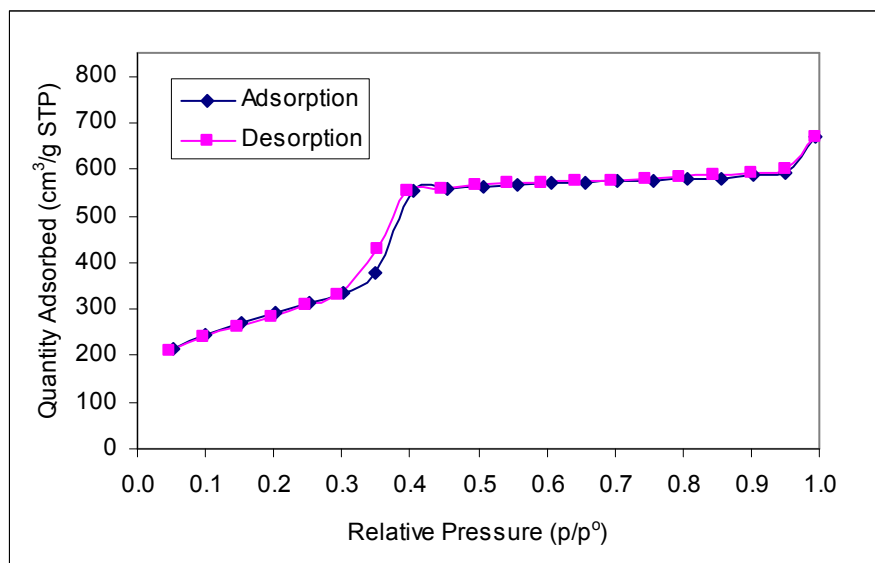


**Figure 8.** Nitrogen adsorption/desorption isotherm of MCM-41 [25]

For the use of ordered mesoporous materials in heterogeneous catalysis, additional catalytic functions are introduced into their structure. This is achieved by the incorporation of active sites in the silica walls or by deposition of active species on the inner surface of the material. The large, adjustable pores of the ordered silicas permit bulky organometallic precursors to be uniformly attached on their inner walls. Their high surface areas and relatively large pores are advantageous since they enable mass transfer and allow a high concentration of active sites per mass of material. By substituting silicon atoms in the framework with metal ions active acidic or redox sites can be created and the resulting materials can be used for various catalytic reactions. However, the wall structure of ordered mesoporous silicate type materials is more like amorphous silica. Thus, the incorporation of metals or metal oxides does not result in the formation of defined structures as in zeolites. Indeed, a variety of different sites with different local environments are created. The active sites in mesoporous materials can be created by direct synthesis, from mixtures containing both silicon and the heteroelement to be incorporated, or by post-synthesis, by treatment of an initially prepared mesoporous silica material. These procedures may be applied by following many pathways. Hence, the properties of the

active sites are variable and can easily be controlled depending on the synthesis procedure applied [19, 26].

There are many studies in literature about the incorporation of Al and also heteroatoms, like B, Fe, Ga, Ti, V, Sn into the siliceous framework in order to modify the composition of the inorganic walls and introduce active sites into the mesoporous material. Some examples would be the incorporation of V [27], Ni [28] and Pd [29] into the mesoporous framework of MCM-41 achieved by direct synthesis.

## CHAPTER 5

### HETEROPOLYACID (HPA) CATALYSTS

#### 5.1. GENERAL PROPERTIES AND CLASSIFICATION OF HPA'S

Heteropoly compounds (heteropolyacids and their salts) have received a great attention in catalysis which resulted in the invention of new industrial processes.

Heteropoly acid catalysts show higher catalytic activity than conventional solid-acid catalysts. They are condensed materials which consist of inorganic oxyacids of P, W, Mo, V, etc. In their structure, HPA's contain an element such as Si, P or As (hetero atom); metals such as W, Mo or V (addenda atom); oxygen and acidic hydrogen atoms [30].

There are many types of heteropoly compounds. The most important three classes of HPA's are listed below [31].

- *Keggin HPA's* have the general formula  $X^{n+}M_{12}O_{40}^{(8-n)-}$  ( $M/X=12$ ). They are the most well-known type of heteropoly compounds. The Keggin heteropolyacids are the most important for catalysis since they are the most thermally stable and more easily available. The fact that they are easier for operation and their high acidic and redox properties also make them favorable. The primary structure of Keggin HPA's is presented in Figures 9 and 10.
- *Wells-Dawson HPA's* have the general formula  $X_2^{n+}M_{18}O_{62}^{(2n-16)-}$  ( $X$  is  $P^{5+}$ ,  $S^{6+}$ ,  $As^{5+}$ ;  $M$  may be either  $W^{6+}$  or  $Mo^{6+}$ ) ( $M/X=9$ ). The primary structure of Wells-Dawson heteropoly compounds is shown in Figure 11.

- *Anderson HPC's* have the general formula.  $\text{XM}_6\text{O}_{24}^{n-}$  ( $\text{M}/\text{X}=6$ ) ( $\text{X}=\text{Mn}^{4+}, \text{Ni}^{4+}, \text{Pt}^{4+}, \text{Te}^{6+}$ ;  $\text{M}=\text{Mo}^{6+}, \text{W}^{6+}$ ). They have a planar structure.



**Figure 9.** The primary structure of Keggin HPA's. [31]

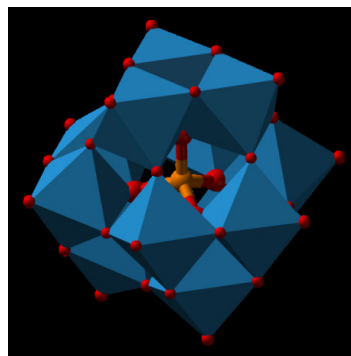


**Figure 10.** Keggin structure [30]

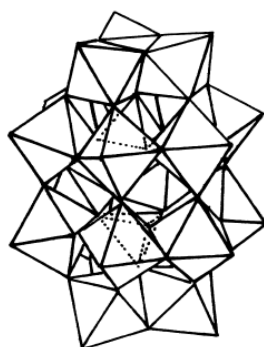


**Figure 11.** The primary structure of Wells-Dawson HPA's. [31]

The advantages of heteropoly compounds as efficient catalysts in industrial applications may be listed as follows:

- *Acidic and redox properties:* An advantage of heteropolyacids is that it is possible to control the acidic and redox properties of them at the atomic and molecular level [32]. Heteropolyacids have strong Brønsted acid sites. They are stronger than the well-known inorganic acids like  $\text{H}_2\text{SO}_4$ ,  $\text{HCl}$ ,  $\text{HBr}$ ,  $\text{HNO}_3$ , etc. [33] Acid strength of tungstophosphoric acid ( $\text{H}_3\text{PW}_{12}\text{O}_{40}$ ) was found to be higher than

sulfuric acid and acetic acid. The three protons in the structure of tungstophosphoric acid (TPA) are as strong as sulfuric acid and perchloric acid [32]. Acidity function measured by Hammett indicator test shows that for TPA  $H_0^a = -13.16$ , whereas for H-ZSM-5 and Silica-Alumina  $H_0^a = -12.70$  [34]. In addition to these, TPA is known to have the highest acidity among the heteropolyacids.

By modifications in the chemical composition of the heteropoly compound, the type of the carrier, the conditions in the preliminary treatment of the catalyst, etc. the nature, strength, and number of the acid sites on the HPA catalyst can be altered [33].

- *High catalytic activity:* As they are stronger acids, heteropolyacids possess high catalytic activity. Solid HPA's show pure Brønsted acidity, whereas oxide systems have both Brønsted and Lewis acid sites. Thus HPA's are stronger than the usual acid catalysts like aluminosilicates,  $H_3PO_4/SiO_2$ , HX and HY zeolites [33]. Owing to the acid strength and oxidizing properties of heteropoly compounds and the unique basic behavior of the polyanions, HPA's are very important in heterogeneous and homogeneous catalysis. Moreover, it is possible to introduce various elements into the structure of the polyanions and the countercations, and the oxidative stability of HPA's is a significant advantage in catalysis [32,35]. Catalytic reactions can take place in various phases such as homogenous liquid, liquid/liquid, liquid/solid, gas/solid systems, etc. [35].

- *Pseudo-liquid phase behaviour:* A very important characteristic of HPA's which contribute to their superior catalytic properties is that they show pseudo-liquid behavior. In spite of their low surface areas certain heteropoly acids, like  $H_3PW_{12}O_{40}$ , and  $H_3PMo_{12}O_{40}$ , in their solid state may easily absorb a large amount of water, alcohols, and ethers. Rather than adsorption in micropores, this is absorption of molecules between the lattice polyanions, which may even expand the lattice. Due to their flexible lattice (variable secondary structure), reactant molecules are absorbed into the three-dimensional solid bulk and the catalytic reaction takes place in this novel bulk phase which can be described as a three-dimensional field. This state is called the "pseudo-liquid phase". This property of HPA's result in high catalytic activities and selectivity values [36,37].

- *Green aspects of HPA's*: HPA's do not lead to any production of toxic wastes and they are considered to be green catalysts. It is possible to work at milder experimental conditions with HPA's with a low proportion of side reactions. Green and sustainable aspects of HPA's have been summarized by Misono et al. [38] by referring to some of their applications such as water-tolerant acid catalysis, catalysis in pseudoliquid phase, solid-phase catalysis, bi-functional catalysis in combination with noble metals, and green processes in bi-phase systems.

## 5.2. CATALYTIC APPLICATIONS OF PURE HPA'S

In their pure form, HPA's have been used in many types of catalytic reactions. They are considered as effective catalysts in alkylation of benzene and alkybenzenes by olefins, synthesis of ethers and esters, acylation of aromatic compounds, etc. [33]. Varisli et al. [39] observed the catalytic activity of tungstophosphoric acid (TPA), silicotungstic acid (STA) and molybdophosphoric acid (MPA) in ethanol dehydration to synthesize diethyl ether. Reactions were carried out between 140-250°C at a space time of 0.27 s.g.cm<sup>-3</sup>. Main products were ethylene and diethyl ether. The trend in catalytic activity was found as STA>TPA>MPA. Also the activities of heteropolyacid catalysts in methanol dehydration reaction to produce dimethyl ether were tested [25]. It was found that with TPA, 15% methanol conversion and 80% dimethyl ether selectivity was obtained at 250°C, whereas with STA, 30% methanol conversion and 100% dimethyl ether selectivity could be obtained. Obviously, pure STA was found to be more active than pure TPA in dehydration of methanol. However, from the results of this work it can be concluded that both of these pure heteropolyacid catalysts showed relatively low activity when it is considered that the equilibrium conversion of methanol dehydration reaction at 250°C is about 90% (as shown in Chapter 7). This low catalytic activity of HPA's is due to some features of them which are given below.

Although they are considered as highly acidic solid acid catalysts which open ways to green and sustainable processes, heteropoly acid catalysts have some major drawbacks [40].

- *Low surface area* : Pure heteropoly acids have surface areas as low as 1-5 m<sup>2</sup>/g, which hinders accessibility to their strong acid sites. Due to their relatively low specific surface area, catalytic activity of HPA's is limited in gas-solid phase reactions.
- *Solubility in polar solvents* : Heteropoly acids in their pure form are very soluble in polar solvents such as alcohols, water, ethers. This property of HPA's causes them to be leached during catalytic reactions involving polar molecules as reactants or products.

### 5.3. SALTS OF HPA'S AND THEIR CATALYTIC APPLICATIONS

In order to increase the efficiency of HPA-catalyzed processes these disadvantages have to be overcome. One of the possible solutions is synthesizing salts of them. In this way, a partial neutralization of HPA's with cations such as K<sup>+</sup>, Ag<sup>+</sup> is achieved and insoluble salts of HPA's are obtained. Haber et al. [41] studied the synthesis of metal salts of HPA's in pure form and also supported them on silica and tested them in dehydration of ethanol and hydration of ethylene. It was reported that the structure of salts of heteropolyacids were affected by the type of counteraction present. Salts with small cations like Fe, Co, Ni or Na resembled the parent HPA, as they were water soluble, nonporous and had low surface areas. On the other hand, salts of HPA with large monovalent cations such as NH<sub>4</sub><sup>+</sup>, K<sup>+</sup>, and Cs<sup>+</sup> were water insoluble, had rigid micro/mesoporous tertiary structure and had high surface areas [41,42]. Allaoui et al. [43] prepared copper salts of molybdophosphoric acid and compared its catalytic activity in methanol conversion to formaldehyde, dimethyl ether, dimethyl carbonate and methyl formate in the presence of CO<sub>2</sub>. Okuhara et al. [34] reported the acidity, micropore structure and catalytic activity of Cs salts. The conclusions achieved in this study showed that the pore size of the acidic Cs salts (Cs<sub>x</sub>H<sub>3-x</sub>PW<sub>12</sub>O<sub>40</sub>) was controlled by the Cs content. Also, shape selective catalysis was observed for the Cs salts of TPA. As for the acidity, it was concluded that the acidic Cs salts as well as H<sub>3</sub>PW<sub>12</sub>O<sub>40</sub> were strongly acidic and when compared to the zeolites SO<sub>4</sub><sup>2-</sup>/ZRO<sub>2</sub>, they were more catalytically active for

decomposition of esters and alkylation in liquid-solid reaction system. Soled et al. [42] synthesized water-insoluble ammonium and cesium heteropolyacid salts of 12-tungstophosphoric acid by gas phase reaction, hydrothermal synthesis, precursor decomposition, in situ reaction and precipitation. Tungsten heteropolyacids are reported to be stable up to around 400°C. When in the form of salts, thermal stability of heteropolyacids is higher than their acid forms [33].

A second solution is to support heteropolyacids on high surface area supports such as silica, alumina or mesoporous molecular sieves like MCM-41, SBA-15. In doing so, both the surface area of the active HPA is increased and compounds which are insoluble in polar solvents are obtained. Examples of related work involving supported HPA's are given in the following section.

#### **5.4. SUPPORTED HPA'S AND THEIR APPLICATIONS IN ALCOHOL DEHYDRATION**

The discovery of mesoporous MCM-41 type materials was a great improvement in catalysis. Incorporation of transition metal ions into the silicate network of such mesoporous materials is the idea which enabled the use of high surface area active catalytic materials in many catalytic processes [44]. Based on this view, dispersing heteropolyacids on high surface area supports is a way of increasing their surface area, thus catalytic activity. Several studies were done on immobilization of HPA's into the silicate matrix of mesoporous materials.

Following a hydrothermal route, Taguchi et al. [44] synthesized new mesoporous materials composed of  $PW_{11}O_{39}^{7-}$  cluster anions and dodecyltrimethylammonium cations with hexagonal phase. Nowinska et al. [45] synthesized tungstophosphoric acid (TPA) modified SBA-13 catalysts with 20% TPA loading. The calcination temperature was changed between 400°C-500°C. The synthesized catalysts had surface area values between 785-1126 m<sup>2</sup>/g and pore diameters in the range 2.1-3.2 nm. Said et al. [46] synthesized supported heteropolyacids by impregnation of TPA on silica by varying the TPA loading on the catalyst between 5-30% and the calcination temperature was changed between 300-500°C. The resulting catalysts had surface areas changing between 166-288 m<sup>2</sup>/g and

pore diameters varied between 33-49 nm. Soled et al. [42] synthesized supported tungstophosphoric acid catalysts by incipient wetness impregnation method. The supports were silica powder and  $\gamma$ -Al<sub>2</sub>O<sub>3</sub>. Calcination was carried out at 300°C and 500°C. The surface areas of the catalysts varied between 102-155 m<sup>2</sup>/g.

Vazquez et al. [47] prepared molybdophosphoric acid and tungstophosphoric acid supported on silica by equilibrium impregnation technique. They were tested in the dehydration of 1,2-diphenylethanol, 1-(3,4-dimethoxyphenyl)-2-phenylethanol and cholesterol. Alcohol dehydration reactions were carried out in liquid phase. Herrera et al. [40] supported TPA on unmodified MCM-41, SBA-15 and also on alumina, zirconia and titania coated MCM-41 and SBA-15 by impregnation. They were tested in 2-butanol and methanol dehydration. Dimethyl ether formation was observed in methanol dehydration. Different from 2-butanol dehydration, significant amount of coke formation was observed after methanol dehydration. It was stated that above 300°C, in the absence of cleaning agents such as oxygen or hydrogen, carbonaceous species could accumulate on the surface of strong acidic catalysts. Carbonaceous deposits on the catalysts were indicated to be a reason for catalyst deactivation during methanol dehydration. Varisli et al. [48] synthesized silica supported silicotungstic acid catalysts by direct hydrothermal synthesis route. W/Si ratios of the catalysts were taken as 0.25 and 0.50. BET surface areas of the samples were found as 393 m<sup>2</sup>/g (pore diameter as 5.5 nm) and 179 m<sup>2</sup>/g (pore diameter as 10 nm), respectively. These catalysts were tested in ethanol dehydration to produce ethylene and diethyl ether. The WO<sub>x</sub>-Silicate acidic catalysts synthesized in this work were found to be much more active when compared to pure HPA's [39]. In another work of Varisli et al. [49] STA incorporated MCM-41 and aluminosilicate catalysts were synthesized by impregnation route and were again tested in dehydration of ethanol.

## CHAPTER 6

### NAFION RESIN AS A CATALYST

#### 6.1. GENERAL PROPERTIES OF NAFION RESIN

Nafion ionomers, developed by the E.I. DuPont Company, are produced by copolymerization of a perfluorinated vinyl ether comonomer with TFE (tetrafluoroethylene). Nafion is a perfluorinated sulfonic acid ion-exchange resin which is considered as an active catalyst for acid-catalyzed reactions. As a superacidic catalyst, nafion resin has a terminal  $-\text{CF}_2\text{CF}_2\text{SO}_3\text{H}$  group and a high concentration of Brønsted acid sites in its structure. The structure of nafion resin is shown in Figure 12 where  $m = 1, 2,$  or  $3$  and  $n$  is about  $6-7$  with  $x$  about  $1000$ . The equivalent weight of the polymeric nafion resin is typically around  $1070$ .

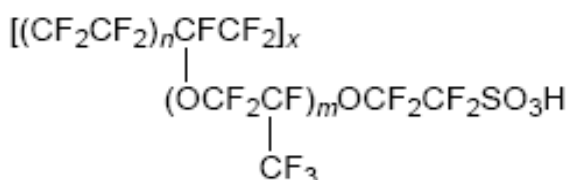


**Figure 12.** Structure of nafion resin [50]

In the structure of nafion resin, perfluorosulfonic acid is present as clusters within the polymer. The perfluorinated resinsulfonic acids are considered as very strong acids with Hammett acidity values between  $-11$  to  $-13$ . The Hammett acidity function of nafion ( $H_0 = \sim 12$ ) is much higher than the Hammett acidity function of Amberlyst-15 ( $H_0 = -2.2$ ), which is also a sulfonic acid ion-exchange resin. In the

structure of nafion resin, there exist terminal sulfonic acid groups attached to a perfluoro polymeric backbone. The presence of electron withdrawing F atoms in the structure increases the acid strength of the terminal sulfonic acid groups to a great extent. Due to this, the acidity of nafion is considered to be comparable to that of pure sulfuric acid. Indeed, the  $H_0$  value of nafion resin was found to be much higher than the acidity of 40% sulfuric acid ( $H_0 = -2.4$ ) and close to the acidity of 100% sulfuric acid ( $H_0 = -12.3$ ). The acid content of nafion resin is about 0.95 meq/g. Due to its superacidic characteristics, nafion has been used as a heterogeneous strong acid catalyst for a wide range of chemical reactions.

The property of nafion resin which widens its application areas is that it is insoluble in polar solvents. Because of this, it can be used in liquid phase reactions and can be treated with polar solvents without being affected. Another advantage of nafion is that it is extremely resistant to chemical attack. Owing to its fluorocarbon backbone, it has a superior chemical stability. Besides, it has a high mechanical strength and thermal stability. Perfluorinated resinsulfonic acids are known to be much more stable than styrene-based resinsulfonic acid catalysts. Nafion resin is thermally stable up to 280°C. Above this temperature the sulfonic acid groups start to decompose. However, the thermal stability of styrene based resinsulfonic acid catalysts is limited to 120-140°C.

Nafion is commercially available in the form of millimeter sized beads known as NR-50. The specific surface area of NR-50 is about 0.02 m<sup>2</sup>/g. The nonporous nature of the pure nafion resin is its major disadvantage which limits its applications in catalysis. The acid sites in nafion, namely the sulfonic acid groups are buried in the bulk of the resin and its nonporous structure leads to poor accessibility to the acid sites on the catalyst. Due to diffusion limitations, the catalytic activity of the resin is decreased to a great extent.

Nafion resin is considered to be an effective acidic catalyst for many reactions such as isomerizations, esterifications, alkylations, acylations, hydrations and dehydrations, nitrations and etherifications. However, as explained above the observed activity of nafion resin in catalytic applications is very low due to its low specific surface area and nonporous structure. To overcome this disadvantage, supported nafion resin catalysts should be prepared by dispersing it on high surface area mesoporous materials in order to increase its efficiency in catalysis [50,51,52].

## 6.2. SUPPORTED NAFION CATALYSTS

Dispersing nafion resin on high surface area supports was first achieved by Harmer et al. [50]. Nafion-silica nanocomposites were synthesized by following a sol-gel synthesis route. The procedure included mixing  $\text{Si}(\text{OMe})_4$ , deionized water and HCl with a mixture of NaOH and 5 wt% Nafion solution. The mixture gelled in a few seconds and then was exposed to nitrogen flow to remove the volatiles. After drying at  $95^\circ\text{C}$ , the solid product was reacidified by stirring with an aqueous HCl solution and then washed with deionized water. Finally, the sample was treated with nitric acid at  $75^\circ\text{C}$ , washed again with DI water and dried in vacuum. The nafion-silica nanocomposites obtained by sol-gel synthesis route had nafion contents of 8 – 80 wt%. Surface area values of the nanocomposites depended on the nafion loading. For example, the catalyst with a nafion loading of 8 wt% had surface area of  $412\text{ m}^2/\text{g}$  and the one with nafion content of 60 wt% had a surface area of  $34\text{ m}^2/\text{g}$ . Pore volumes were in the range of  $0.15\text{-}1.05\text{ cm}^3/\text{g}$  and the pore diameters of the catalysts were changing between 6.5-15 nm.

Fujiwara et al. [53] prepared MCM-41/nafion composites by the following synthesis route. Nafion gel was dissolved in ethanol and it was added to a mixture of tetramethyl ammonium hydroxide and cetyltrimethylammonium bromide in distilled water. To this mixture, tetraethoxy silane was added. The material was synthesized in an autoclave at  $130^\circ\text{C}$  for 24 hours. The white solid product was washed with distilled water, dried and then refluxed in sulfuric acid solution in ethanol for 18 hours. After two further refluxes in ethanol the product was dried at  $150^\circ\text{C}$ . The X-ray diffraction peaks of the catalyst revealed that the MCM-41 structure was preserved. The BET surface area of the catalyst was  $619\text{ m}^2/\text{g}$  and the pore volume was  $0.64\text{ cm}^3/\text{g}$ .

In another work of Fujiwara et al. [54], by following three different synthesis procedures, polymer sulfonates like nafion were incorporated into the mesoporous silica framework. Firstly, to an aqueous solution of NaOH and hexadecyltrimethylammonium bromide, 5 wt% nafion solution was added. Then tetraethoxy silane was added and the mixture was stirred at room temperature. After filtering and washing, the product was dried at  $80^\circ\text{C}$ . The sample was refluxed with 1M of sulfuric acid solution of ethanol for 12 hours and then filtered. The resulting

material was further refluxed with pure ethanol for 12 hours. In this work, in addition to the mesoporous silica-nafion nanocomposite material, a nafion-silica composite was prepared from the amorphous nafion-silica composite (SAC-13) produced by Harmer et al. [50]. To an aqueous solution of NaOH and hexadecyltrimethylammonium bromide, appropriate amount of SAC-13 was added and stirred for 1 hour. The synthesis was carried out in an autoclave at 110°C for 24 hours. The rest of the procedure is similar to the procedure described for the mesoporous nafion-silica composite above. Thirdly, a mesoporous silica-poly (4-styrenesulfonate) composite material was synthesized by adding poly(sodium 4-styrenesulfonate) and TEOS to the solution of NaOH and hexadecyltrimethylammonium bromide. The nanocomposites synthesized in this work had nafion contents of 5-25 wt%. The BET specific surface areas of the catalysts changed between 1239-333 m<sup>2</sup>/g, pore volumes were in the range 0.26-1.26 and BJH adsorption pore diameters varied between 2.52-2.75 nm depending on the nafion loading and synthesis procedure of the catalysts.

By following impregnation technique, Wang et al. [55] synthesized supported nafion catalysts. 5 wt % nafion in water-alcohol solution was impregnated on various supports by stirring at 60°C for 2 hours. After evaporating the water and alcohols the sample was dried at 60°C. Török et al. [56] also synthesized 10 % Nafion-H/Silica nanocomposites by impregnation method. Silica was dispersed in 2-propanol/1-propanol/water mixture which contained the appropriate amount of nafion-H. After stirring at room temperature for 2 hours, the solvents were evaporated and the sample was dried under vacuum. Bringué et al. [57] used silica, alumina and silica-alumina as carriers. In the impregnation procedure, the carrier was washed, dried and then mixed with a solution of 2-propanol:water. Commercial nafion resin solution was added and the mixture was stirred for 6 hours. After evaporating the solvents, the impregnated catalyst was dried and washed with methanol to get rid of the non-bonded nafion.

In the work of Alvaro et al. [58], by a condensation reaction between the surface silanol groups of the mesoporous silicas and 1,2,2-trifluoro-2-hydroxy-1-trifluoromethyl-ethane sulfonic acid beta-sultone hybrid organic-inorganic MCM-41 silicas were functionalized with perfluoroalkylsulfonic acid groups analogous to Nafion. The XRD analysis indicated that the ordered mesoporous structure of MCM-

41 was not affected with the incorporation of perfluoroalkyl sulfonic acid groups. But it was also observed that at higher loading (more than 2wt%) of perfluoroalkyl sulfonic acid groups, the mesoporous structure was destroyed and the materials had an amorphous structure. This was attributed to the high concentration of Brønsted acid sites formed on the catalyst. The resulting materials had surface areas between 680-912 m<sup>2</sup>/g. Sulfur content of the final solid was found to be between 0.12-0.45 mmol/g depending on the 1,2,2-trifluoro-2-hydroxy-1-trifluoromethyl-ethane sulfonic acid beta-sultone added per gram of solid (0.5-1.5 mmol/g). The C/S ratios were found as approximately 3.0 for all the samples. In another work of Alvaro et al. [59], in addition to MCM-41, functionalization of SBA-15 type mesoporous materials with 1,2,2-trifluoro-2-hydroxy-1-trifluoromethyl-ethane sulfonic acid sultone was also described. Martinez et al. [60] synthesized Nafion/SBA-15 catalysts by following impregnation route. Nafion alcoholic solution was added to the dispersion of powder SBA-15. The synthesis was carried out at 60°C by stirring for 2 hours at atmospheric pressure. Nafion loadings of the catalysts changed between 10-20 wt% and the surface areas decreased from 601 m<sup>2</sup>/g to 432 m<sup>2</sup>/g with an increase in nafion loading.

### **6.3. CATALYTIC APPLICATIONS OF NAFION BASED CATALYSTS**

In the majority of the kinetic studies where nafion-silica nanocomposites were used as catalysts, the synthesis procedure described by Harmer et al. [50] was applied and the synthesized nafion-silica nanocomposites were tested in a range of chemical reactions. In some of the studies, commercialized SAC-13 (13wt% nafion containing nafion-silica nanocomposite produced by DuPont synthesized based on the study of Harmer et al. (1996)) and pure Nafion NR-50 were purchased and used in the kinetic studies.

Sun et al. [61] used the 13 wt% nafion-silica nanocomposite in Friedel-Crafts benzylation of benzene at 80°C and p-xylene at 100°C with methylbenzyl alcohol at ambient pressure. The novel composite was found to be twice as active as the nafion resin beads (NR-50). The activity of nafion-silica nanocomposites were tested in liquid phase alkylation of isobutene [62], in the reaction of resorcinol with ethyl

acetoacetate or with acrylic acid [63], in the alkylation of benzene with linear C<sub>9</sub>-C<sub>13</sub> alkenes [64] and in the acylation of anisole with acetic anhydride [65].

The catalytic activity of nafion resin in methanol dehydration reaction was presented in the work of Varisli and Dogu [66]. The commercial nafion resin beads (NR-50) were used as catalyst and the methanol dehydration experiments were carried out in vapor phase at atmospheric pressure. The catalytic activity of nafion resin was observed as a function of temperature in the range of 120-220°C. To observe the effect of space time on the methanol conversion and DME yield, the amount of catalyst loaded to the differential reactor was changed from 0.2 g to 1.0. At a space time of 1.35 s.g.cm<sup>-3</sup>, about 0.4 methanol conversion was achieved at 220°C. DME selectivity reached to 1.0 at temperatures over 200°C and the selectivity of the by-product formaldehyde decreased with an increase in temperature.

## CHAPTER 7

### THERMODYNAMIC ANALYSIS

The chemical reaction which occurs during the vapor phase methanol dehydration process is;



In this chapter, theoretical information about the thermodynamic analysis and the results concerning equilibrium curves at different pressures (1 bar and 30 bar) are presented.

To analyse the thermodynamics of this reaction, at first heat capacity,  $C_p$  values were calculated.  $C_p$  is a function of temperature and it is written for one substance in the form;

$$C_{p,i}(T) = a + bT + cT^2 + \dots \quad (2)$$

The molar heat capacity coefficients of the species involved in the methanol dehydration reaction are presented in Table 4.

For the enthalpy of the reaction, the summation of the constants in  $C_p$  equation was used, as it is in equation 3.

$$C_p(T) = \Delta a + \Delta bT + \Delta cT^2 + \dots \quad (3)$$

**Table 4.** The molar heat capacity coefficients of species in the  $C_p = a + bT + cT^2$ ,  
where  $C_p$  is in J/mol.K

Chemical Species	a	b	c
CH <sub>3</sub> OH	19.038	$9.146 \times 10^{-2}$	$-1.218 \times 10^{-5}$
CH <sub>3</sub> OCH <sub>3</sub>	17.249	$18.00 \times 10^{-2}$	$-6.0 \times 10^{-5}$
H <sub>2</sub> O	30.54	$0.79 \times 10^{-2}$	$0.3 \times 10^{-5}$

After finding the heat capacity, calculations for reaction's enthalpy and Gibbs free energy were done. For this reason, enthalpy of formation and Gibbs free energy of formation values were determined for each reactant and product which are listed in Table 5.

**Table 5.** Standard Enthalpies and Gibbs Energies of Formation at 298.15 K  
for one mole of Each Substance from its Elements

Chemical Species	State	$\Delta H_f^\circ$ (kJ/mol)	$\Delta G_f^\circ$ (kJ/mol)
CH <sub>3</sub> OH	gas	-200.7	-162.0
CH <sub>3</sub> OCH <sub>3</sub>	gas	-184.2	-113.0
H <sub>2</sub> O	gas	-241.8	-228.6

And then, for any given temperature, enthalpy of the reaction is calculated from equation 4.

$$\Delta H_{\text{rxn}}(T) = \Delta H_R^\circ + \int (\Delta a + \Delta bT + \Delta cT^2) dT \quad (4)$$

Critical pressures and critical temperatures are needed for equilibrium calculations. Table 6 represents these values for each material.

**Table 6.** Critical temperature (K) and critical pressure (MPa) values for methanol, DME and water vapor.

Chemical species	T <sub>c</sub> (K)	P <sub>c</sub> (MPa)
CH <sub>3</sub> OH	512.6	8.1
CH <sub>3</sub> OCH <sub>3</sub>	400.05	5.35
H <sub>2</sub> O	647.3	22.048

Expressions for the equilibrium constant are determined as equations 5 and 6.

$$K_{298} = \exp(-\Delta G_{298} / RT) \quad (5)$$

$$\ln \frac{K(T)}{K_{298}(298\text{ K})} = \int_{298\text{ K}}^T \frac{\Delta H_{rxn}(T)}{RT^2} dT \quad (6)$$

The equilibrium constant of the reaction was calculated as  $1.212 \times 10^3$  at 298 K using equation 5. The reaction is highly favored for the products side since K is larger than 1. However, considering that the reaction is exothermic, the equilibrium constant is expected to decrease as temperature increases.

In the next step, the equilibrium constant was written considering non-ideal gas behavior and assuming that the solution is ideal.

$$K = K_{f/P} K_P \quad (7)$$

$$K_{f/P} = \frac{(f/P)_{CH_3OCH_3} \times (f/P)_{H_2O}}{(f/P)_{CH_3OH}^2} \quad (8)$$

$$K_P = \frac{(y_{CH_3OCH_3} P) \times (y_{H_2O} P)}{(y_{CH_3OH} P)^2} \quad (9)$$

The  $f/P$  ratios for each species are determined for each temperature value by Peng-Robinson equation. Molar compositions of the species at equilibrium are derived as shown in Table 7. The inlet molar flow rate was taken as 100 mol/hr as basis.

**Table 7.** Flow rates and molar compositions of the species at equilibrium conversion

<b>Component</b>	<b>Initial flow rate (<math>F_{i0}</math>) (mol/hr)</b>	<b>Equilibrium value (<math>F_{ieq}</math>) (mol/hr)</b>	<b>Molar composition at equilibrium (<math>y_i</math>)</b>
CH <sub>3</sub> OH	100	$100(1-x_{eq})$	$100(1-x_{eq})/100$
CH <sub>3</sub> OCH <sub>3</sub>	-	$50x_{eq}$	$50x_{eq}/100$
H <sub>2</sub> O	-	$50x_{eq}$	$50x_{eq}/100$
Total	100	100	

By equating the  $K$  values found from equation 6 to the  $K$  expression in equation 7, equilibrium conversions were calculated at different temperatures up to 600°C by using MATHCAD. Equilibrium conversion versus temperature graph was plotted and equilibrium curve is drawn for two different pressure values, namely 1 bar and 30 bar as shown in Figure 13.

It is clear that the reaction is pressure insensitive. Even if the pressure is changed from atmospheric pressure to 30 bar, there is almost no change in the equilibrium conversion values attained. Therefore, operating the reaction system at pressures higher than the atmospheric pressure would not make a difference in the methanol conversion values that can be reached.

Between 120-400°C, which is the temperature range the catalysts synthesized in this study were tested, the equilibrium conversion is higher than 0.80. Thus, we can conclude that the reaction is not strongly limited by equilibrium constraints.

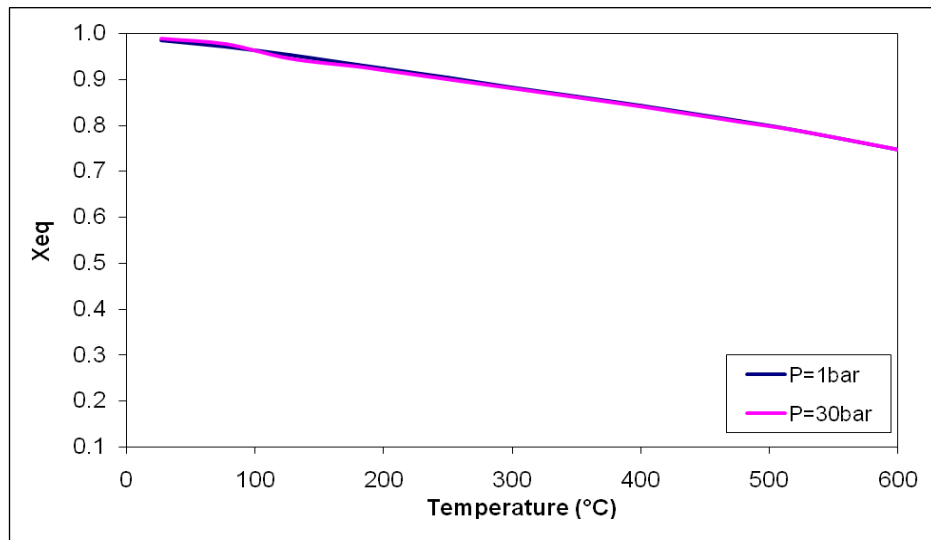


**Figure 13.** The equilibrium curves for methanol dehydration at 1 bar and 30 bars

## CHAPTER 8

### EXPERIMENTAL

In this chapter, experimental studies concerning the synthesis of Silicotungstic acid(STA)/Silica, Tungstophosphoric acid (TPA)/Silica, Nafion/Silica, Nafion/Aluminosilicate and Nafion/ $\alpha$ -Alumina catalysts are explained in detail. The characterization techniques used are described and the experimental set-up where methanol dehydration reaction experiments were carried out is presented.

#### 8.1. SYNTHESIS OF STA/SILICA MESOPOROUS CATALYSTS

STA/SiO<sub>2</sub> catalysts were synthesized by following a one-pot hydrothermal synthesis route. In this route, the synthesis procedure of MCM-41 was applied with some modifications as described by Varisli [25]. The W/Si molar ratio was adjusted to 0.40. The synthesis was carried out under acidic conditions.

The chemical reagents used during the synthesis are listed below.

- *Source of Silica:* TEOS (Tetraethylorthosilicate) C<sub>8</sub>H<sub>20</sub>O<sub>4</sub>Si (Merck)
- *Source of surfactant:* Cetyltrimethylammonium bromide (CTMABr), C<sub>16</sub>H<sub>33</sub>(CH<sub>3</sub>)<sub>3</sub>NBr, (MW 364.46 g/mol, powder, 99% pure, Merck)
- *Source of Solvent:* Deionized water, obtained from Millipore Ultra-Pure Water System (Milli-QPlus)
- *Active Component:* Silicotungstic acid (STA), (Sigma-Aldrich)

The steps followed in the synthesis of STA/Silica catalysts can be summarized as follows.

- **Preparation of the Synthesis Solution:** 13.2 grams of surfactant was dissolved in 87 mL of deionized water and mixed with a magnetic stirrer at 30°C. When a clear mixture was obtained, 15.64 mL TEOS was added. A few minutes later, predetermined amount of silicotungstic acid (STA) dissolved in 5 mL of deionized water was added dropwise to the solution and it was mixed for 1 hour. The pH of the synthesis mixture was measured as 1.0.
- **Hydrothermal Synthesis:** The mixture was transferred into a Teflon bottle which was placed in a stainless steel autoclave. Hydrothermal synthesis was carried out at 120°C for 96 hours.
- **Washing with deionized water:** The material obtained after 96 hours was washed with deionized water and filtered. For each washing step, 300 mL of deionized water was added and the mixture was mixed for about 30 minutes. Filtering and washing of the material was continued until a constant pH value of the residual washing liquid was obtained. The resulting solid material was dried in a vacuum oven at 40°C. After the material was dried, it was obtained as a white block. Since it was not in powder form, it could be crushed into smaller pieces to be used in the reactions in desired size.
- **Calcination:** Calcination was carried out in a quartz tubular reactor placed in a temperature controlled tubular furnace. Dry air was passed over the sample at 350°C for 8 hours with a flow rate of about 1 dm<sup>3</sup>/min. The synthesized catalyst was denoted as TRC-75(L). To compare the effect of calcination temperature, a part of the material was calcined at 400°C and named as TRC-75-400. Alternatively, to see the effect of supercritical carbon dioxide extraction on the activity of the catalyst, to a part of the sample supercritical CO<sub>2</sub> extraction was applied at 350 bar, 100°C for 3 hours with a carbon dioxide flow of 1 mL/min based on the study of Kawi et al. [67]. The experiment was carried out with a SFX 3560 extractor in METU Central Laboratory.

The synthesis procedure of STA/Silica catalysts is illustrated in Figure 14.

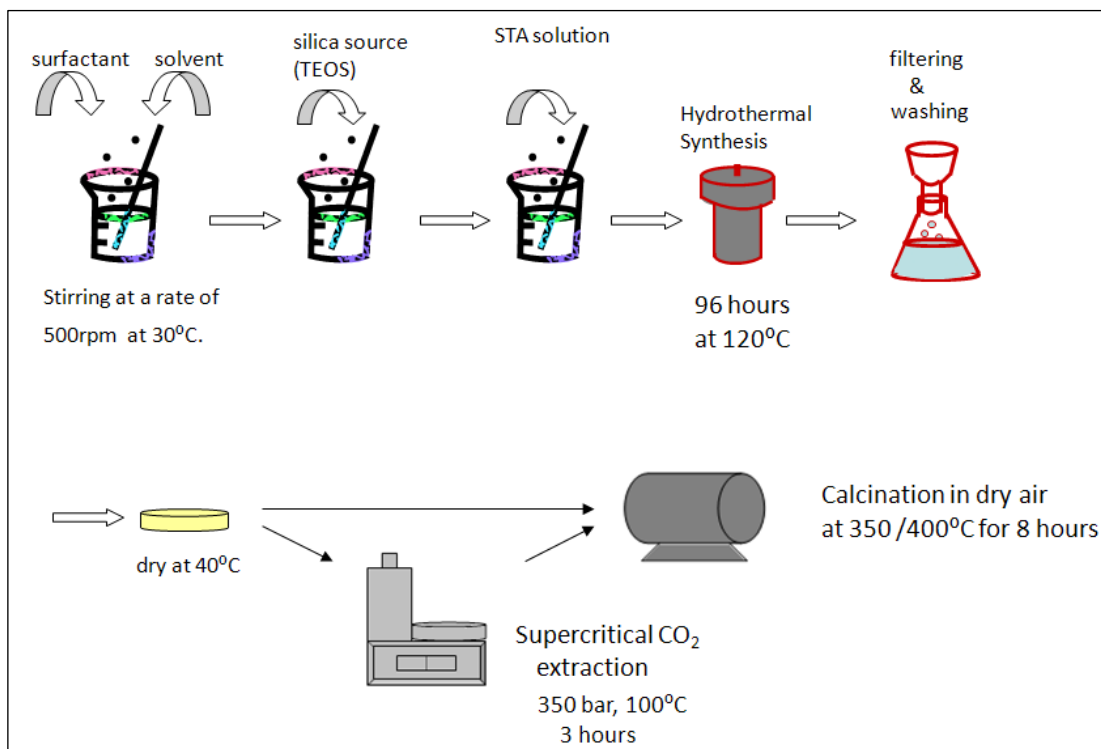


**Figure 14.** Synthesis procedure of STA/Silica catalysts

Depending on the treatments applied to the catalysts, they were denoted by different symbols as shown in Table 8.

**Table 8.** Denotation of the synthesized STA/Silica catalysts

Treatment	Resulting catalyst
Calcination @ 350°C	TRC75-(L)
Calcination @ 400°C	TRC75-400
Supercritical CO <sub>2</sub> extraction and calcination @ 350°C	TRC-75(L)-CO2

## 8.2. SYNTHESIS OF TPA/SILICA MESOPOROUS CATALYSTS

For the synthesis of TPA/SiO<sub>2</sub> catalysts one-pot hydrothermal route was applied. The synthesis procedure developed for these materials is similar to that of the STA/SiO<sub>2</sub> catalysts. The W/Si molar ratio was again adjusted to 0.40.

The chemical reagents used during the synthesis are listed.

- *Source of Silica:* TEOS (Tetraethylorthosilicate) C<sub>8</sub>H<sub>20</sub>O<sub>4</sub>Si (Merck)
- *Source of surfactant:* Cetyltrimethylammonium bromide (CTMABr), C<sub>16</sub>H<sub>33</sub>(CH<sub>3</sub>)<sub>3</sub>NBr, (MW 364.46 g/mol, powder, 99% pure, Merck)
- *Source of Solvent:* Deionized water, obtained from Millipore Ultra-Pure Water System (Milli-QPlus)
- *Active Component:* Tungstophosphoric acid (TPA), (Acros Organics)

The steps applied during the synthesis are similar to those applied for STA/Silica catalysts. The drawing is shown below in Figure 15. The synthesis mixture was quite acidic with a pH below 0.5. The material was again obtained as a white solid block and crushed into smaller pieces prior to calcination.

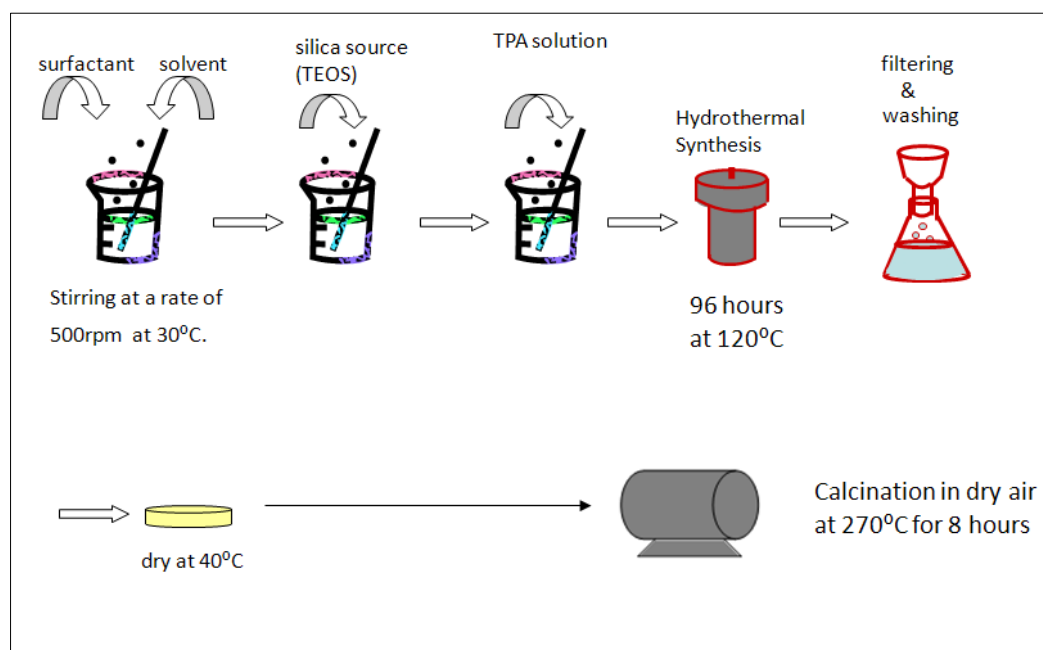


**Figure 15.** Synthesis procedure of TPA/Silica catalysts

Different from the synthesis of STA/Silica catalysts, TPA/Silica catalysts were calcined at 270°C based on the thermogravimetric analysis (TGA) which is discussed later in Section 9.2.1.

### 8.3. SYNTHESIS OF NAFION/SILICA MESOPOROUS CATALYSTS

Novel Nafion/SiO<sub>2</sub> catalysts were synthesized by following a one-pot hydrothermal route.

The chemical reagents used during the synthesis are listed below.

- *Source of Silica:* TEOS (Tetraethylorthosilicate) C<sub>8</sub>H<sub>20</sub>O<sub>4</sub>Si (Merck)
- *Source of surfactant:* Cetyltrimethylammonium bromide (CTMABr), C<sub>16</sub>H<sub>33</sub>(CH<sub>3</sub>)<sub>3</sub>NBr, (MW 364.46 g/mol, powder, 99% pure, Merck)
- *Source of Solvent:* Deionized water, obtained from Millipore Ultra-Pure Water System (Milli-QPlus)
- *Nafion source:* Two different nafion sources were used.
  1. Nafion® 117 solution, ~5% in mixture of lower aliphatic alcohols and water (Fluka). Nafion 117 is the commonly available Nafion film having a nominal thickness of 0.007 in. and EW of 1100.
  2. Nafion perfluorinated ion-exchange resin, 5 wt% in mixture of lower aliphatic alcohols and water (Aldrich)

The studies in literature on supported nafion catalysts (as discussed in Section 6.2) were mainly based on sol-gel synthesis procedure. Direct synthesis was also followed, but either a solution of hexadecyltrimethylammonium bromide and sodium hydroxide or a solution of cetyltrimethylammonium bromide and tetramethylammonium hydroxide were used while preparing the precursor solution. In this study, acidic hydrothermal synthesis procedure was followed since the resulting catalysts are aimed to have strong acid sites for obtaining high catalytic activity in alcohol dehydration reactions. As listed above, a solution of cetyltrimethyl ammonium bromide and deionized water were used as the sources of surfactant and solvent. Furthermore, different conditions and methods were applied in surfactant

removal to compare the effect of alternative routes on the characteristics of the resulting material.

The steps followed in the synthesis of Nafion/Silica catalysts are explained below.

- **Preparation of the Synthesis Solution:** 13.2 grams of surfactant was dissolved in 87 mL of deionized water and mixed on a magnetic stirrer at 30°C. When a clear mixture was obtained, predetermined amount of nafion source was added dropwise to the mixture. A few minutes later, 15.64 mL TEOS was added and the mixture was mixed for 1 hours. For NS1 the pH was measured as 1.6. The pH of NS3 was adjusted to 1.6 by addition of a few drops of 1 N NaOH. The pH values of NS4 and NS5 were found as 0.9 and 0.7, respectively.
- **Hydrothermal Synthesis:** The mixture was transferred into a Teflon bottle placed in a stainless steel autoclave. Hydrothermal synthesis was carried out at 120°C for 96 hours.
- **Washing with deoized water:** The material obtained after 96 hours was washed with deionized water and filtered. For each washing step, 300 mL of deionized water was added and the mixture was mixed for about 30 minutes. The resulting solid material was dried in a vacuum oven at 50°C and before any treatment was applied it was dried at 110°C for 2 hours. After drying, the materials were obtained as one-piece, hard, white solid blocks and were crushed to get smaller pieces.
- **Calcination:** For surfactant removal, the materials were calcined at 350°C based on the thermogravimetric analysis of the samples which is discussed in Section 9.3.1. To compare the effect of temperature, calcination at 250°C was also applied.
- **Washing in Sulfuric Acid Solution of Ethanol (SAE):** As an alternative technique, surfactant removal by washing in sulfuric acid-ethanol (SAE) mixture was applied. Different conditions were used during the washing

procedure. Some of the catalysts were refluxed in 1 M of SAE solution for 12 hours (1 g/ 150 mL solution) based on the study of Fujiwara et al. [54]. In the case of using 2 M of SAE solution, the materials were refluxed for 6 hours. Also keeping in 2 M of SAE solution for 24 hours at room temperature was applied to some part of the catalysts. After treatment with SAE solution, in order to get rid of the remaining sulfuric acid at the surface of the catalysts, the samples were further washed in pure ethanol. Finally, they were dried at 100°C for 8 hours. The synthesis procedure is illustrated in Figure 16. The different types of catalysts synthesized, their nafion sources, nafion loadings and pH of the synthesis mixtures are listed in Table 9. The different treatments applied to the Nafion/Silica catalysts are shown in Table 10.

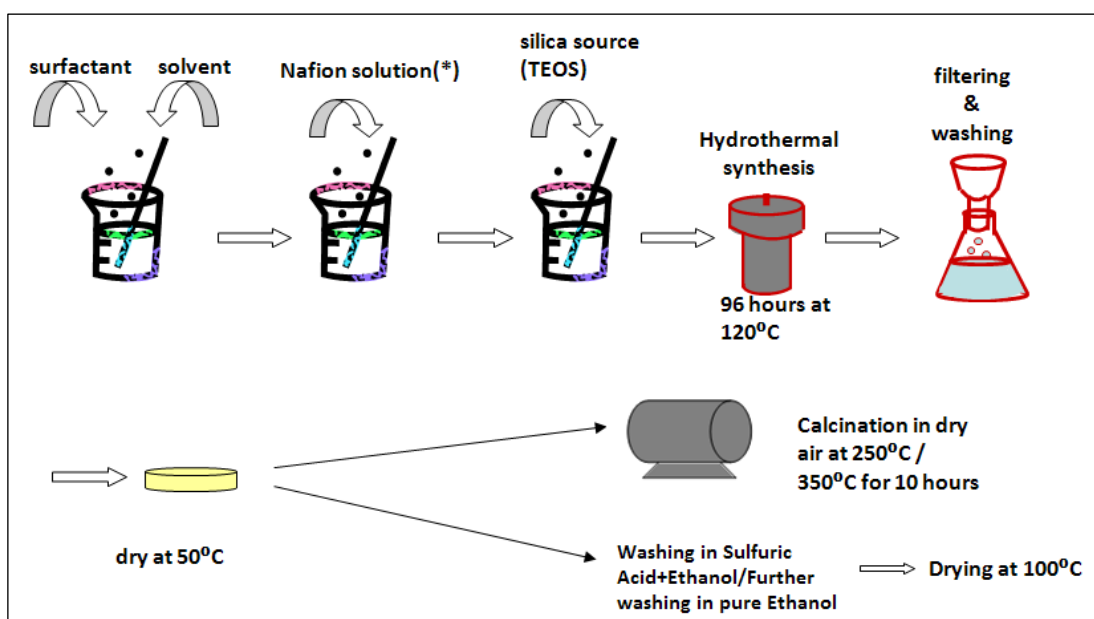


**Figure 16.** Synthesis procedure of the Nafion/Silica catalysts

**Table 9.** The nafion sources, starting Nafion/Silica weight ratios and pH of the synthesis mixtures

Catalyst	Nafion source	Nafion/Silica (wt ratio) in the starting solution	pH
NS1	1 *	0.05	1.6
NS3		0.15	1.6
NS4	2 **	0.15	0.9
NS5		0.25	0.7

\*Nafion® 117 solution, ~5% in mixture of lower aliphatic alcohols and water (Fluka)

\*\*Nafion perfluorinated ion-exchange resin, 5 wt% in mixture of lower aliphatic alcohols and water (Aldrich)

**Table 10.** Applied treatments and the denotation of the samples

Applied to	Treatment	Resulting catalyst
NS1	Calcination @ 350°C	NS1350
	Calcination @ 250°C	NS1250
	Refluxing with 1M SAE for 12 hours + Refluxing with pure EtOH for 12 hours	NS1R
NS3	Refluxing with 1M SAE for 12 hours + Refluxing with pure EtOH for 12 hours	NS3R1
	Refluxing with 2M SAE for 6 hours + Refluxing with pure EtOH for 6 hours	NS3R2
	Keeping in 1M SAE for 24 hours @ RT + Keeping in pure EtOH for 6 hours	NSA
NS4	Refluxing with 2M SAE for 6 hours + Refluxing with pure EtOH for 6 hours	NS4R2
NS5		NS5R2

#### 8.4. SYNTHESIS OF NAFION IMPREGNATED CATALYSTS

By following the impregnation technique, nafion/aluminosilicate and nafion/ $\alpha$ -alumina catalysts were synthesized. As the nafion source, Nafion perfluorinated ion-exchange resin (5 wt% in a mixture of lower aliphatic alcohols and water) purchased from Aldrich was used. Support material, namely aluminosilicate (purchased from Aldrich) or  $\alpha$ -alumina (purchased from Toyo Engineering), was dispersed in ethanol and then appropriate amount of nafion solution was added. The procedure is as shown in Figure 17.

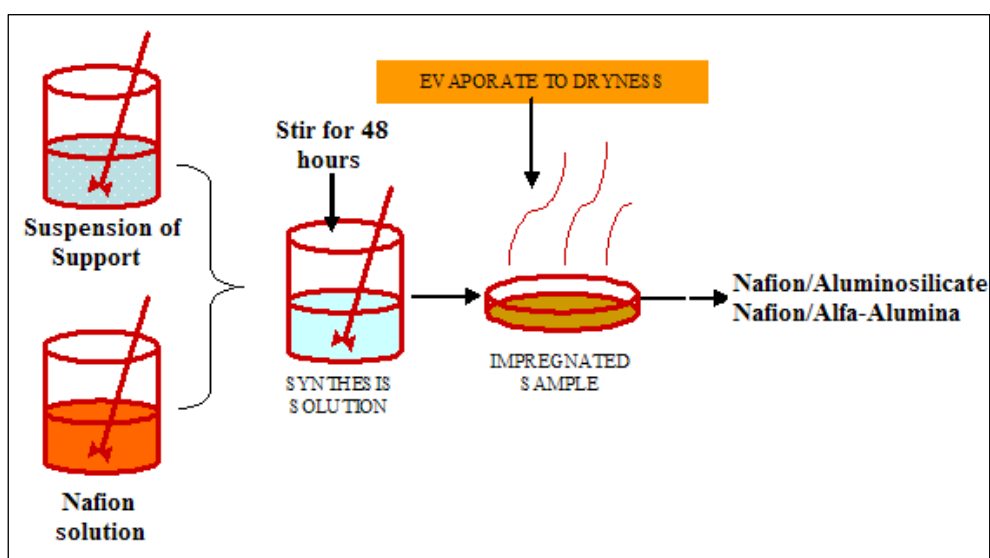


**Figure 17.** Synthesis procedure of nafion impregnated catalysts

The nafion/support ratios in the synthesis solutions are given in Table 11. NFMAS1, NFMAS2 and NFMAS3 are nafion/aluminosilicate catalysts synthesized with nafion/aluminosilicate weight ratios of 0.05, 0.10 and 0.20 respectively. NFALFA1 is a nafion/ $\alpha$ -alumina catalyst synthesized with a nafion/ $\alpha$ -alumina weight ratio of 0.05.

**Table 11.** The nafion impregnated catalysts and their nafion/support starting ratios

Catalyst	Nafion/Support ratio (synthesis soln.)
NFMAS1	0.05
NFMAS2	0.10
NFMAS3	0.20
NFALFA1	0.05

## 8.5. MATERIAL CHARACTERIZATION

The synthesized catalysts were characterized by using various techniques in order to get information about their chemical composition, morphologies, surface areas, pore sizes, nature of the acid sites on their surface, etc. The techniques applied are explained below.

### 8.5.1. X-Ray Diffraction (XRD)

X-Ray diffraction is a method to identify the crystalline phases in a material. Diffraction is a property of crystals that are physically large compared to the wavelength of X-rays. The diffraction pattern of a metal is an identification of the packing structure of its metal phase if the metal is crystalline, in sufficiently large particles and if its diffraction pattern cannot be obscured by the support. A beam of X-rays parallel to each other, with wavelengths of  $\lambda \sim 0.5 - 2 \text{ \AA}$ , is incident on a specimen and it is diffracted by the crystalline phases in the specimen following the Bragg's law,  $\lambda = 2d\sin\theta$  ( $d$  is the spacing between the atomic planes in the crystalline phase). The intensity of the diffracted X-rays measured as a function of the diffraction angle and the specimen's orientation gives a diffraction pattern which is used to identify the crystalline phases of the specimen [68].

XRD is a useful tool to get information about the pore architecture of the porous materials. In order to determine the presence of an MCM-41-like ordered pattern in the porous structure of the synthesized materials, the catalysts were

characterized by X-Ray Diffraction (XRD) analysis in METU Metallurgical and Materials Engineering Department using the Rigaku D/MAX2200 diffractometer with a CuK radiation source with a  $2\theta$  scanning range between  $1^\circ$  and  $50^\circ$ .

### **8.5.2. N<sub>2</sub> Physisorption**

Adsorption techniques are applied to determine the porosity and specific surface area of the catalytic materials. Surface area determination by using nitrogen as the molecular probe is a common technique for measuring the amount of catalyst surface available for interaction with the reactant molecules. Different models have been developed for calculating the pore size distribution such as BET (Brunauer, Emmett, Teller), BJH (Barrett, Joyner, Halenda), etc. [19,68].

Nitrogen adsorption analyses were done by a Quantachrome Autosorb-1-C/MS instrument in the METU Central Laboratory. Before the analyses, the samples were degassed at  $100^\circ\text{C}$  for 16 hours and the analyses were performed at a relative pressure range of  $5 \times 10^{-2}$  to 0.99 at liquid nitrogen temperature. Multipoint BET surface area values, BJH adsorption and desorption pore diameters and pore volumes of the samples were determined by this characterization technique. Nitrogen adsorption and desorption isotherms were plotted and the pore size distributions were determined. Additionally, single point BET surface area analyses were done by using a Quantachrome Autosorb 1C instrument in the Chemical Engineering Department of Gazi University. Before the analyses, degassing was performed at  $140^\circ\text{C}$  for 30 minutes under the flow of N<sub>2</sub>-He gas mixture. Measurements were done at liquid nitrogen temperature (77 K) under the flow of a gas mixture composed of 30% nitrogen and 70% helium.

### **8.5.3. Scanning Electron Microscopy (SEM)**

SEM is an analytical instrument which provides a high magnification imaging of a material. In Scanning Electron Microscopy, an electron beam is focused into a fine probe and scanned over a small rectangular area of the sample. As a result of the interaction between the beam and the sample, various signals are created. These signals are used to modulate the brightness of a cathode ray tube, which is also

scanned with the electron beam at the same time and an image is observed on the screen. This is a highly magnified image with a much greater depth than the traditional microscopic image [19].

Scanning Electron Microscopy (SEM) analyses were done in Middle East Technical University (METU) Central Laboratory by a Quanta 400F Field Emission SEM instrument and in Metallurgical and Materials Engineering Department by using JSM-6400 (JEOL) equipped with NORAN system Six. Samples were coated with gold for the analyses. Morphologies of the materials were observed by this technique.

#### **8.5.4. Energy Dispersive X-Ray Spectroscopy (EDS-EDX)**

The atoms in a material emit characteristic X rays when they are ionized by a high energy radiation. EDS is a technique which is based on the collection and energy dispersion of characteristic X rays. The elements in an EDS unit are a source of high-energy radiation (electrons), a sample, a solid state detector and signal processing electronics. The resulting X-ray spectrum contains a series of peaks which represent the type and relative amount of each element in the sample [68].

Energy Dispersive X-Ray Spectroscopy (EDS) analyses were carried out in METU Metallurgical and Materials Engineering Department by a JSM-6400 (JEOL) instrument equipped with NORAN System Six. Samples were coated with gold before the analyses. Bulk chemical composition of the synthesized materials were determined by EDS.

The dispersion of specific elements on the surface of the catalysts were observed by Energy Dispersive X-Ray (EDX) elemental mapping. The analyses were performed in the Bilkent University Chemistry Department, using a scanning electron (SE) microscope, equipped with an EDX spectrometer. SEM and EDX data were acquired using a Zeiss EVO40 environmental SEM that is equipped with a LaB6 electron gun, a vacuum SE detector, an elevated pressure SE detector, a backscattering electron detector (BSD), and a Bruker AXS XFlash 4010 detector. Samples were prepared by grinding the particles into fine powder and mechanically dispersing them on an electrically conductive carbon film which was placed on an aluminum sample holder. SEM images were obtained using a vacuum SE detector

where electron acceleration voltage of the incident beam was varied within 10-20 kV and the samples were kept at  $\leq 5 \times 10^{-5}$  Torr inside the SEM. EDX data were collected using an electron acceleration voltage of 20 kV and a working distance of 15 mm. EDX revealed the elemental surface distribution of the samples on the order of a few micrometers.

#### **8.5.5. X-Ray Photoelectron Spectroscopy (XPS)**

In XPS, the sample is bombarded with monoenergetic soft X-rays and electrons are ejected. The elements present in the sample are identified from the kinetic energies of the ejected photoelectrons. Also, the chemical states of the elements present can be identified from the small variations in the determined kinetic energies. The measured photoelectron intensities gives information about the relative concentrations of the elements. XPS is useful in determining the elemental and chemical state compositions in the top 30 Å [68].

In order to get information about the surface composition of the materials, XPS analyses were done with the SPECS EA-200 instrument in the METU Central Laboratory by using Al as the X-ray anode, with an excitation power of 260 W, step size of 0.10 eV, dwell time of 1 s and pass energy of 96 eV.

#### **8.5.6. Fourier Transform Infrared Spectroscopy (FTIR)**

The use of FTIR as a characterization technique is based on the vibrational frequencies of the chemical bonds. The vibrational motions of the chemical bonds in a material have frequencies in the infrared regime. In the infrared technique, the intensity of a beam of infrared radiation is measured before ( $I_0$ ) and after ( $I$ ) its interaction with the sample as a function of light frequency. The plot of  $I/I_0$  versus frequency is the “infrared spectrum”. By using FTIR, information about the identities, surrounding environments, and concentrations of the chemical bonds in the material can be obtained [68].

Fourier Transform Infrared Spectroscopy analyses of the HPA/Silica catalysts were done by a Bruker FTIR-IFS66/S instrument in METU Central Laboratory. The

samples were grinded and mixed with KBr (1 mg sample, 300 mg KBr) and pressed to obtain pellets. The chemical bonds present in the structure of the materials were identified by this analysis technique.

#### **8.5.7. Thermal Analyses (TGA-DTA)**

In thermal analyses the sample is exposed to a gaseous environment and the temperature is increased with time. The response of the system is monitored by measuring the sample weight change by thermogravimetric analysis (TGA) and by measuring the change in temperature for constant heating by differential thermal analysis (DTA) [68].

Thermal analyses (TGA and DTA) of the synthesized materials were done by the Dupont 951 thermal analyses system found in the METU Chemical Engineering Department by passing air over the samples. The analyses were carried out by increasing the temperature of the samples from room temperature to 600°C with a heating rate of 10°C/min. This technique gave information for the selection of the calcination temperature of the HPA/Silica materials. Results of the thermogravimetric analyses were also used to determine the nafion content in the Nafion/Silica catalysts.

#### **8.5.8. Diffuse Reflectance Infrared Fourier Transform Spectroscopy (DRIFTS) of Pyridine Adsorption**

DRIFTS of pyridine adsorption is a technique to determine the nature of acid sites on a catalyst. The synthesized materials were dried at 110°C for 16 hours and then 1 mL of pyridine was adsorbed on them. Samples were prepared by mixing 0.035 g of the pyridine adsorbed or fresh catalysts with 0.07 g KBr. A reference spectrum was recorded with KBr. For the acid site determination, the spectra of the clean samples were subtracted from the spectra of the pyridine adsorbed samples.

DRIFTS analyses of pyridine adsorption were carried out by using a Perkin Elmer Spectrum One instrument in the Kinetic Laboratory in METU Chemical Engineering Department in order to get information about the Brønsted and Lewis acid sites of the synthesized catalysts.

## 8.6. EXPERIMENTAL SET-UP OF THE METHANOL DEHYDRATION REACTION SYSTEM

The vapor phase methanol dehydration reaction was carried out in a fixed bed flow reactor system. Helium was used as the carrier gas and also as the reference gas for the gas chromatograph. Liquid methanol was fed through a syringe pump to an evaporator where it was mixed with helium. Gaseous methanol and helium were fed to a stainless steel differential reactor (1/4 in.) placed in a temperature controlled tubular furnace. The catalyst was placed in the middle of the stainless steel reactor and fixed by quartz wool. Flow rate of helium and the total flow rate were 23 ml/min and 44.42 ml/min, respectively. The ratio of the volumetric flow rate of methanol to the total volumetric flow rate in the system was adjusted as 0.48. The products and the unreacted gases were analyzed on-line by a Varian CP 3800 GC equipped with Porapak T and a thermal conductivity detector (TCD). The TCD detector and the gas sampling valve were heated to 225°C and 200°C, respectively. A temperature ramped-program was used in order to separate the species involved in the reaction. The column was heated to 75°C and it was held at this temperature for 2 minutes. Then the temperature was increased to 170°C with a ramp of 10°C/min and held there for 3 minutes. The connection lines were kept at 150°C in order to avoid any condensation of the reactants or products. After finishing each experiment, the whole system was purged with helium for 1 hour. The drawing of the experimental set-up is shown in Figure 18. GC calibration factors and the retention times of the species involved in the reaction are presented in Appendix A.1. Calculations for the flow rates of methanol and helium are given in Appendix A.2 and the equations derived for methanol conversion, product selectivities and yields are shown in Appendix A.3.

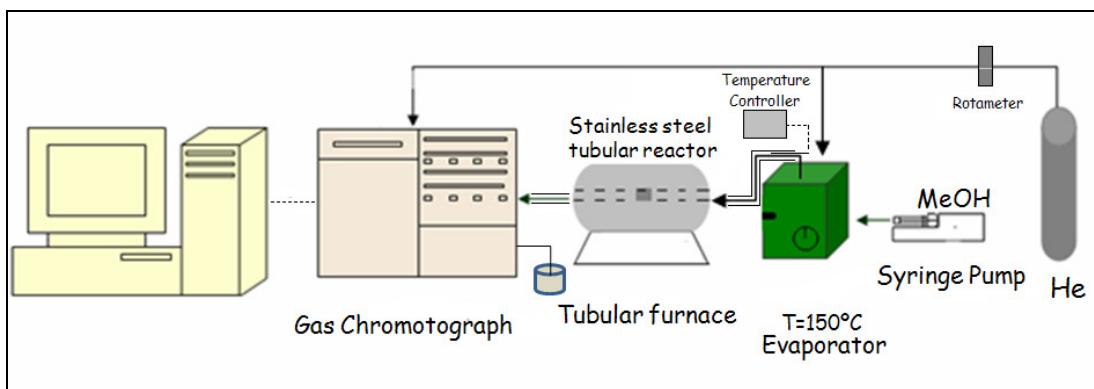


**Figure 18.** Experimental set-up of the methanol dehydration reaction system

The kinetic experiments were carried out at different temperature ranges depending on the type of the catalyst tested. The activities of the STA/Silica catalysts were tested at 180°C-350°C and the TPA/Silica catalysts were tested at 180-250°C. Depending on the decomposition temperature of the heteropolyacid phase, conducting the experiments at higher temperatures was avoided. The experiments with the Nafion/Silica catalysts were carried out at 120-300°C since nafion containing catalysts are expected to be catalytically active at low temperatures also. In order to distinguish between the effect of the support and the nafion resin on the catalytic activity, Nafion/Aluminosilicate and Nafion/ $\alpha$ -Alumina catalysts were tested at a wide temperature range, namely at 120-400 and 180-400°C, respectively.

Space time, calculated by dividing the mass of the catalyst put in the reactor by the total volumetric flow rate in the system (44.42 ml/min), was adjusted to 0.27 s.g.cm<sup>-3</sup>. For some of the catalysts, the effect of space time was also investigated by changing the mass of the catalyst put in the reactor system. All the conditions in the reaction experiments are listed in Table 12.

At least three successive data points were taken at each temperature and the average of these data points was used in the evaluation of conversion, selectivity and yield. Results of a blank test carried out in the absence of catalyst indicated that there was no non-catalytic dehydration of methanol at these reaction conditions.

**Table 12.** The catalysts and the conditions used in the activity tests

Catalyst		Amount of catalyst (g)	Space time (s.g.cm <sup>-3</sup> )	Temperature interval (°C)
STA/SiO <sub>2</sub>	TRC-62(L)*	0.2	0.27	180-350
	TRC-82(L)*	0.2	0.27	180-350
	TRC-92(L)*	0.2	0.27	180-350
	TRC-75(L)	0.1	0.14	180-350
	TRC-75(L)	0.2	0.27	180-350
	TRC-75(L)	0.3	0.41	180-350
	TRC-75-400	0.2	0.27	180-350
	TRC-75(L)-CO <sub>2</sub>	0.2	0.27	180-350
	STAMAS*	0.2	0.27	180-350
TPA/SiO <sub>2</sub>	TPA-75(L)	0.2	0.27	180-250
Nafion/SiO <sub>2</sub>	NS1	0.2	0.27	120-300
	NS1R	0.2	0.27	120-300
	NS1350	0.2	0.27	120-300
	NS1250	0.2	0.27	120-300
	NS2350	0.2	0.27	120-300
	NS3R1	0.2	0.27	120-300
	NS3R2	0.2	0.27	120-300
	NS3A	0.2	0.27	120-300
	NS4R2	0.2	0.27	120-300
	NS5R2	0.2	0.27	120-300
Nafion/Al <sub>2</sub> O <sub>3</sub> -SiO <sub>2</sub>	NFMAS1	0.2	0.27	120-400
	NFMAS2	0.2	0.27	120-400
	NFMAS3	0.2	0.27	120-400
Nafion/ $\alpha$ -Alumina	NFALFA1	0.2	0.27	180-400
Stability Tests (for 6-8 hours)	TRC-75(L)	0.2	0.27	200°C
	TRC-75(L)	0.2	0.27	250°C
	STAMAS*	0.2	0.27	250°C
	TRC-75(L) deactivated at 250°C and re-calcined at 350°C	0.2	0.27	250°C
	NS1	0.2	0.27	350°C
	NS4R2	0.2	0.27	300°C

\*Synthesized by Varisli [25]

## CHAPTER 9

### RESULTS AND DISCUSSION

#### 9.1. CHARACTERIZATION OF STA/SILICA CATALYSTS

##### 9.1.1. X-Ray Diffraction (XRD)

The X-ray diffraction patterns of the STA/Silica catalysts synthesized by taking the W/Si molar ratios as 0.4 are shown in Figure 19. From 1°-10°, diffraction peaks belonging to the 100 plane of MCM-41 and its reflections are observed but there is a significant loss in the sharpness of the peaks when compared with the XRD pattern of pure MCM-41. These patterns imply the existence of a mesoporous structure but it is clear that the MCM-41 structure was destructed and the catalysts are rather amorphous. No peak was observed related to the presence of  $WO_x$  in the structure of the catalysts synthesized in the present study, which suggest that the new STA/Silica catalysts have well-dispersed structures. The XRD patterns of the previously synthesized STA/Silica catalysts (TRC-62(L), TRC-82(L) and TRC-92(L)) by Varisli [25] on the other hand, showed the presence of sharp peaks corresponding to  $W_{20}O_{58}$  dispersed within the mesoporous silicate matrix of the materials.

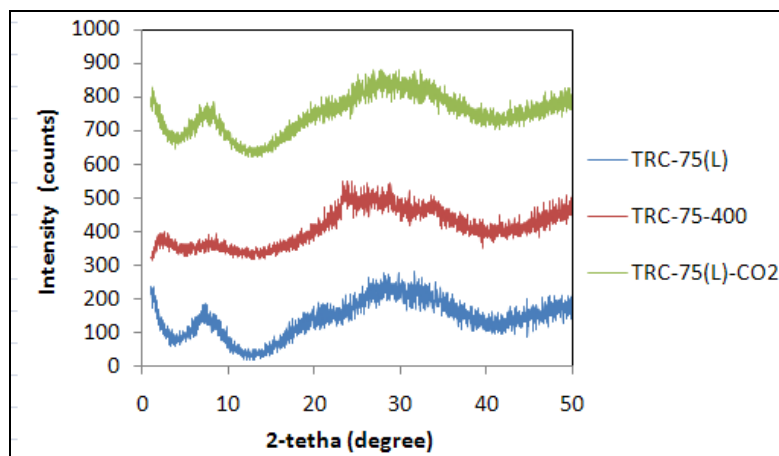


**Figure 19.** XRD patterns of STA/Silica catalysts

The difference between the XRD patterns of the new catalysts (TRC-75(L), TRC-75-400 and TRC-75(L)-CO<sub>2</sub>) and the former ones (TRC-62(L), TRC-82(L) and TRC-92(L)) is thought to be due to the modification of the hydrothermal synthesis procedure. In the present study, the synthesis of the new catalysts was achieved in a fully sealed autoclave, while in the previous synthesis procedure the material had been allowed to be in touch with air at atmospheric pressure, during the synthesis step. XRD results (Figure 19) indicated well dispersion of tungsten in the silicate lattice.

### 9.1.2. Energy Dispersive Spectroscopy (EDS)

The results of EDS analyses are shown in Table 13. The results indicate that STA was successfully incorporated into the structure of the catalysts. In the synthesis solution, W/Si ratio was adjusted as 0.40 and finally after calcination the catalyst used in the reaction (TRC-75(L)) was found to contain a W/Si ratio of 0.33, which means that STA was only slightly lost from the catalyst during the washing and calcination steps and most of it was preserved in the structure of the material.

**Table 13.** EDS results of the STA/Silica catalysts

Catalyst	W/Si atomic ratio EDS	W/Si atomic ratio Soln.
TRC-75(L)	0.33	0.40
TRC-75(L)-CO <sub>2</sub>	0.33	0.40

### 9.1.3. Scanning Electron Microscopy (SEM)

Morphologies of the samples were observed by SEM analyses. In Figures 20 and 21, SEM photographs of the catalyst calcined at 350°C are shown. From Figure 20, the average particle size of the STA/Silica catalyst was determined as 90 µm. In the 1500 times magnified image of the material (Figure 21), agglomerated sites can be observed on the surface of the catalyst. In Figure 22, SEM image of the catalyst calcined at 400°C is presented. Here at a magnification level of 100000, formation of rod-like structures on the surface of the catalyst can be clearly observed. Such a structure was also observed by Varisli [48] in a catalyst containing a W/Si ratio of 0.47. In that work it was concluded that these rod-like structures have a tungsten oxide structure.

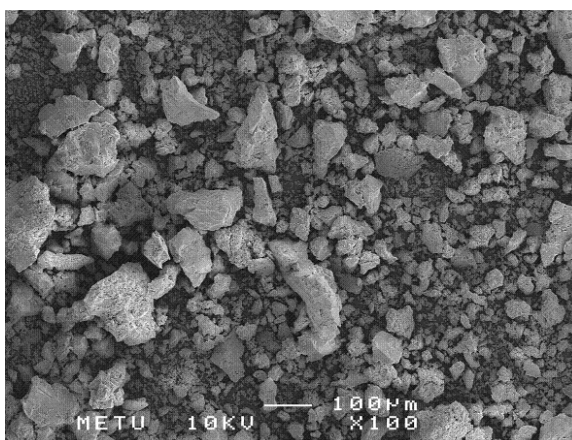


**Figure 20.** SEM image of TRC-75(L)

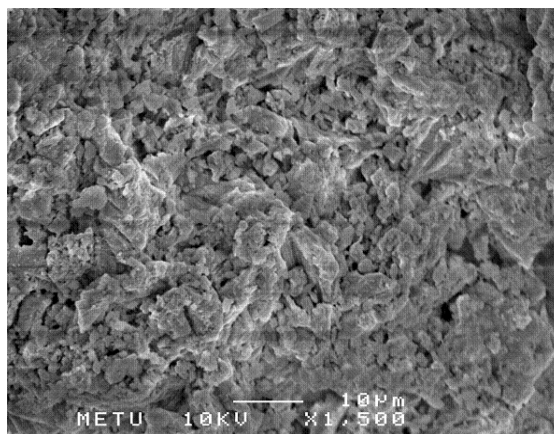


**Figure 21.** SEM image of TRC-75(L)

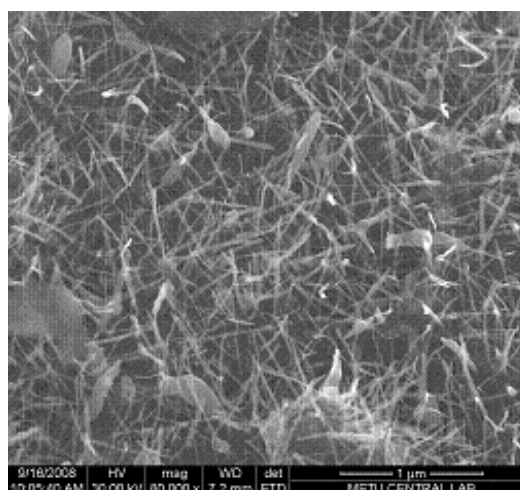


**Figure 22.** SEM image of TRC-75-400

#### **9.1.4. Energy Dispersive X-Ray Spectroscopy (EDX)**

The elemental mapping analyses of the catalysts are presented in Figures 23 and 24. The images show EDX mapping of single catalyst particles. It is observed that W (shown in red) and Si (shown in yellow) are very well dispersed in the structure of the STA/Silica catalysts synthesized by following a one-pot hydrothermal procedure. The even distribution of W in the porous network of silica

proves the success of the synthesis method in obtaining STA incorporated silica supported catalysts.

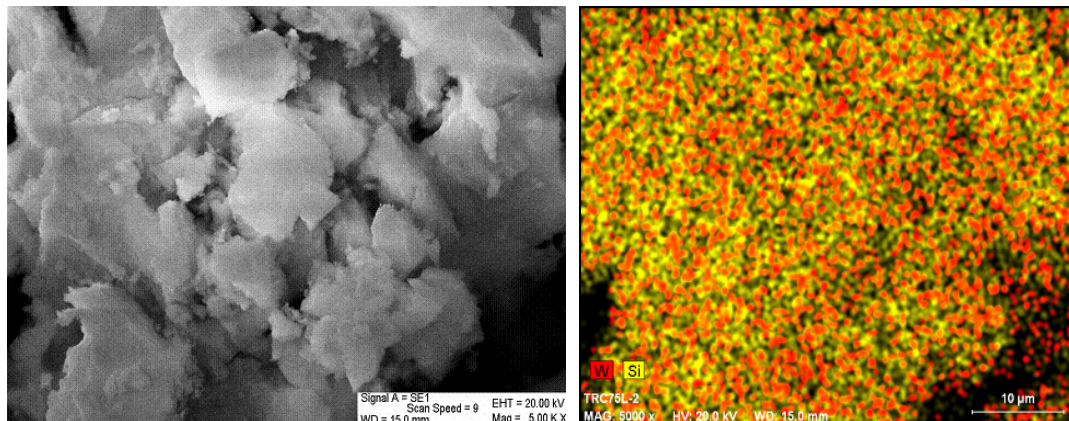


**Figure 23.** EDX elemental mapping analysis of TRC-75(L)

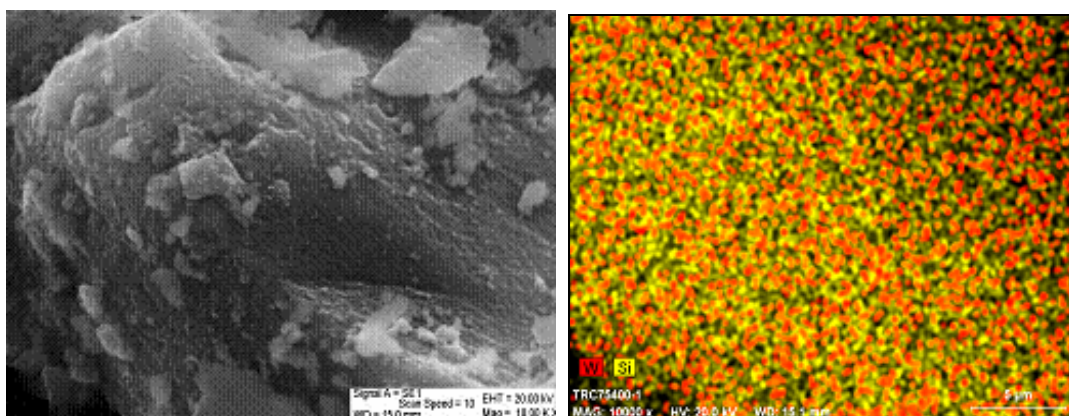


**Figure 24.** EDX elemental mapping analysis of TRC-75-400

### 9.1.5. Nitrogen Physisorption

The nitrogen physisorption analyses gave information about the multipoint BET surface areas, pore volumes and average pore diameters of the catalysts. The results obtained are shown in Table 14.

**Table 14.** Physical properties of the STA/Silica catalysts

Catalyst	W/Si atomic ratio EDS	Multipoint BET Surface Area (m <sup>2</sup> /g)	BJH Des. Pore volume (cm <sup>3</sup> /g)	BJH Des. Avg pore diameter (nm)
TRC-75(L)	0.33	252	0.37	7.8
TRC-75(L)-CO <sub>2</sub>	0.33	187	0.32	7.8
TRC-75-400		241	0.47	7.8
TRC-62(L) *	0.16	393	0.55	5.5
TRC-82(L) *	0.47	179	0.45	10.0
TRC-92(L) *	0.78	108	0.21	7.8

(\*) Adapted from Varisli [25]

The pore volumes of the catalysts are found to be between 0.37-0.47 cm<sup>3</sup>/g and their pore diameters are 7.8 nm. The multipoint BET surface areas of the catalysts are found to be between 187-252 m<sup>2</sup>/g. When considered together with the previously synthesized STA/Silica catalysts, it is concluded that as the W/Si ratios increase the multipoint BET surface areas of the catalysts decrease because of the increasing STA content at the surface of the catalyst. The nitrogen adsorption-desorption isotherms of the catalysts are Type IVa according to IUPAC classification, indicating the mesoporous structure of the materials as shown in Figure 25. Formation of a hysteresis loop was observed and it was classified as a Type H1 loop. Hysteresis formation is related to capillary pore condensation and it results from the differences between the adsorption and desorption mechanisms. During adsorption, pores are filled from the wall inward. On the other hand, in the course of desorption the liquid evaporates from the pore opening.

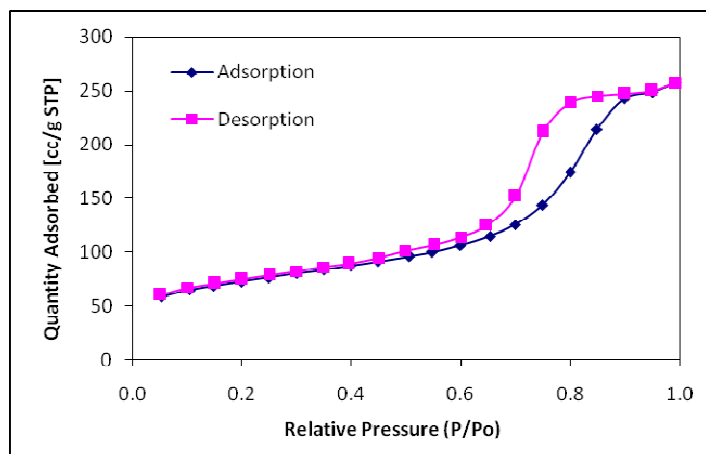


**Figure 25.** Nitrogen adsorption-desorption isotherm of TRC-75(L)

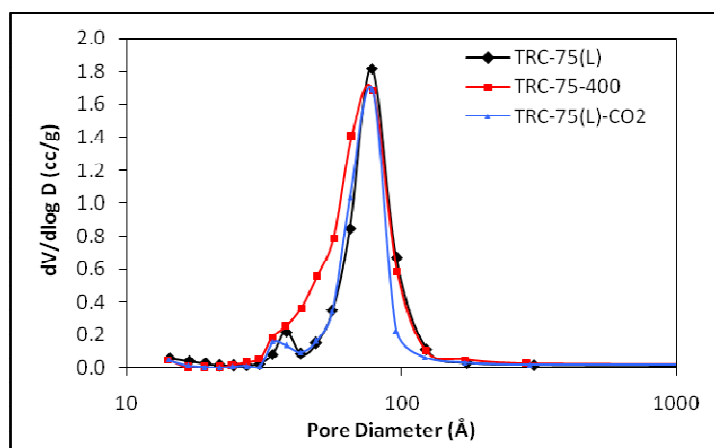


**Figure 26.** Pore size distributions of the STA/Silica catalysts

The pore size distributions are presented in Figure 26. This figure showed that these materials have quite narrow pore size distributions. Above 400°C, protons of STA were reported to be lost and decomposition of the synthesized material started [48]. When the pore volumes of TRC-75(L) and TRC-75-400 are compared, it can be seen that calcination at 400°C also caused an increase in the porosity of the material. Besides, the catalyst calcined at 400°C seems to have a wider peak at 7.8 nm than the one calcined at 350°C.

### 9.1.6. Fourier Transform Infrared Spectroscopy (FTIR)

FTIR spectrum of pure STA (adapted from Varisli et al. [48]) showed the characteristic IR peaks at  $780\text{ cm}^{-1}$  (W-O-W),  $876\text{ cm}^{-1}$  (W-O<sub>corner</sub>-W),  $921\text{ cm}^{-1}$  (Si-O) and  $977\text{ cm}^{-1}$  (W=O). The presence of the same bands is observed in the FTIR spectrum of TRC-75(L) as shown in Figure 27. Except for the band corresponding to W-O<sub>corner</sub>-W, the other bands were equally sharp. These results indicated that the STA structure was not significantly distorted within the lattice of the synthesized materials. The broad band at about  $1060\text{ cm}^{-1}$  with a shoulder at  $1200\text{ cm}^{-1}$  corresponds to Si-O-Si.

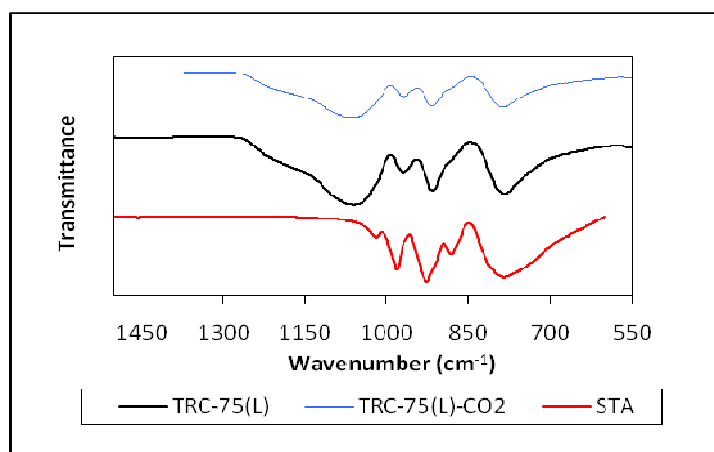


**Figure 27.** FTIR spectra of STA/Silica catalysts and pure STA

### 9.1.7. DRIFTS of Pyridine Adsorbed Samples

Pyridine adsorbed samples gave IR absorption bands at  $1539$ ,  $1488$  and  $1445\text{ cm}^{-1}$  (Figure 28). The first band at  $1539\text{ cm}^{-1}$  corresponds to pyridinium ion adsorbed on the Brønsted acid sites on the catalyst surface. The second band is associated with both the Brønsted and Lewis acid sites. The third band belongs to the adsorbed molecules on the Lewis acid sites [69]. All these bands were observed for TRC-75(L), however it is clear that Brønsted acid sites are much stronger than Lewis acid

sites. In the case of the material prepared with supercritical CO<sub>2</sub> extraction, the relative intensity of the Brønsted acid sites is even stronger. Presence of Brønsted acid sites is the major indication of the catalytic activities of these catalysts for alcohol dehydration reactions.

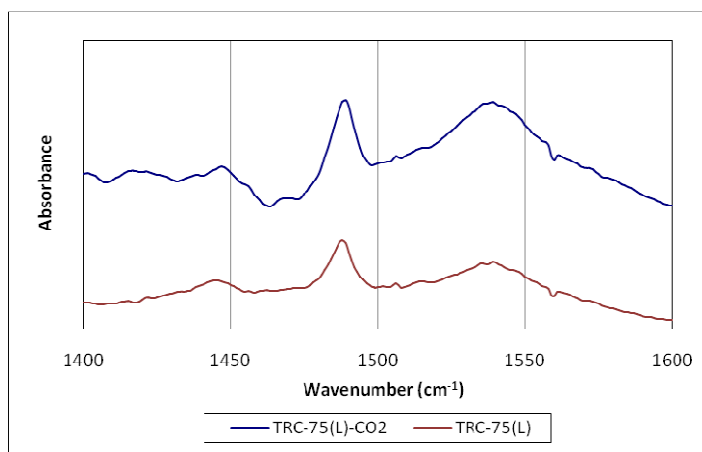


**Figure 28.** DRIFTS spectra of the STA/Silica catalysts

## 9.2. CHARACTERIZATION OF TPA/SILICA CATALYSTS

### 9.2.1. Thermal Analyses (TGA-DTA)

The result of the thermal analysis of the uncalcined TPA/Silica catalyst is shown in Figure 29. It was observed that over 300°C, TPA structure started to decompose based on the presence of two sharp peaks at 378°C and 493°C on the DTA curve. The major weight loss between 200-300°C corresponds to the removal of surfactant. Based on this result, the material was calcined at 270°C in dry air.

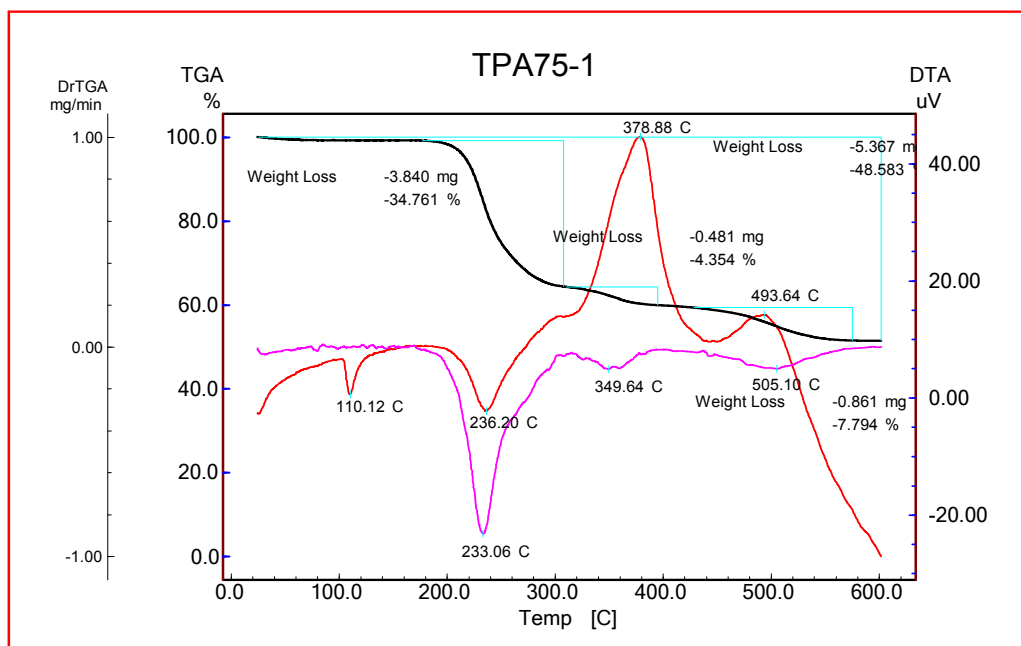


**Figure 29.** TGA-DTA analysis of TPA-75(L)

### 9.2.2. X-Ray Diffraction (XRD)

The XRD pattern of the calcined TPA/Silica catalyst (TPA-75(L)) is shown in Figure 30.

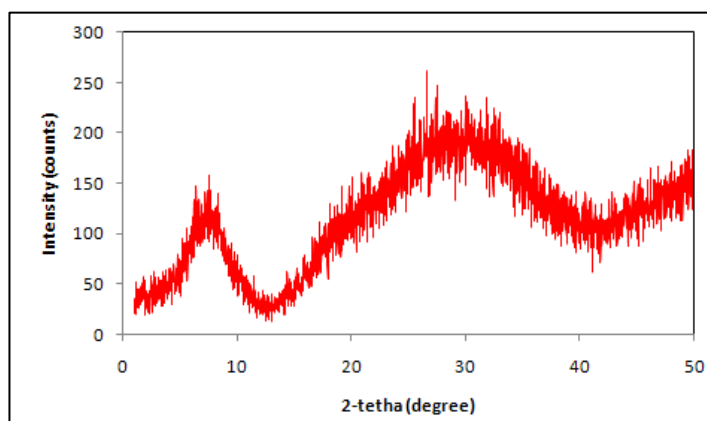


**Figure 30.** X-ray diffraction pattern of TPA-75(L)

Similar to TRC-75(L), TPA-75(L) is also amorphous with a rather destructed mesoporous framework and a well-dispersed structure.

### 9.2.3. Energy Dispersive Spectroscopy (EDS)

TPA-75(L) was prepared by taking the same W/Si molar ratio of 0.40 in the synthesis solution as TRC-75(L) in order to compare the effect of TPA and STA as the active phase on the characteristics and catalytic activity of the resulting silicate structured catalyst. The comparison of the W/Si ratios for TPA-75(L) and TRC-75(L) are shown in Table 15. The EDS results show that TPA-75(L) has a higher W/Si ratio (0.52). Therefore, it can be concluded that when TPA is used as the active phase, it better incorporates into the material.

**Table 15.** The comparison of the EDS results of TPA-75(L) and TRC-75(L)

Catalyst	Active Phase	W/Si atomic ratio EDS	W/Si atomic ratio Soln.
TPA-75(L)	TPA	0.52	0.40
TRC-75(L)	STA	0.33	0.40

### 9.2.4. Scanning Electron Microscopy (SEM)

SEM images of TPA-75(L) are presented in Figures 31 and 32. From Figure 31, the average particle size of the catalyst was determined as 110  $\mu\text{m}$ .

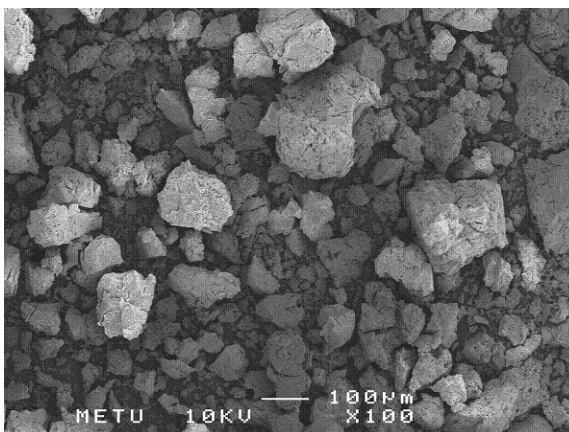


**Figure 31.** SEM image of TPA-75(L)

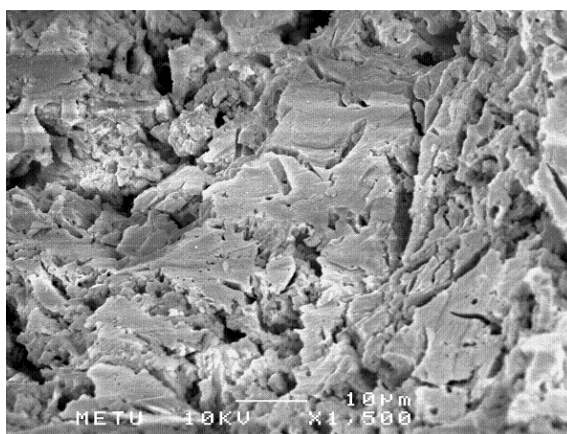


**Figure 32.** SEM image of TPA-75(L)

### 9.2.5. Nitrogen Physisorption

The Multipoint BET surface area, pore volume and pore diameter of the samples were characterized by N<sub>2</sub> physisorption (Table 16). When compared with the STA/Silica catalyst, TPA/Silica has a lower multipoint BET surface area (143 m<sup>2</sup>/g), and a smaller pore volume (0.23 cm<sup>3</sup>/g) with narrower pores (5.6 nm). This supports our previous conclusion that when TPA is used as the active phase it seems to incorporate better than STA into the silicate network.

**Table 16.** Physical properties of TPA-75(L) and TRC-75(L)

Catalyst	Active Phase	Multipoint BET Surface Area ( $\text{m}^2/\text{g}$ )	BJH Des. Pore volume ( $\text{cm}^3/\text{g}$ )	BJH Des. Avg pore diameter (nm)
TPA-75(L)	TPA	143	0.23	5.6
TRC-75(L)	STA	252	0.37	7.8

The nitrogen adsorption-desorption isotherm of TPA-75(L) is Type IVa (Figure 33). Its pore size distribution is shown in Figure 34.

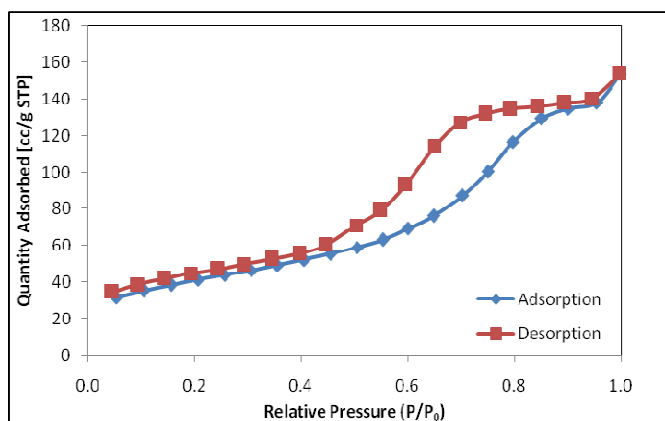


**Figure 33.** Nitrogen adsorption-desorption isotherm of TPA-75(L)

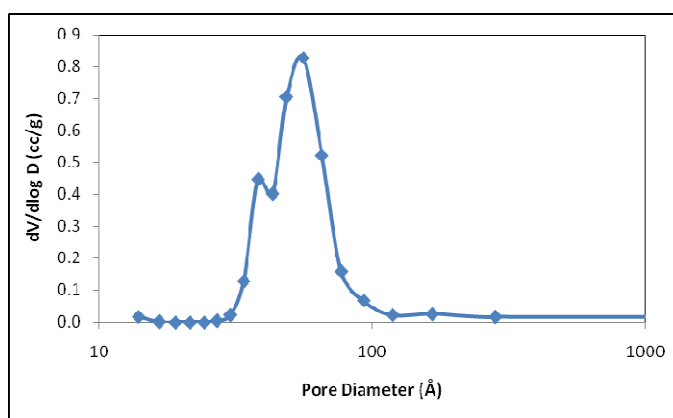


**Figure 34.** Pore size distribution of TPA-75(L)

### 9.2.6. Fourier Transform Infrared Spectroscopy (FTIR)

The FTIR spectra of pure TPA and the TPA-75(L) catalyst are given together in Figure 35. The pure TPA showed IR peaks at 1080, 981, 889, 796, 594, 522  $\text{cm}^{-1}$ . The first five bands are due to the stretching vibrations P-O<sub>a</sub>, W-O<sub>d</sub>, W-O<sub>b</sub>-W, W-O<sub>c</sub>-W, and to the bending vibration O<sub>a</sub>-P-O<sub>a</sub>, respectively. The subscripts signify oxygen bridging the W and the heteroatom (a), corner-sharing (b) and edge-sharing oxygen(c) belonging to octahedral WO<sub>6</sub> and terminal oxygen (d) [47].

The peaks belonging to the pure TPA were observed in the case of TPA-75(L) but there seems to be a decrease in their intensities, which imply some distortion of the TPA phase in the lattice of the material. The broad band at about 1075  $\text{cm}^{-1}$  with a shoulder at 1200  $\text{cm}^{-1}$  corresponds to Si-O-Si.

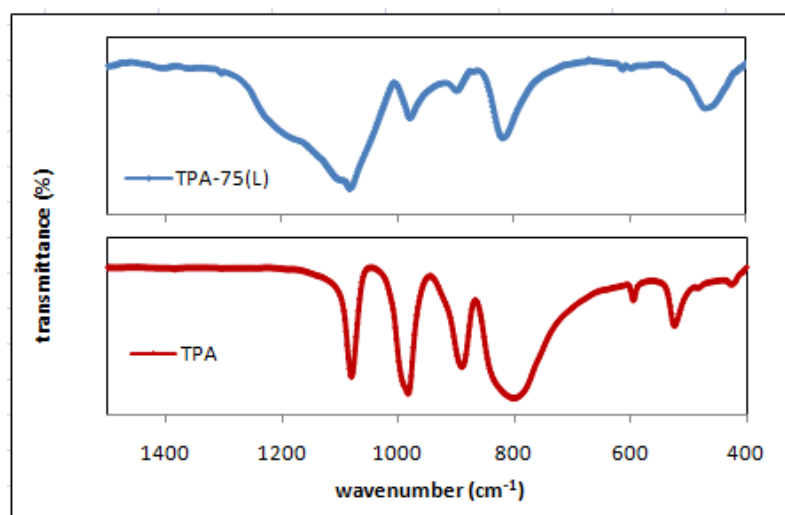


**Figure 35.** FTIR spectra of pure TPA and TPA-75(L)

### 9.2.7. DRIFTS of Pyridine Adsorbed Samples

Pyridine adsorbed samples gave two distinct IR absorption bands at 1537 and 1488  $\text{cm}^{-1}$  (Figure 36). The broad band at 1442  $\text{cm}^{-1}$ , which belonged to pyridinium ion adsorbed on the Lewis acid sites, was observed to be quite low in intensity.

Similar to the STA/Silica catalysts, this TPA/Silica catalyst has a very intense peak corresponding to the Brønsted acid sites ( $1537\text{ cm}^{-1}$ ), which is the major indication for the dehydration efficiency of this catalyst.

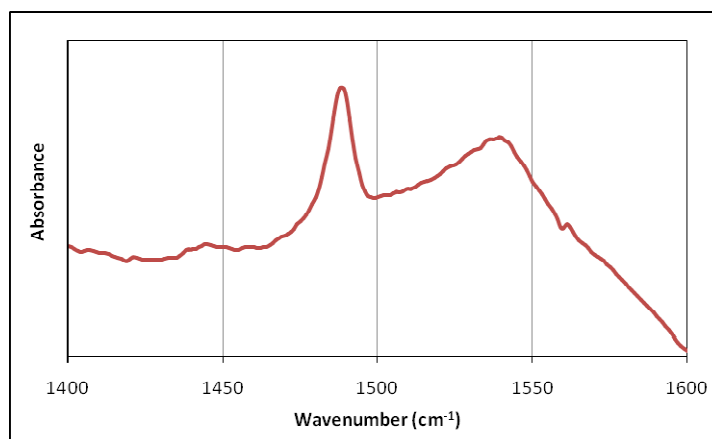


**Figure 36.** DRIFTS spectra of TPA-75(L)

### 9.3. CHARACTERIZATION OF NAFION/SILICA CATALYSTS

#### 9.3.1. Thermal Analyses (TGA-DTA)

The thermogravimetric analyses were conducted between room temperature and  $600^{\circ}\text{C}$  with flow of dry air. The result belonging to one of the Nafion/Silica nanocomposites (NS3) after washing several times with deionized water is shown in Figure 37.

The first weight loss between room temperature and  $100^{\circ}\text{C}$  corresponds to the water evaporated from the material. The second weight loss belongs to the surfactant (cetlytrimethyl ammonium bromide) decomposed and left from the structure between  $200^{\circ}\text{C}$  to about  $350\text{-}400^{\circ}\text{C}$ . The final weight loss in the perfluorocarbon region (from  $400^{\circ}\text{C}$  to  $550\text{-}600^{\circ}\text{C}$ ) signify the decomposition of nafion resin which was also stated by Harmer et al. [50]. The nafion contents of the catalysts were calculated from TGA analyses by ignoring the weight of water evaporated and the surfactant. The results

are shown in Table 17. They all show that nafion was successfully incorporated into the materials.

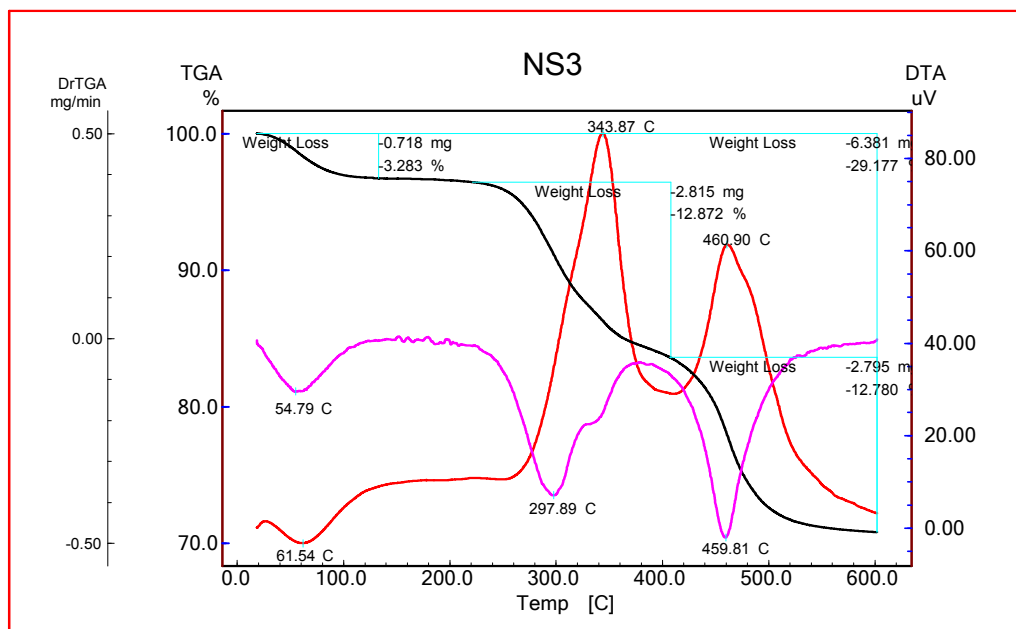


**Figure 37.** TGA-DTA analysis of NS3

**Table 17.** Starting nafion/silica ratios of the catalysts and their nafion contents

Catalyst	Nafion/Silica (wt ratio) in the starting solution	Nafion wt% in the nanocomposite (TGA results)
NS1	0.05	5.0
NS3	0.15	15.2
NS4	0.15	16.8
NS5	0.25	23.0

### 9.3.2. X-Ray Diffraction (XRD)

The X-ray diffraction pattern of the Nafion/Silica catalyst containing 5% nafion in its structure (NS1) is shown in Figure 38. XRD patterns of this catalyst after calcination at 350°C (NS1350) and after refluxing with sulfuric acid solution of ethanol (NS1R) are also illustrated. The sharp peaks at about 1° indicate the presence of the mesoporous structure in the catalysts. These peaks result from the MCM-like structure but the absence of the reflection peaks between 1°-10° show that the MCM-structure has collapsed and the materials do not have an ordered MCM-41 form. Alvaro et al. [58] had also observed the destruction of the ordered mesoporous structure by incorporation of more than 2wt% perfluoralkyl sulfonic acid groups into MCM-41. The broad peaks between 20°-30° in the X-ray diffraction patterns of NS1, NS1350 and NS1R belong to the amorphous silica.

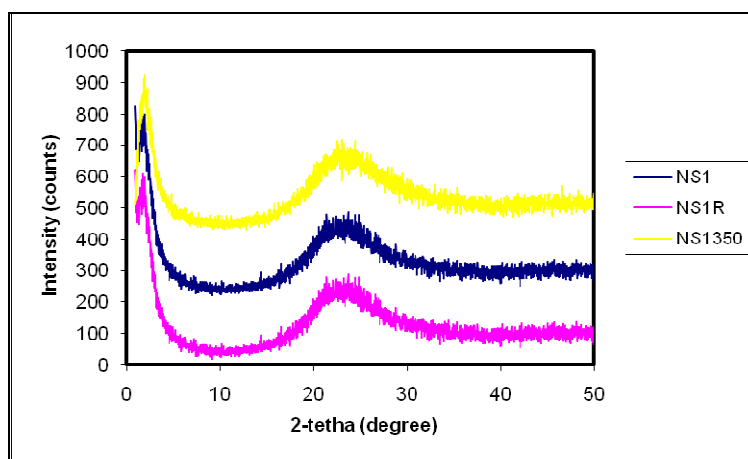


**Figure 38.** XRD patterns of NS1, NS1R and NS1350 catalysts

### 9.3.3. Energy Dispersive Spectroscopy (EDS)

EDS analysis showed the presence of sulfur in the structure of the Nafion/Silica catalyst (NS1) after washing with deionized water (Table 18). Sulfur content is related to the sulfonic groups in nafion resin. The fluorine content of the

catalysts could not be measured by this technique since elements lighter than sodium (atomic number of 11) cannot be detected by EDS. The presence of fluorine could be detected by XPS analyses.

**Table 18.** EDS analysis of NS1

Element	Weight Conc %	Atom Conc %
Si	92.84	97.02
S	0.63	0.58
Br	6.53	2.40

#### 9.3.4. Scanning Electron Microscopy (SEM)

Morphologies of the samples were observed by SEM analyses (Figures 39, 40 and 41). After drying, the materials were obtained as one-piece, hard, solid blocks. They were crushed into smaller pieces to get the desired size. From the SEM images (Figures 39 and 40) we can see that the average particle sizes of the Nafion/Silica catalysts are about 250  $\mu\text{m}$ .

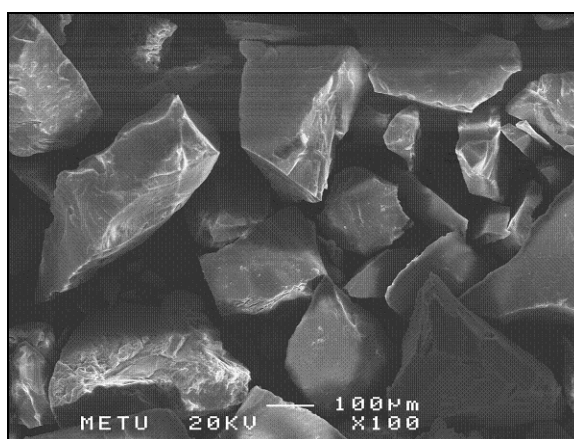


**Figure 39.** SEM image of NS3R1

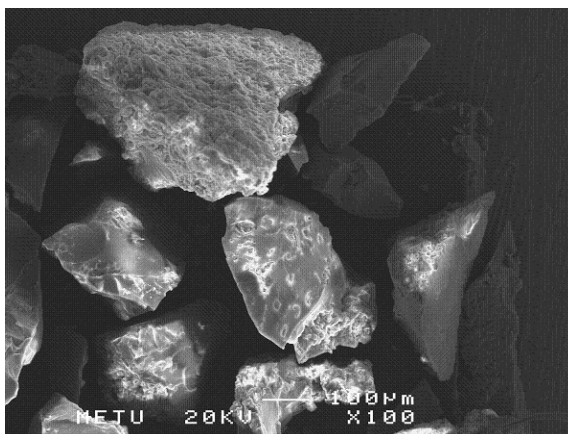


**Figure 40.** SEM image of NS4R2

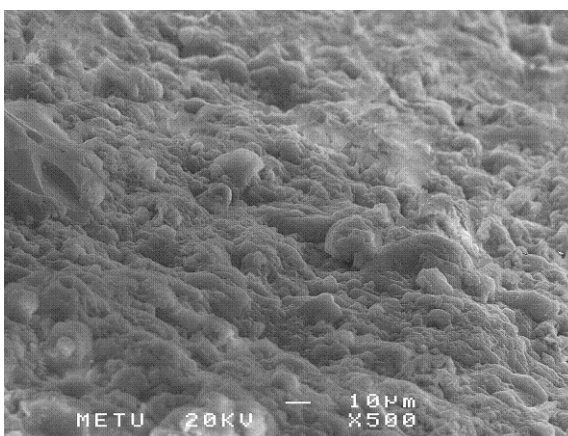


**Figure 41.** SEM image of NS4R2

The rest of the SEM images for all the catalysts synthesized are presented in Appendix B.

### **9.3.5. Energy Dispersive X-Ray Spectroscopy (EDX)**

The elemental mapping analysis of NS1R is shown in Figure 42. EDX images show that the single catalyst particles have very well dispersed F (shown in green)

and Si (shown in red) elements in their structure which means that nafion and silica are perfectly dispersed in the nanocomposite.

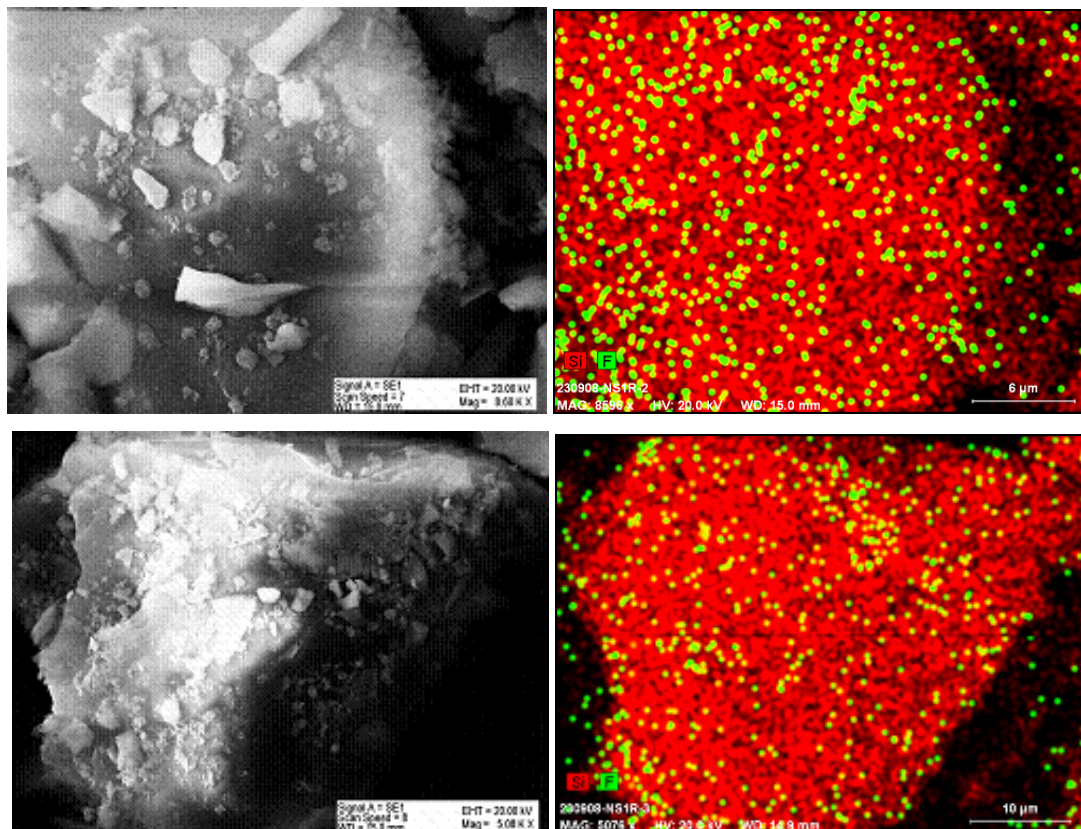


**Figure 42.** EDX elemental mapping of Nafion/Silica nanocomposite (NS1R)

### 9.3.6. X-Ray Photoelectron Spectroscopy (XPS)

The composition of a group of elements present at the surface of the nafion-silica catalysts were analyzed by XPS. A typical XPS spectrum of nafion/silica catalysts is shown in Figure 43.

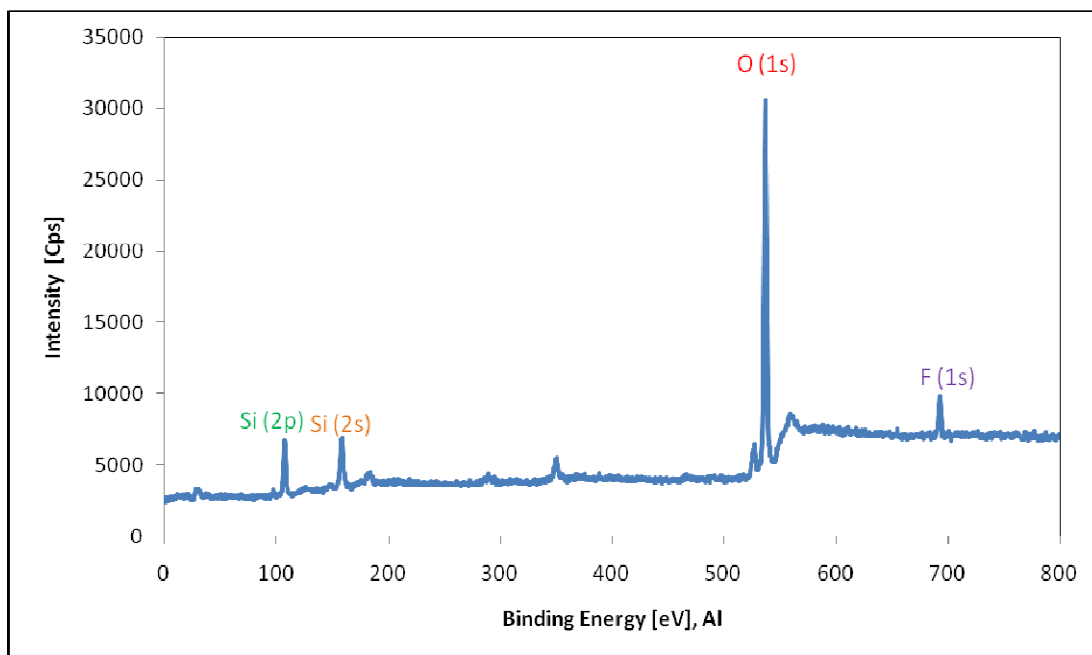


**Figure 43.** XPS spectrum of NS4R2

Table 19 shows the F/Si ratios and the C contents at the surface of the catalysts which were just washed with deionized water. The XPS results of the catalysts after applying further treatments such as calcination and washing in sulfuric solution-ethanol mixture are listed in Table 20.

When the results in these tables are compared, it is observed that F/Si ratios at the surface of the catalysts are preserved and even increased in some of the samples after applying further treatments for surfactant removal (NS1R, NS3R2). Based on this, we can conclude that nafion was not lost from the structure after washing in sulfuric acid solution of ethanol. The Carbon contents as revealed by XPS analyses have significantly decreased after washing in SAE solution or calcination. This means that cetyltrimethylammonium bromide was successfully removed from the catalyst surface.

**Table 19.** XPS results of the as-synthesized catalysts

Catalyst	Nafion/Silica (wt ratio) in the starting solution	F/Si atomic ratio in the nanocomposite (XPS results)	C content, atom% (XPS results)
NS1	0.05	0.08	19.4
NS3	0.15	0.27	25.0
NS4	0.15	0.31	15.2
NS5	0.25	0.36	15.6

**Table 20.** XPS results of the final form of the catalysts (after surfactant removal)

Catalyst	Nafion/Silica (wt ratio) in the starting solution	F/Si atomic ratio in the nanocomposite (XPS results)	C content, atom% (XPS results)
NS1R	0.05	0.16	3.4
NS1350	0.05	0.17	7.0
NS3R1	0.15	0.24	14.8
NS3A	0.15	0.20	9.3
NS3R2	0.15	0.34	7.2
NS4R2	0.15	0.26	5.9
NS5R2	0.25	0.36	4.1

Nafion resin does not have a certain molecular weight. Based on the information given in Chapter 6, m, n and x in the structure of nafion may have different values which alter the length of the chains in the resin. By taking average numbers for each of them, the molecular weight of the nafion resin was calculated as about 731460 g/mol. By using this value, the expected F/Si ratios were calculated as 0.12, 0.36 and 0.60 for the materials synthesized by taking nafion/silica weight ratio as 0.05 (NS1 group), 0.15 (NS3 and NS4 groups) and 0.25 (NS5 group), respectively. A sample calculation is given in Appendix C.

For NS1R and NS1350, XPS results gave the F/Si ratios as 0.16 and 0.17, respectively. They are higher than the expected value of 0.12, which may be an indication of silica loss from the structure of the catalyst during synthesis. However, we also know that XPS gives information about the elemental composition at the surface of the catalyst up to a depth of 3 nm. So, we may also conclude that most of the incorporated nafion resin is located at the surface of the catalyst rather than being hidden in the bulk of the material, which enables a good interaction between the reactants and the active nafion species. Therefore, this is desired in terms of obtaining good catalytic activity. In the case of NS3 group (NS3R1, NS3A, NS3R2) the highest F/Si ratio was obtained with NS3R2 as 0.34 which is very close to the expected value of 0.36. This can be explained by an increase in the F/Si at the catalyst surface with an increase in nafion content and also with an increase of acid strength of the SAE solution used in washing. For NS4R2, XPS results showed a slight decrease in F/Si ratio at the surface. Finally, NS5R2 had an F/Si ratio of 0.36 which is much less than the expected value of 0.60. This is probably because there is an optimum value of nafion loading for the hydrothermally synthesized nafion/silica catalysts developed in this work. Even if the nafion/silica weight ratio was increased up to 0.25 in the synthesis solution, it did not have an effect in the resulting nafion content of the synthesized material.

### **9.3.7. Nitrogen Physisorption**

The results of the nitrogen physisorption analyses of the catalysts are given in Tables 21 and 22. Even before calcination or washing in SAE solution, the multipoint BET surface areas of the catalysts were around 300 m<sup>2</sup>/g which is quite high when compared to the surface area of pure nafion resin (0.02 m<sup>2</sup>/g). Further increase in multipoint BET surface areas and pore volumes were observed for the catalysts after applying treatments for surfactant template removal (Table 22).

**Table 21.** Physical properties of the as-synthesized catalysts

Catalyst	Nafion/Silica (wt ratio) in the starting solution	Multipoint BET surface area (m <sup>2</sup> /g)	BJH Des. Pore Volume (cm <sup>3</sup> /g)	BJH Des. Avg Pore Diameter (nm)
NS1	0.05	313.9	0.48	4.3
NS3	0.15	277.6	0.45	4.3
NS4	0.15	274.1	0.42	4.3
NS5	0.25	282.7	0.44	4.3

**Table 22.** Physical properties of the final form of the catalysts (after surfactant removal)

Catalyst	Nafion/Silica (wt ratio) in the starting solution	Multipoint BET surface area (m <sup>2</sup> /g)	BJH Des. Pore Volume (cm <sup>3</sup> /g)	BJH Des. Avg Pore Diameter (nm)
NS1R	0.05	792.4	0.97	4.3
NS1350	0.05	658.8	0.83	4.3
NS3R1	0.15	678.3	0.87	4.3
NS3A	0.15	678.8	0.88	4.3
NS3R2	0.15	658.7	0.84	4.3
NS4R2	0.15	594.8	0.71	4.3
NS5R2	0.25	745.8	0.93	4.3

The final catalysts obtained after washing in SAE solution had surface areas in the range 594.8-792.4 m<sup>2</sup>/g. This is an indication of the effectiveness of the surfactant removal technique. Calcination also seems to have increased the surface area of the catalyst (658.8 m<sup>2</sup>/g). Pore volumes of the catalysts were in the range 0.71-0.97 cm<sup>3</sup>/g.

The BJH adsorption-desorption isotherms of the catalysts are Type IVb according to the IUPAC classification (Figures 44 and 45), indicating the

mesoporous structure of the materials. Type H2 hysteresis loops were observed. The steep desorption branch signifies that there is interconnectivity in the porous network of the nanocomposite [70].

Single point surface areas of some of the catalysts were determined and they are presented in Appendix D. They are in agreement with the multipoint BET surface areas.

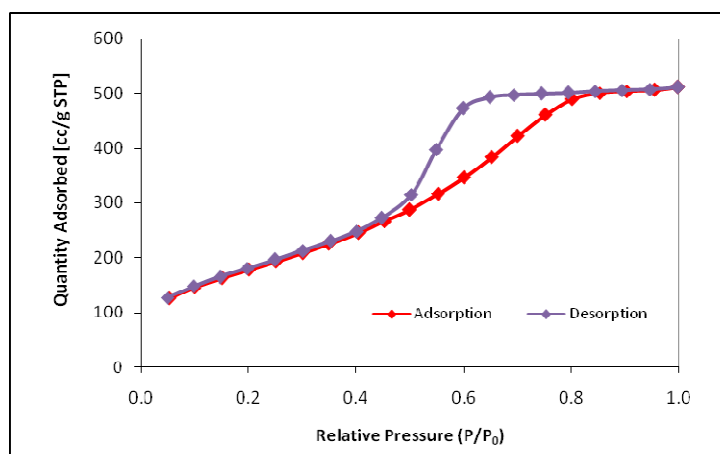


**Figure 44.** Nitrogen adsorption-desorption isotherm of NS3R2

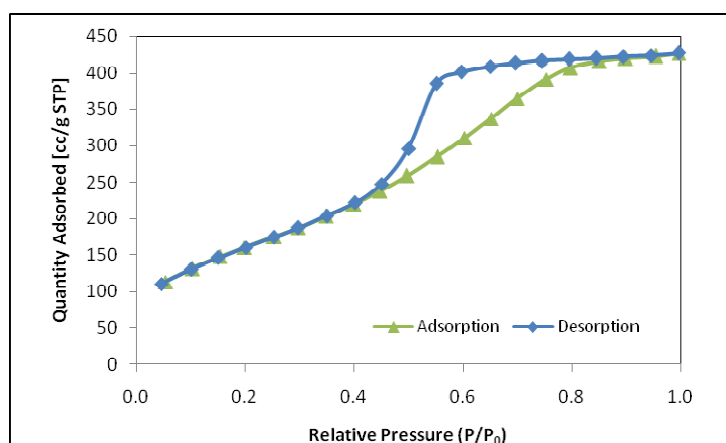


**Figure 45.** Nitrogen adsorption-desorption isotherm of NS4R2

The pore size distributions of the catalysts are given in Figure 46. As observed from the figure, pore size distributions show that the pore diameters of all the materials are in the mesoporous range giving a peak at 4.3 nm. All the samples had average BJH desorption pore diameters of 4.3 nm.

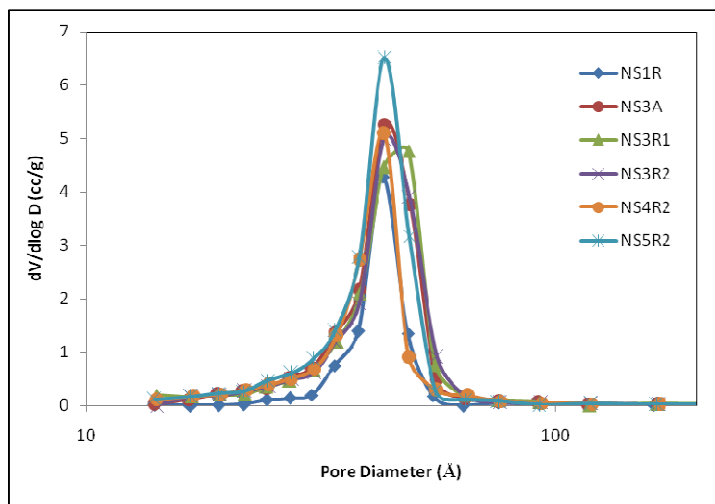


**Figure 46.** Pore size distributions of Nafion/Silica catalysts

### 9.3.8. DRIFTS of Pyridine Adsorbed Samples

Pyridine adsorbed samples gave IR absorption bands at 1598, 1543, 1490 and 1446  $\text{cm}^{-1}$  as presented in Figure 47. The band at 1543  $\text{cm}^{-1}$  corresponds to pyridinium ion adsorbed on the Brönsted acid sites on the catalyst surface. The band at 1490  $\text{cm}^{-1}$  is associated with both the Brönsted and Lewis acid sites. The bands at 1598 and 1446  $\text{cm}^{-1}$  belong to the adsorbed molecules on the Lewis acid sites. NS4R2 has the most intense peaks when compared to the other catalysts. The Brönsted acidities of the catalysts are increasing in the following order : NS1R, NS5R2, NS3A, NS3R1, NS3R2, NS4R2. Since Brönsted acidity is the key parameter for the activity of a catalyst in methanol dehydration reactions, highest DME yield in methanol dehydration is expected to be obtained in the presence of NS4R2.

The band appearing at 1445–1450  $\text{cm}^{-1}$  is an indication of the Lewis acidity which is due to the interaction of pyridine with the silica matrix through donor–acceptor-type bonds [56].

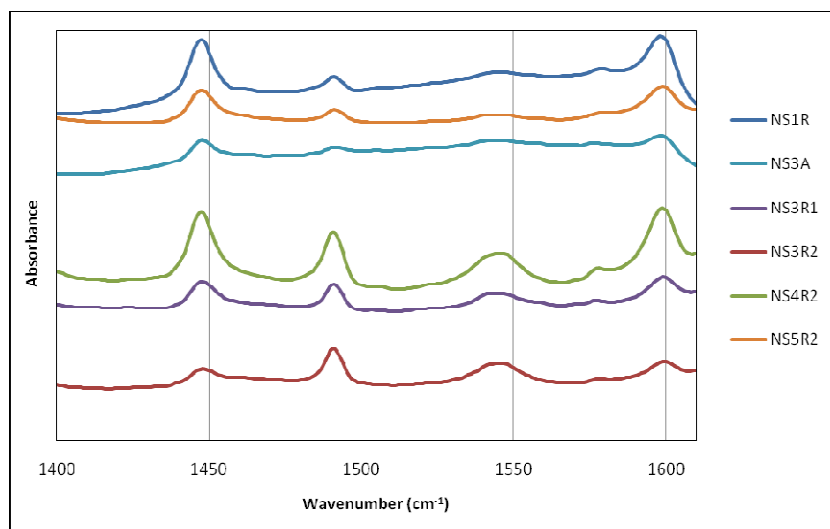


**Figure 47.** DRIFTS spectra of the Nafion/Silica catalysts

#### 9.4. CHARACTERIZATION OF NAFION IMPREGNATED CATALYSTS

The XPS and Nitrogen Physisorption analyses results of the nafion impregnated catalysts are shown in Table 23.

The multipoint BET surface areas of these catalysts indicate that nafion was not successfully incorporated into the pores. BET surface areas of pure aluminosilicate and  $\alpha$ -alumina are 903  $\text{m}^2/\text{g}$  [71] and 232  $\text{m}^2/\text{g}$  [72], respectively. As a result of nafion impregnation, no decrease was observed in the surface area values of the catalysts. However, XPS results indicate the presence of F at the surface of the materials. This is probably due to the presence of nafion as chunks at the surface of the catalyst rather than being incorporated into the mesoporous structure of the supports.

**Table 23.** Physical properties of the nafion impregnated catalysts

Catalyst	Nafion/Alumino silicate or $\alpha$ -Alumina wt ratio (synthesis soln.)	XPS (Atom%)				N <sub>2</sub> Physisorption			
		C 1s	F 1s	Al 2p	Si 2p	S 3s	Multipoint BET surface area (m <sup>2</sup> /g)	BJH Des. Pore Volume (cm <sup>3</sup> /g)	BJH Des. Avg Pore Diameter (nm)
NFMAS1	0.05	19.2	25.3	0.0	55.5	0.0	1262	1.54	3.05
NFMAS2	0.10	8.4	19.1	4.3	68.0	0.2	1385	1.77	3.04
NFMAS3	0.20	24.8	6.2	4.6	64.3	0.1	1089	1.38	2.72
NFALFAI	0.05	-	-	-	-	-	391.6	0.72	5.64

## 9.5. ACTIVITY RESULTS OF STA/SILICA CATALYSTS

In this part, STA/Silica catalysts (TRC-75(L), TRC-75-400, TRC-75(L)-CO<sub>2</sub> synthesized in this work, and the previously synthesized TRC-62(L), TRC-82(L), TRC-92(L)) [25] were tested in methanol dehydration reaction to produce dimethyl ether (DME). The methanol conversion, DME selectivity and DME yield values were plotted as a function of temperature. The comparison of the activities of the catalysts was done in terms of the effect of the W/Si ratio and the effect of the surfactant removal step. In the presence of TRC-75(L), which was found to be the most active catalyst, the effect of space time on DME yield was observed.

### 9.5.1. The effect of the W/Si ratio

By carrying out activity tests with four different STA/Silica (TRC-62(L), TRC-75(L), TRC-82(L), TRC-92(L)) catalysts containing different W/Si ratios in their structure (0.16, 0.33, 0.47, 0.78), the effect of the W/Si ratio on methanol conversion and dimethyl ether (DME) selectivity of the catalysts were observed (Figures 48 and 49).

As presented in Figure 48, TRC-62(L) which contains the lowest W/Si ratio (0.16) gave the lowest methanol conversion between 180-350°C. The activity tests with the other three catalysts showed similar trends. As far as DME selectivity is concerned, with TRC-75(L) the highest DME selectivity was obtained approaching to 100% between 180-350°C. With this catalyst, about 60% DME yield was obtained at 250°C. Formaldehyde formation was observed as the byproduct following the dehydrogenation reaction below.



There is a decrease in activity for TRC-62(L), TRC-82(L) and TRC-92(L) after 250°C due to coke deposition and deactivation of STA above this temperature. However, TRC-75(L) preserves its maximum catalytic activity up to 300°C. Thus,

we can conclude that the tolerance of TRC-75(L) to coke deposition is obviously higher than the other three catalysts.

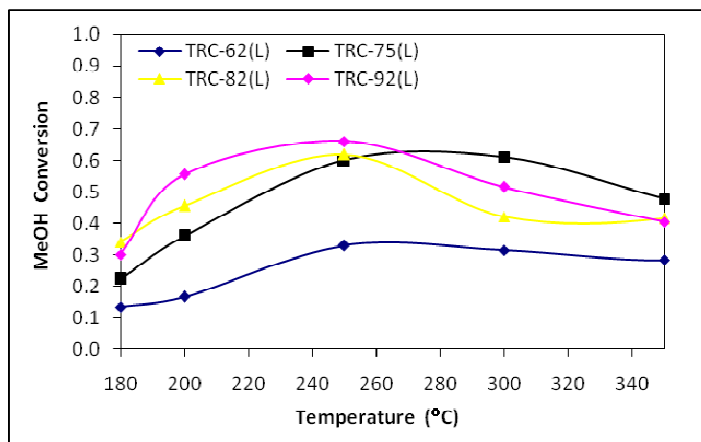


**Figure 48.** MeOH conversion over TRC-62(L), TRC-75(L), TRC-82(L) and TRC-92(L) at 0.27 s.g/cm<sup>3</sup> between 180-350°C

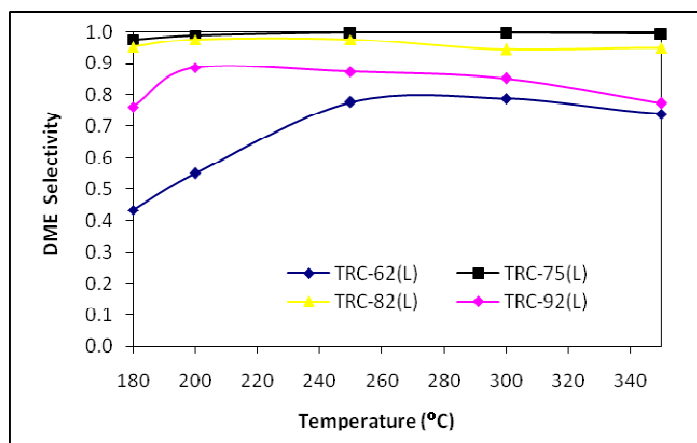


**Figure 49.** DME selectivities over TRC-62(L), TRC-75(L), TRC-82(L) and TRC-92(L) at 0.27 s.g/cm<sup>3</sup> between 180-350°C

### 9.5.2. The effect of the surfactant removal step

The catalytic activity tests of TRC-75(L) which was calcined at 350°C, TRC-75-400 which was calcined at 400°C and TRC-75(L)-CO<sub>2</sub> to which supercritical carbon dioxide extraction was applied as an alternative technique are compared in Figure 50. Methanol conversion values seem to be very close for all three catalysts. However, a slight decrease is observed for TRC-75-400, which indicates that by calcining the catalyst at 400°C some decrease in activity was observed. This is due to the fact that over 350°C, STA structure begins to decompose and protons of the active STA phase are partly lost.

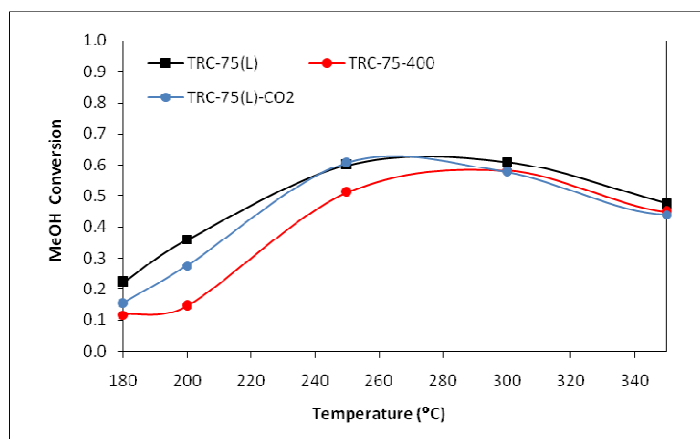


**Figure 50.** MeOH conversion over TRC-75(L), TRC-75(L)-CO<sub>2</sub> and TRC-75-400 at 0.27 s.g/cm<sup>3</sup> between 180-350°C

Supercritical CO<sub>2</sub> seems to cause no loss in activity which means that the structure of the catalyst was not destructed by applying this technique.

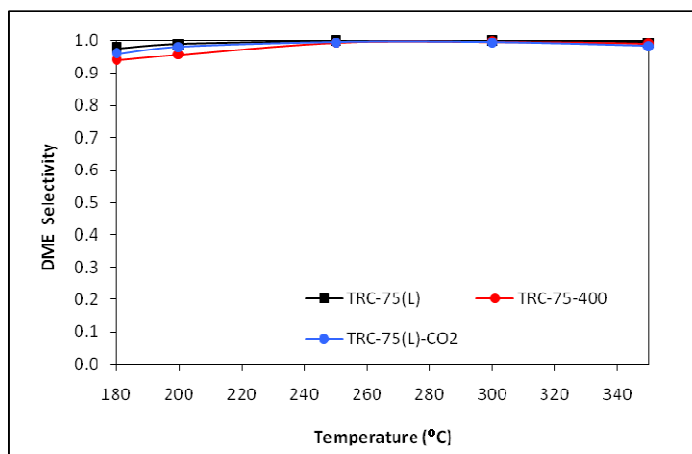


**Figure 51.** DME selectivities over TRC-75(L), TRC-75(L)-CO<sub>2</sub> and TRC-75-400 at 0.27 s.g/cm<sup>3</sup> between 180-350°C

DME selectivities are shown in Figure 51. All three catalysts show nearly 100% DME selectivity between 180-350°C.

### 9.5.3. The effect of space time

With TRC-75(L), which showed the highest activity in dehydration of methanol among the STA/Silica catalysts tested, activity tests were done by using different amounts of catalysts (0.1 g, 0.2 g, 0.3 g), at different space times (0.14 s.g.cm<sup>-3</sup>, 0.27 s.g.cm<sup>-3</sup>, 0.41 s.g.cm<sup>-3</sup>).

Methanol conversion and DME selectivity results are presented in Figures 52 and 53. DME yields were calculated by multiplying methanol conversion values by DME selectivities. As expected, as the space time increased the methanol conversion and DME selectivities, hence the DME yields increased. The highest DME yield was obtained as 80% at 250°C at a space time of 0.41 s.g.cm<sup>-3</sup>. The considerably high activity of this catalyst was attributed to its high Brönsted acidity, which is known to play a major role in alcohol dehydration reactions. The presence of undistorted Keggin units incorporated into the mesoporous siliceous framework (as observed by

FTIR) is the main reason for the high Brønsted acidity and the enhanced catalytic activity of this STA/Silica catalyst.

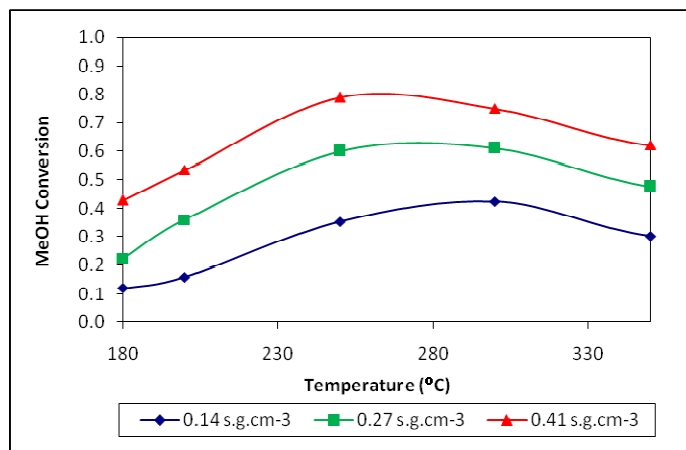


**Figure 52.** MeOH conversion over TRC-75(L) at different space times between 180-350°C

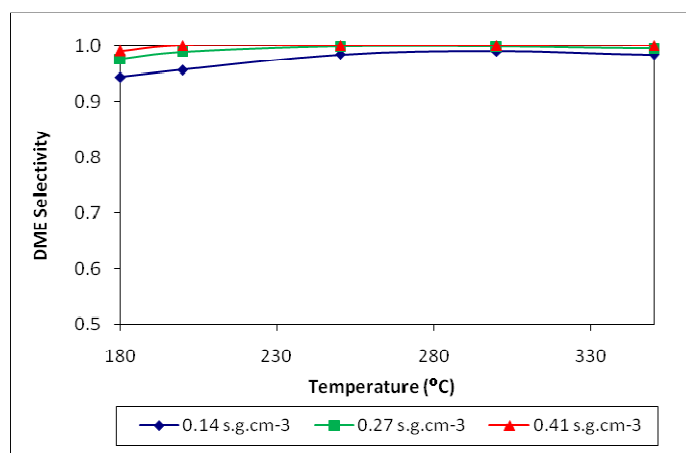


**Figure 53.** DME selectivities over TRC-75(L) at different space times between 180-350°C

The stability of the activity of TRC-75(L) in methanol dehydration reaction was tested by carrying out two reaction experiments at 200°C and 250°C for 6 hours. Some decrease in activity was observed due to coke formation. Carbon deposition on the catalyst surface was proved by XPS analyses. After 6 hours of reaction, the C/Si ratio at the surface of the catalyst increased from 1.2 to 1.5. Catalyst deactivation due to coke formation was also observed in the work of Herrera et al. [40] on TPA impregnated mesoporous silica catalysts used in methanol dehydration. However, in this work TRC-75(L) was successfully regenerated. By re-calcining in dry air at 350°C the spent catalyst could easily be reactivated to its original activity. The results of the stability tests and the catalytic activity obtained after regeneration are given in Table 24. DME selectivity was found to be almost 100% between 180-350°C at the space time of 0.27 s.g.cm<sup>-3</sup> and no significant decrease was observed during the stability tests.

**Table 24.** Results of the stability tests and regeneration experiments over TRC-75(L) at 0.27 s.g.cm<sup>-3</sup>

	<b>Methanol conversion (%)</b>
<b>During the 1<sup>st</sup> hour at 250°C (Averaged over 3 data points)</b>	60
<b>At the end of 6 hours at 250°C</b>	22
<b>During the 1<sup>st</sup> hour at 200°C (Averaged over 3 data points)</b>	36
<b>At the end of 6 hours at 200°C</b>	13
<b>During the 1<sup>st</sup> hour at 250°C <i>After regeneration</i></b>	58

## 9.6. ACTIVITY RESULTS OF TPA/SILICA CATALYSTS

By synthesizing two types of HPA/Silica catalysts each containing W/Si ratios of 0.40 but prepared by using two different HPA's, namely STA and TPA, the effect of the active heteropoly compound phase was tested on the catalytic activity of the materials in DME synthesis by dehydration of methanol.

Figure 54 shows the methanol conversion values obtained with STA/Silica (TRC-75(L)) and TPA/Silica (TPA-75(L)) catalysts. It can be concluded that STA/Silica is much more active than TPA/Silica in methanol dehydration reaction. With TPA-75(L), about 30% methanol conversion was obtained at 250°C.

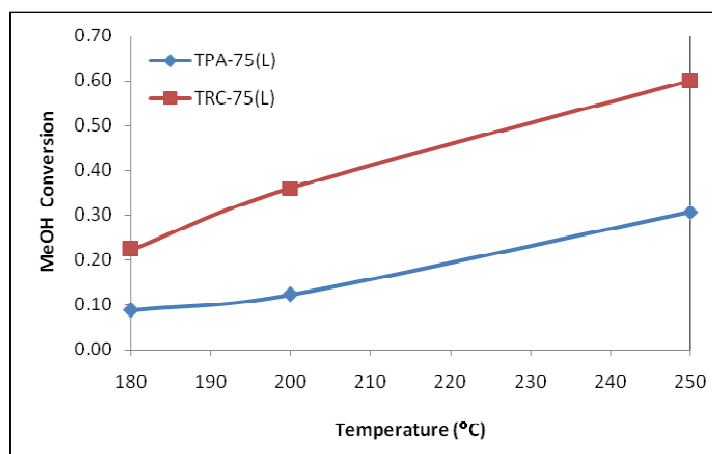


**Figure 54.** MeOH conversion over TPA-75(L) and TRC-75(L) at 0.27 s.g/cm<sup>3</sup> between 180-250°C

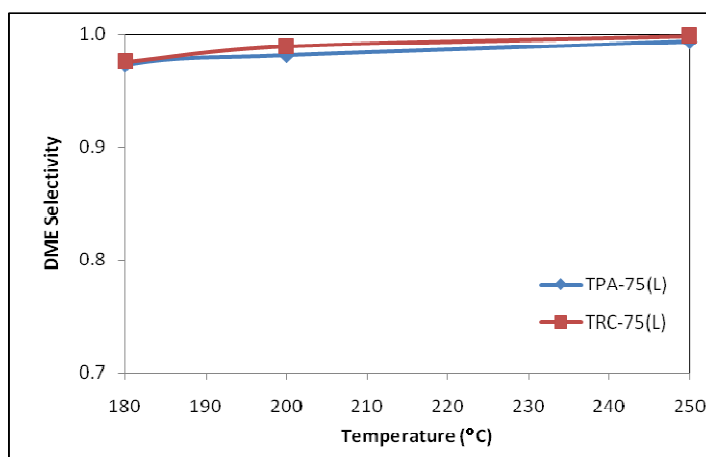


**Figure 55.** DME selectivities over TPA-75(L) and TRC-75(L) at 0.27 s.g/cm<sup>3</sup> between 180-250°C

The activities of pure STA and pure TPA in methanol dehydration were tested in literature [25]. At a space time of  $0.27 \text{ s.g.cm}^{-3}$  at  $250^\circ\text{C}$  highest methanol conversion was found as 0.32 and 0.14 for STA and TPA, respectively. In this study, the hydrothermally synthesized HPA incorporated mesoporous catalysts having high surface areas and pore volumes were found to be twice as active as their pure forms with over 99% DME selectivities (Figure 55).

## 9.7. ACTIVITY RESULTS OF AN STA/ALUMINOSILICATE CATALYST

The activity of an STA(Silicotungstic acid)/Aluminosilicate catalyst prepared by impregnation method [25] was tested in methanol dehydration reaction. The results are given in Figures 56 and 57.

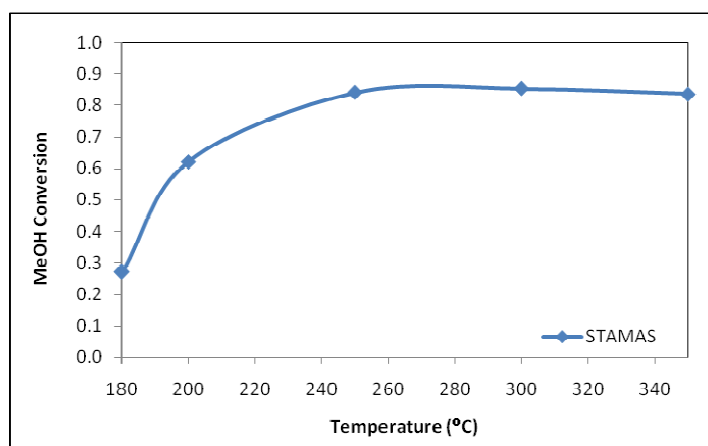


**Figure 56.** Methanol conversion over STAMAS at  $0.27 \text{ s.g/cm}^3$  between  $180\text{-}350^\circ\text{C}$

A very high methanol conversion was obtained with STAMAS. At  $250^\circ\text{C}$  84% methanol conversion, 90% DME selectivity and about 75% DME yield was achieved. For the STA/Silica catalysts synthesized by one-pot hydrothermal synthesis route, the methanol conversion values decreased with an increase in temperature over  $250^\circ\text{C}\text{-}300$ . However, for the case of STAMAS no deactivation

was observed due to temperature increase. This implies that STAMAS, prepared by impregnation of STA into aluminosilicate, is a more stable catalyst in methanol dehydration reaction.

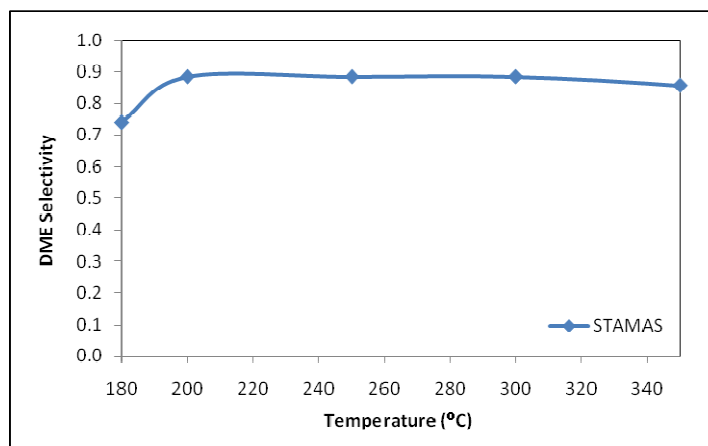


**Figure 57.** DME selectivities over STAMAS at  $0.27 \text{ s.g/cm}^3$  between 180-350°C

Also, the activity of STAMAS was found to be highly stable when tested for 8 hours of run at 250°C. It was observed that there was no loss in the activity of this catalyst as shown in Figure 58.

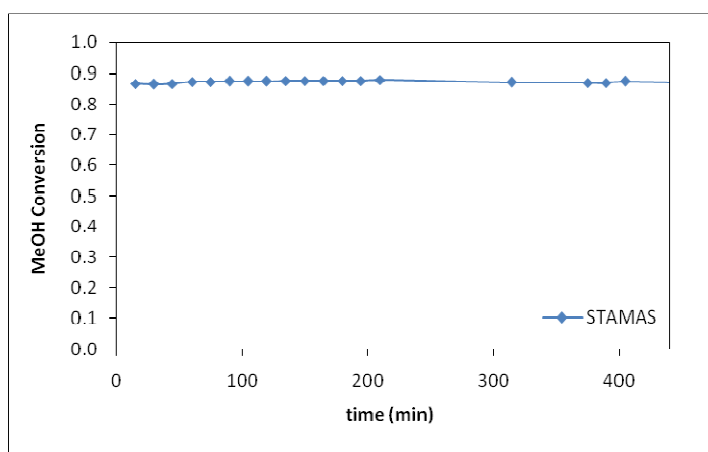


**Figure 58.** Stability test over STAMAS at 250°C at  $0.27 \text{ s.g.cm}^{-3}$

## 9.8. ACTIVITY RESULTS OF NAFION/SILICA CATALYSTS

In this part, activity results of the nafion/silica catalysts synthesized by following a one-pot hydrothermal synthesis procedure is presented. The results of the activity tests in methanol dehydration reaction are compared in terms of the difference between calcination and washing with sulfuric acid-ethanol mixture as surfactant removal techniques, different washing conditions (changes in the molarity of the SAE solution used, temperature, time, etc.), nafion loading on the catalyst and nafion source used during the synthesis of the materials.

### 9.8.1. The comparison of calcination and washing with SAE solution

By carrying out activity tests with NS1 catalysts which contain 5% nafion in their structure, the effects of calcination and refluxing on the catalytic activity of the materials was compared. As shown in Figures 59 and 60, NS1R which was refluxed with 1M sulfuric acid solution of ethanol for 12 hours seems to be much more active than the catalysts which were calcined at 250°C and 350°C with dry air. Also the activity of the untreated NS1, which was only washed with deionized water after hydrothermal synthesis, was tested. This catalyst as well showed very low methanol conversion and DME selectivity when compared to NS1R.

In fact, the low DME selectivity values of NS1250, NS1350 and NS1 especially below 250°C showed that the trace amount of methanol conversion obtained with these catalysts belonged to the formation of formaldehyde as a result of methanol dehydrogenation. Methanol dehydration capacities of these catalysts were very low when compared to NS1R.

The surface area of NS1 is limited (314 m<sup>2</sup>/g) due to the unremoved surfactant template on its surface. The surface area of the calcined N1350 was found to be 659 m<sup>2</sup>/g, which is comparable to the surface area of NS1R (792 m<sup>2</sup>/g). However, the active sulfonic acid groups of the nafion resin decompose over 280°C. [50] Thus, the catalytic activity of NS1350 was significantly inhibited by exposure to high temperature during calcination. As a result, refluxing in SAE solution proved to be the best treatment in terms of catalytic activity and NS1R, which has the highest

surface area and active sulfonic acid groups in its structure, showed the highest methanol conversion and DME selectivity among these catalysts.

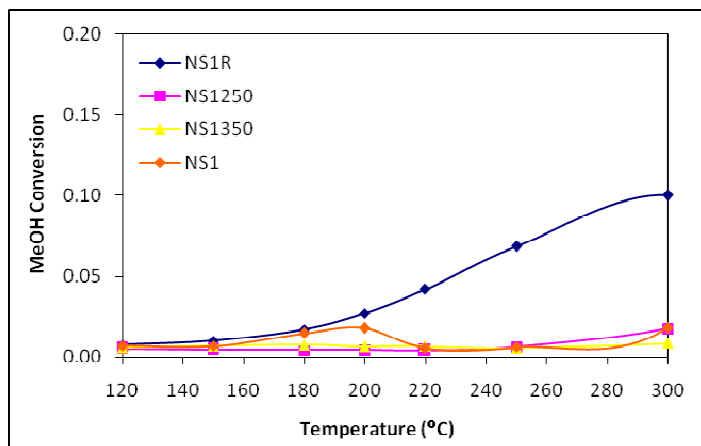


**Figure 59.** MeOH conversion over NS1R, NS1250, NS1350 and NS1 at 0.27 s.g/cm<sup>3</sup> between 120-300°C

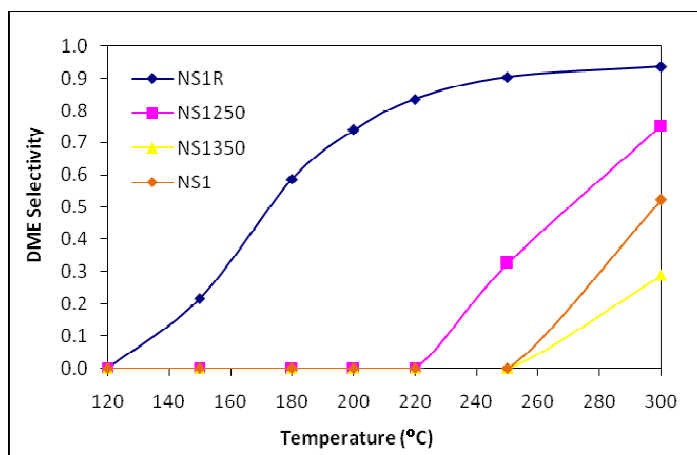


**Figure 60.** DME selectivities over NS1R, NS1250, NS1350 and NS1 at 0.27 s.g/cm<sup>3</sup> between 120-300°C

### 9.8.2. The effect of different washing conditions

For NS3 catalysts, which contain about 16% nafion in their structure, the effect of different washing conditions was investigated. Methanol conversion and DME selectivities are presented in Figures 61 and 62.

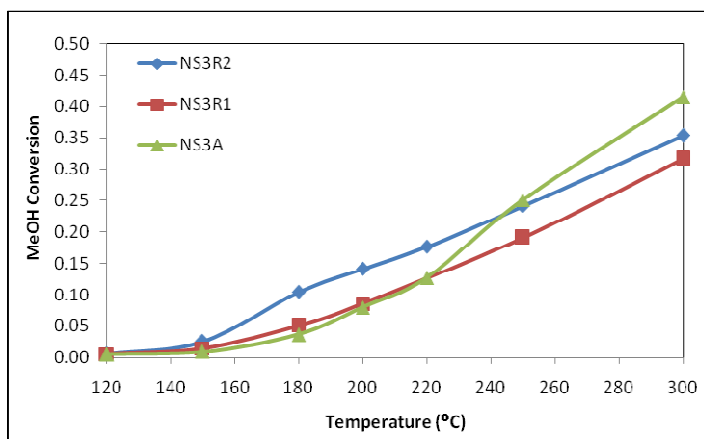


**Figure 61.** MeOH conversion over NS3R2, NS3R1 and NS3A at 0.27 s.g/cm<sup>3</sup> between 120-300°C

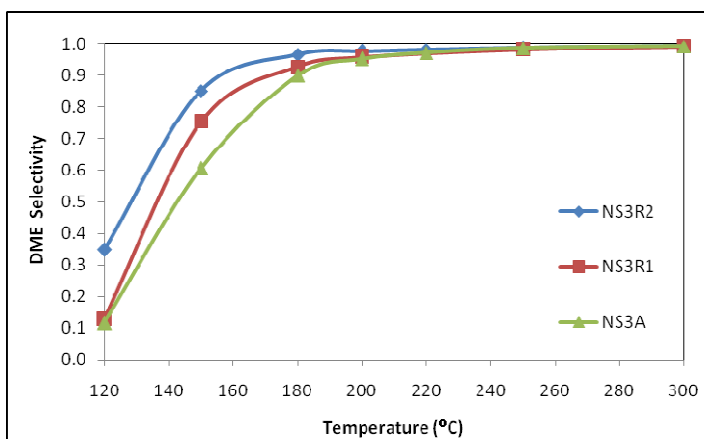


**Figure 62.** DME selectivities over NS3R2, NS3R1 and NS3A at 0.27 s.g/cm<sup>3</sup> between 120-300°C

Among the NS3 catalysts, NS3R2 showed the highest methanol conversion up to 250°C. Also, the highest DME selectivity was obtained with this catalyst between 120-300°C. The different washing conditions applied to NS3 group catalysts were shown in Table 10. Based on the comparison of the activity results of the NS3 group, the best conditions for washing seem to be those applied to NS3R2, namely using 2 M of sulfuric acid solution of ethanol, refluxing the solid particles at 78°C for 6 hours and further refluxing in pure ethanol for 6 hours.

### **9.8.3. The effect of nafion loading**

The highest methanol conversion obtained with N1R was about 10% at 300°C. As presented in the previous section, NS3 group catalysts led to a much higher methanol conversion and DME selectivity when compared to NS1R. Thus, we can conclude that by increasing the nafion/silica weight ratio in the synthesis solution from 0.05 to 0.15 a significant increase in catalytic activity was achieved. This was also proved by the higher concentration of Brönsted acid sites in NS3R1, NS3R2 and NS3A when compared to NS1R.

The most effective method for surfactant template removal was identified as the one applied to NS3R2. Therefore, NS4 and NS5, for the synthesis of which a different nafion source was used, were refluxed with 2 M sulfuric acid solution of ethanol for 6 hours and then further refluxed with pure ethanol for 6 hours. They were given the names NS4R2 and NS5R2 and were synthesized by taking the nafion/silica weight ratio in the starting synthesis mixture as 0.15 and 0.25, respectively. As shown in Figure 63, NS4R2, similar to NS3R2, showed better catalytic activity than NS1R due to its higher nafion content. However, both NS3R2 and NS4R2 were found to be more active than NS5R2 which indicates that further increasing the nafion content in the synthesis solution from 0.15 to 0.25 did not result in an increase in activity. This suggests that there is an optimum nafion loading for the Nafion/Silica catalysts. Therefore, based on the catalytic activity, the optimum nafion/silica weight ratio in the starting solution was identified as 0.15 for the catalysts synthesized in this work.

NS3R2 and NS4R2 were synthesized by taking the nafion/silica ratio as 0.15 but by using different nafion sources. The nafion source of NS4R2 is apparently better for catalytic applications based on the higher methanol conversion and DME selectivity (Figure 64) obtained with this catalyst over the entire temperature range.

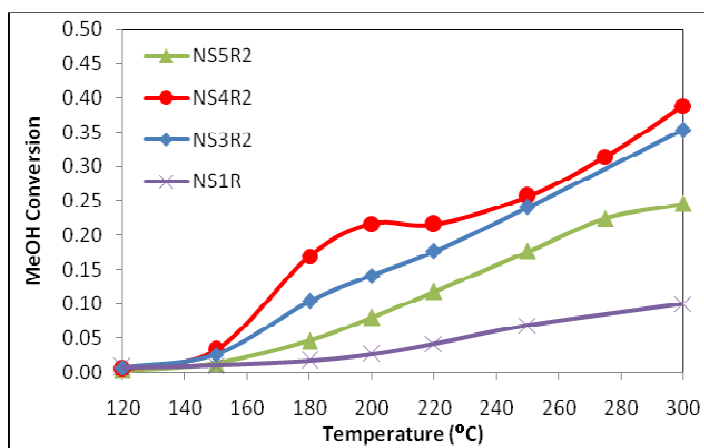


**Figure 63.** MeOH conversion over NS5R2, NS4R2, NS3R2 and NS1R at 0.27 s.g/cm<sup>3</sup> between 120-300°C

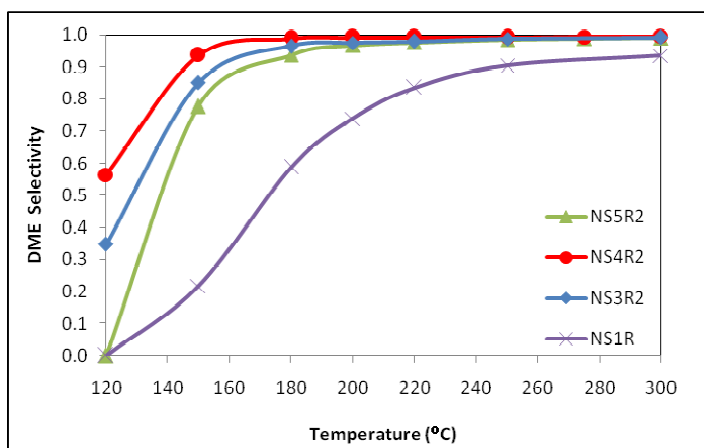


**Figure 64.** DME selectivities over NS5R2, NS4R2, NS3R2 and NS1R at 0.27 s.g/cm<sup>3</sup> between 120-300°C

Highest methanol conversion obtained with the Nafion/Silica catalysts synthesized in this work was 40% in the presence of NS4R2 at 300°C with approximately 100% DME selectivity over 180°C. This catalyst was also found to be the one with the highest Brönsted and Lewis acidity among all the Nafion/Silica catalysts synthesized in this work.

The surface areas and the pore volumes of the nafion/silica catalysts are also indications of the incorporation of nafion into the silicate structure. For example, the surface area and pore volume of NS4R2 were found to be 595 m<sup>2</sup>/g and 0.71 cm<sup>3</sup>/g, respectively. These values are slightly lower than the surface areas and pore volumes of the other nafion/silica catalysts implying better incorporation of nafion resin into NS4R2, which was also proved by its highest catalytic activity.

Increasing the selectivity towards DME formation has been a major challenge in solid-acid catalyzed methanol dehydration reaction. In the case of Nafion/Silica catalysts, no loss in activity due to coke deposition was observed during the reaction experiments. Moreover, the stability test performed with NS4R2 showed that its activity was highly stable at a temperature as high as 300°C after 6 hours of run as shown in Figure 65.

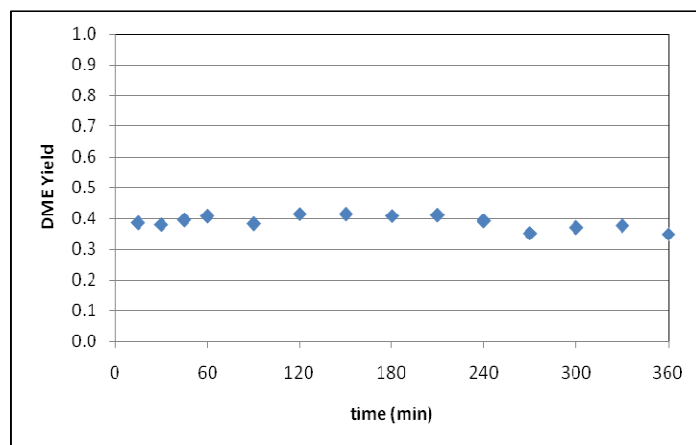


**Figure 65.** Stability test over NS4R2 at 300°C at 0.27 s.g.cm<sup>-3</sup>

Actually, sulfonic acid groups of nafion resin are expected to start decomposing over 280°C. However, stability test showed that no decomposition took place in the structure of Nafion/Silica catalyst even at 300°C. This is an indication of the increased thermal stability due to strong binding of the sulfonic acid groups to the surface of the mesoporous silicate network achieved by one-pot hydrothermal synthesis.

The reproducibility of the experiments was tested with NS4R2 and the results were found to be highly reproducible as shown in Figure 66.

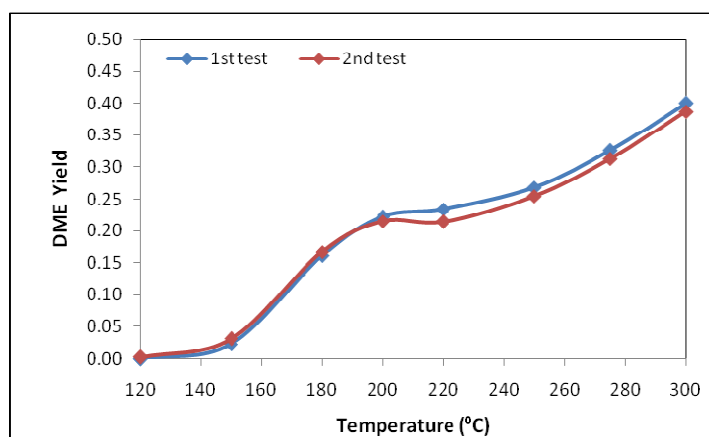


**Figure 66.** Reproducibility check over NS4R2 at  $0.27 \text{ s.g.cm}^{-3}$

The catalytic activity of the pure nafion resin (NR-50) was tested in methanol dehydration in a study in literature [66]. By adjusting the space time as  $0.27 \text{ s.g.cm}^{-3}$  (by loading 0.2 g of nafion resin in the reactor), the highest methanol conversion achieved was about 0.20 at 220°C, whereas in this work it was observed that by loading 0.2 g of NS4R2 (in which the nafion/silica weight ratio was 0.15 during the synthesis), the same methanol conversion (0.20) could be achieved at 200°C. This is because the catalytic activity of the nonporous nafion resin is limited, whereas the hydrothermally synthesized silicate structured nafion/silica catalyst (NS4R2) has a surface area as high as  $594.8 \text{ m}^2/\text{g}$  which considerably increases the amount of accessible sites to the reactant molecules. Thus, by dispersing nafion in the silicate

structured lattice, it is possible to use much less amount of nafion resin to get the same catalytic activity at a lower temperature.

Also, a nanocomposite nafion/silica catalyst (SAC-13) synthesized by sol-gel route by DuPont [50] had a surface area of 235 m<sup>2</sup>/g and was tested in our laboratory in methanol dehydration reaction by Tokay [72]. It was found to give 0.26 conversion and 90% DME selectivity at 250°C when the space time was adjusted to 0.27 s.g.cm<sup>-3</sup>. The same methanol conversion could be achieved with NS4R2 at 250°C at the same space time but with a higher DME selectivity approaching to 100% at all temperatures over 180°C.

## 9.9. ACTIVITY RESULTS OF NAFION IMPREGNATED CATALYSTS

### 9.9.1. Activity Results of Nafion/Aluminosilicate Catalysts

The nafion impregnated Nafion/Aluminosilicate catalysts were tested in methanol dehydration reaction and their results were compared with the activity of commercial aluminosilicate (AlSi(c)). The results are shown in Figures 67 and 68.

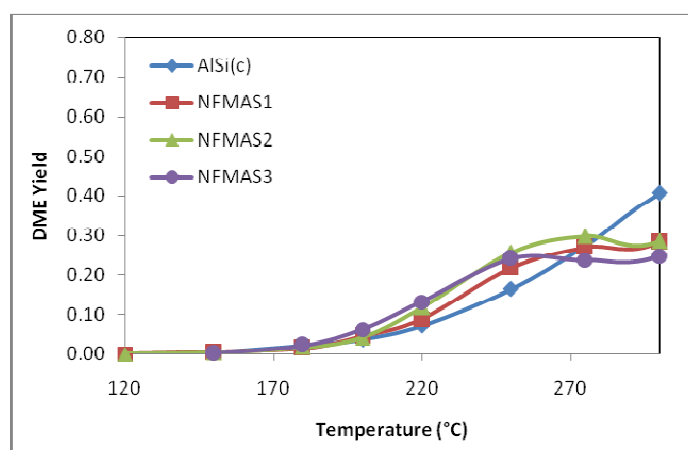


**Figure 67.** DME yield over nafion/aluminosilicate catalysts at 0.27 s.g/cm<sup>3</sup> between 120-300°C

As can be observed in Figure 67, between 120-250°C there is an increase in DME yield values due to the impregnation of nafion in the structure of aluminosilicate. However, as shown in Figure 68, the DME yield values start to decrease over 275°C due to the decomposition of the sulfonic groups of nafion.

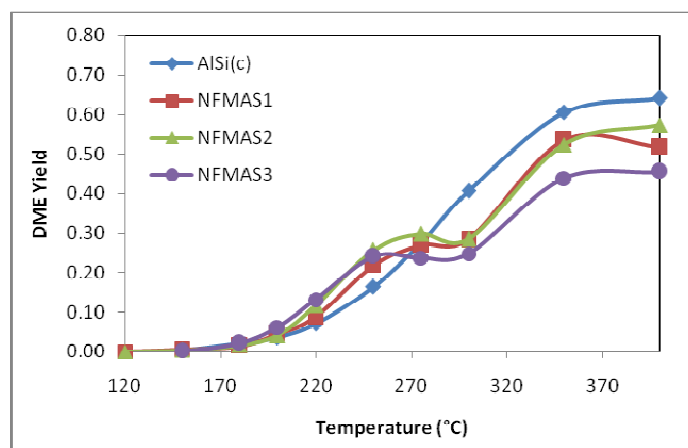


**Figure 68.** DME yield over nafion/aluminosilicate catalysts at 0.27 s.g/cm<sup>3</sup> between 120-400°C

### 9.9.2. Activity Results of Nafion/ $\alpha$ -Alumina Catalysts

The activity results of the nafion/ $\alpha$ -alumina catalysts synthesized by impregnation are compared with the activity of pure  $\alpha$ -alumina (adapted from [72]). The results are presented in Figure 69. It is seen that impregnation of nafion by a nafion/ $\alpha$ -alumina weight ratio of 0.05 did not have a significant effect on the catalytic activity of  $\alpha$ -alumina.

The reason why nafion impregnation on aluminosilicate or  $\alpha$ -alumina did not cause a significant rise in the methanol dehydration activity of the catalysts was that since impregnation was done by dispersing the support and nafion solution, which actually is a dispersion of nafion resin in lower aliphatic alcohols and water, in ethanol and mixing for several hours, nafion as a bulk polymeric compound may not have incorporated into the porous structure of the catalyst. Instead, it was probably

located at the surface as chunks because as discussed before, no significant decrease in surface areas of nafion impregnated aluminosilicate or  $\alpha$ -alumina catalysts was observed due to nafion loading. Consequently, one-pot hydrothermal synthesis proved to be a better technique for incorporation of nafion resin into mesoporous silicates.

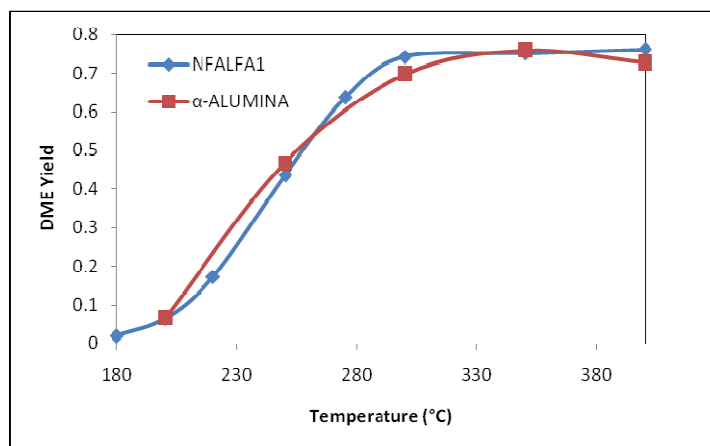


**Figure 69.** DME yield over nafion/ $\alpha$ -alumina and pure  $\alpha$ -alumina at 0.27 s.g/cm<sup>3</sup> between 180-400°C

#### 9.10. IN-SITU INFRARED STUDIES : METHANOL AND DME ADSORPTION AND DESORPTION ON THE CATALYSTS SYNTHESIZED

Adsorption and desorption of methanol and dimethyl ether on the mesoporous catalysts synthesized in this work were studied by in situ FT-IR. The experiments were done in the Laboratory of Heterogeneous Catalysis of Eindhoven University of Technology by using a Bruker IFS 113v instrument. The spectra were recorded at a 2 cm<sup>-1</sup> resolution and averaged over 30 scans. Prior to each experiment, the following steps were applied.

First the sample was prepared as a thin self-supporting wafer of about 10 mg/cm<sup>2</sup>. Then the wafer was placed inside a controlled environment infrared transmission cell and out-gassed until the residual pressure was below 5x10<sup>-5</sup> mbar.

The sample was dried at appropriate conditions before being exposed to methanol or DME and a spectrum was recorded at room temperature (30°C) as the reference spectrum. Then the wafer was exposed to 5 mbar of methanol or DME for 15 minutes. Afterwards the chamber was evacuated to get rid of the unadsorbed gas and a spectrum was recorded at room temperature (RT). Desorption was carried out by evacuation at the desired temperatures (100°C-500°C) for 30 minutes and spectra were recorded at room temperature after desorption at each temperature. The spectra presented in this section are subtracted from the reference spectra of the clean dried wafers recorded at room temperature.

### 9.10.1. Methanol Adsorption on Nafion/Silica Catalysts

Hydrated nafion resin contains dissociated and strongly hydrated sulfonic acid groups, which upon drying transform into undissociated sulfonic groups, associated by hydrogen bonds [73]. The hydrated form of Nafion is shown in Figure 70.

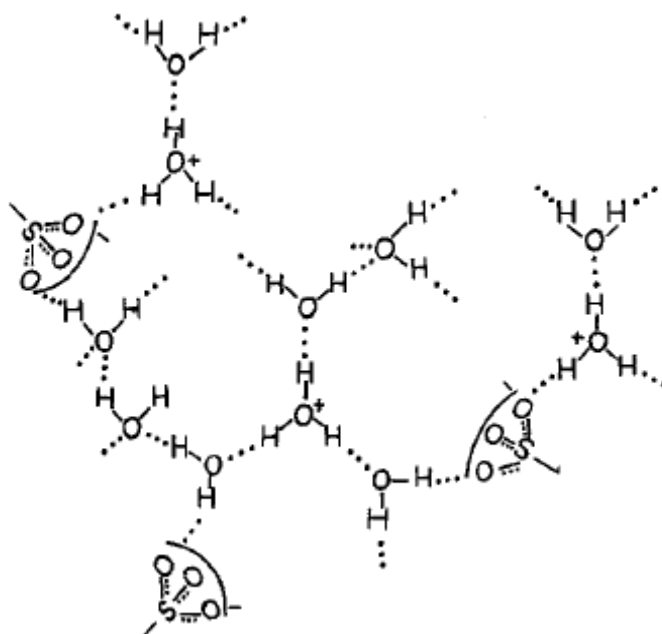


**Figure 70.** Hydrate structures in Nafion membrane swollen with water [73]

Two of the nafion/silica catalysts synthesized by one-pot hydrothermal synthesis route, namely NS4R2 and NS3R1, were tested in in-situ methanol adsorption and desorption experiments. Dehydration was carried out at 150°C for 60 minutes. The FT-IR spectra of the samples after dehydration are given in Figure 87 in Appendix E. The dried samples, NS4R2 and NS3R1, gave absorption bands at 1401  $\text{cm}^{-1}$  and 1399  $\text{cm}^{-1}$ , respectively. These bands are due to the  $\nu(\text{S}=\text{O})$  stretching vibrations of undissociated sulfonic acid groups ( $-\text{SO}_3\text{H}$ ) present in the structure of nafion [73]. As a result of drying, the network of hydrate structures are broken and the association of sulfonic groups is observed by the emergence of the peaks around 1400  $\text{cm}^{-1}$ . The FT-IR spectra of the commercial nafion-silica nanocomposite (SAC-13) was also recorded and the  $\nu(\text{S}=\text{O})$  stretching vibration for this catalyst was observed at 1414  $\text{cm}^{-1}$ . The bands around 3740  $\text{cm}^{-1}$  for the hydrothermally synthesized Nafion/Silica catalysts are due to the lone silanol groups ( $\text{SiO}-\text{H}$  stretch) on the surface of the silica network [74].

In Figure 71, the spectra of methanol adsorbed on NS4R2 are shown. The bands observed in the C-H stretching region, 2854  $\text{cm}^{-1}$ , 2928  $\text{cm}^{-1}$ , 2955  $\text{cm}^{-1}$  and 2994  $\text{cm}^{-1}$  suggest the dissociative adsorption of methanol and the formation of methoxy functional groups ( $\text{CH}_3-\text{O}$ ) on the surface of the catalyst. These bands belong to asymmetric and symmetric C-H stretching bands of  $\text{CH}_3-\text{O}$  groups [74]. The bands 2854  $\text{cm}^{-1}$ , 2955  $\text{cm}^{-1}$  and 2994  $\text{cm}^{-1}$  are in agreement with the previous studies in literature where they were assigned to methoxide on silica ( $\text{CH}_3\text{O}-\text{Si}$ ) [75]. In the study of Fisher and Bell [75], the peak at 2926  $\text{cm}^{-1}$  was attributed to methoxide on Cu for the  $\text{Cu}/\text{SiO}_2$  catalyst and the peak at 2933  $\text{cm}^{-1}$  was said to be due to methoxide on Zr for the  $\text{Cu}/\text{ZrO}_2/\text{SiO}_2$  catalyst. Thus, the additional band at 2928  $\text{cm}^{-1}$  in the C-H stretching region may be due to the methanol adsorbed on the active nafion sites on the catalyst.

The broad band (between 3000-3400  $\text{cm}^{-1}$ ) is due to the O-H stretch of hydrogen-bonded network of adsorbed methanol molecules [74]. The OH groups of alcohols form hydrogen bridges with the  $-\text{SO}_3\text{H}$  groups of the catalyst and also among themselves. Alcohols enter between the hydrogen bonded network of  $-\text{SO}_3\text{H}$  groups and cause swelling [76]. A large fraction of the acid sites are expected to be covered by these physically adsorbed methanol molecules. By desorption with increasing temperature, the intensity of this broad band decreases due to methanol

dehydration reaction. Thus, these sites are identified as “type 1” sites ( $S_1$ ) involved in methanol adsorption on the catalyst surface during methanol dehydration. The negative peak at  $3743\text{ cm}^{-1}$  is due to the consumption of silanol groups.

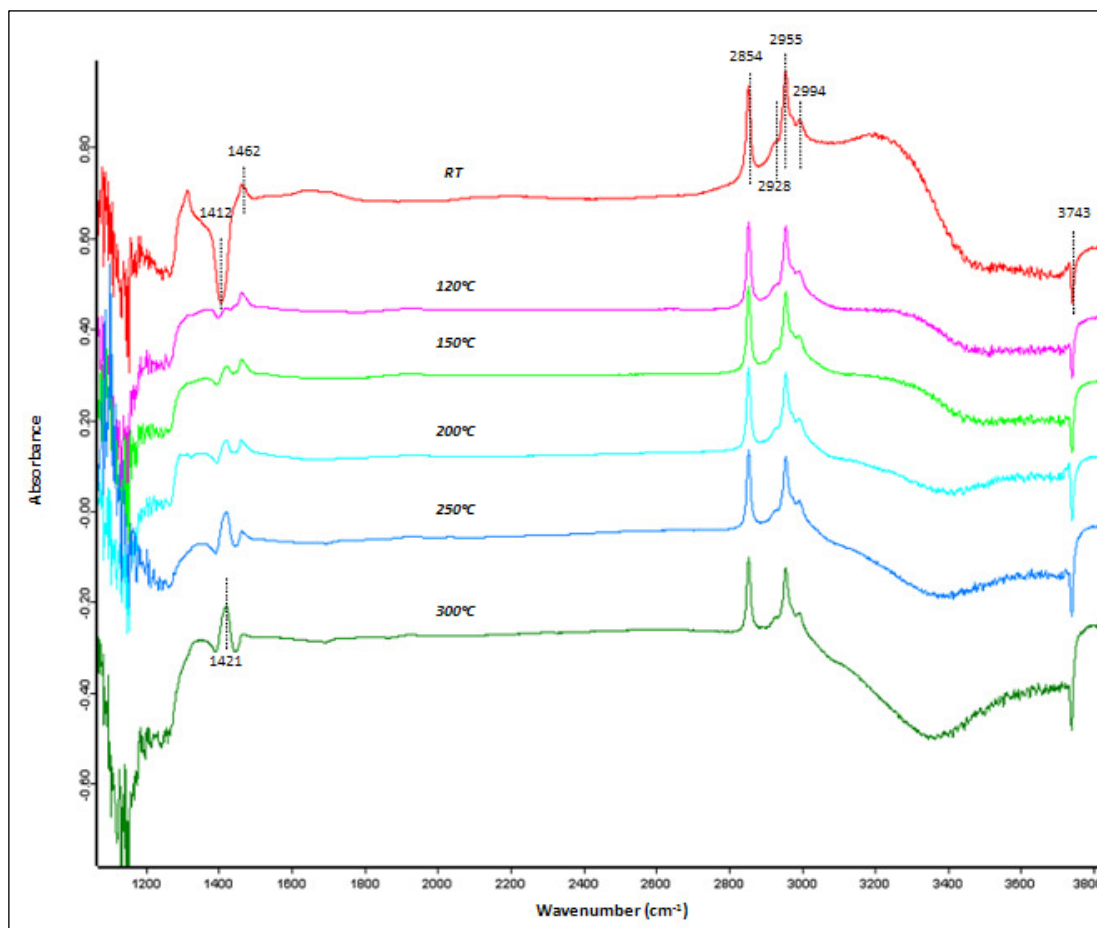


**Figure 71.** FT-IR spectra for methanol adsorption and desorption on NS4R2 catalyst at different temperatures : RT, 120°C, 150°C, 200°C, 250°C, 300°C

Alcohols are adsorbed on the acid sites of ion-exchange resin catalysts. The negative peak at  $1412\text{ cm}^{-1}$  is probably related to the broadening of the peak corresponding to the  $-\text{SO}_3\text{H}$  groups due to the interaction of methanol with the sulfonic acid sites. Methanol adsorption leads to the dissociation of the sulfonic acid groups which is reflected by a negative peak in the difference spectra (Figure 71).

This is due to the disappearance of the S=O bonds, hence the disappearance of the undissociated groups upon methanol adsorption [77]. As temperature increases, by desorption of methanol the peak corresponding to the sulfonic acid groups reemerge but a shift to the right is observed. This suggests an increase in the S=O bond strength due to the interaction of methanol with the proton of the sulfonic group. As temperature increases the SO-H bond in interaction with methanol weakens and consequently an increase in the S=O bond strength is expected. Also, a second peak at  $1462\text{ cm}^{-1}$  is identified at all temperatures, which is thought to be due to the formation of methoxy species for DME synthesis related to methanol adsorbed on sulfonic acid sites. It is also in agreement with literature since the  $\text{CH}_3$  umbrella mode for the methoxy groups are expected to be observed between  $1440\text{-}1470\text{ cm}^{-1}$  [74]. At higher temperatures this peak decreases in intensity due to DME release. This idea was supported by DME adsorption on the same catalyst, results of which will be presented in the next sections. These suggest that methanol is probably adsorbed in methoxy form on the sulfonic acid sites by dissociation of one hydrogen atom. These sites are identified as “type 2” sites ( $\text{S}_2$ ).

Similar peaks were observed for methanol adsorption and desorption on NS3R1 as shown in Figure 72. Same conclusions can be drawn for this catalyst also. The negative peak appearing at  $1405\text{ cm}^{-1}$ , which is thought to be due to the dissociation of sulfonic acid groups with methanol adsorption, is relatively small in intensity when compared with the intensity of the negative peak appearing at  $1412\text{ cm}^{-1}$  for NS4R2. This is because the strength of the sulfonic acid groups in NS3R1 is lower due to the differences in the synthesis procedure which were discussed before. Also, the methanol dehydration activity of NS4R2 was found to be higher than that of NS3R1.

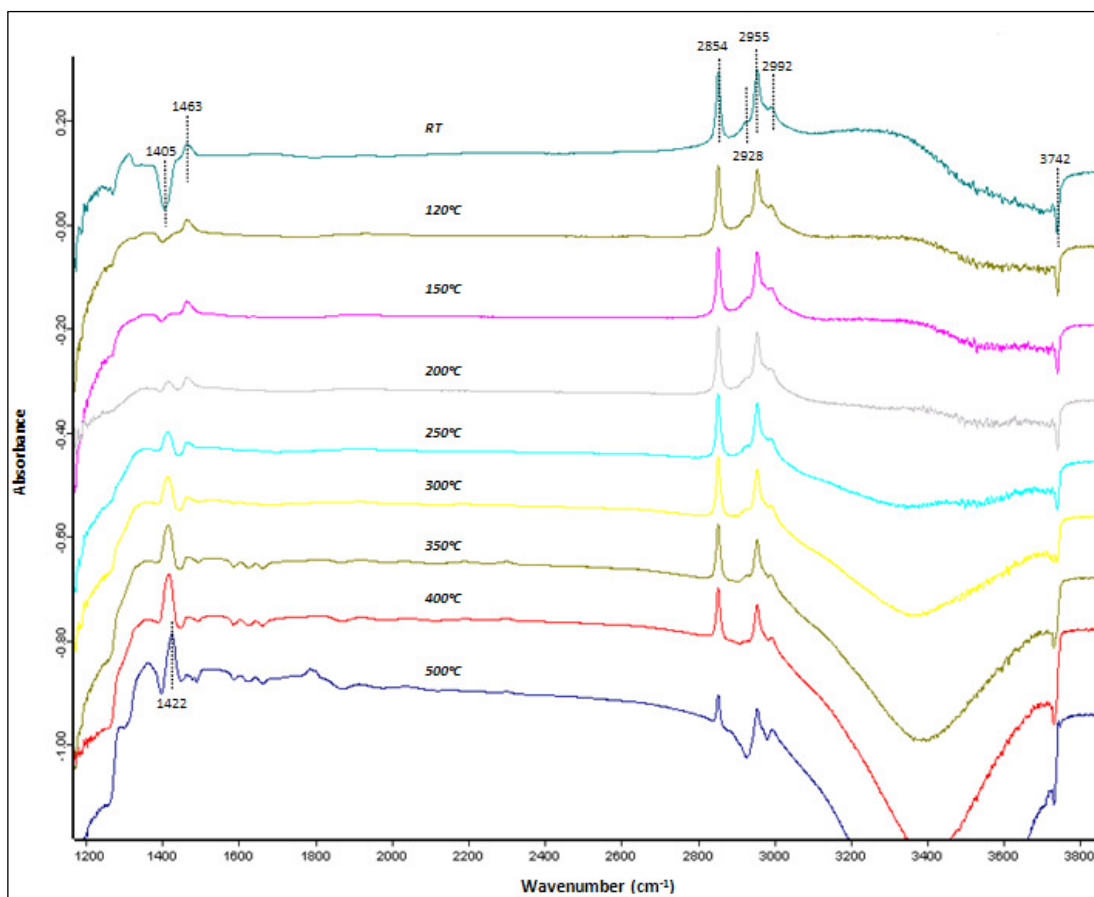


**Figure 72.** FT-IR spectra for methanol adsorption and desorption on NS3R1 catalyst at different temperatures : RT, 120°C, 150°C, 200°C, 250°C, 300°C, 350°C, 400°C, 500°C

Based on the results of the in situ FT-IR analyses of methanol adsorption and desorption on Nafion/Silica catalysts, we may suggest that DME is formed by the reaction of methoxy species adsorbed on the catalyst surface and the physisorbed methanol in molecular form. A possible reaction mechanism for methanol dehydration reaction to produce DME is proposed in Figure 73.

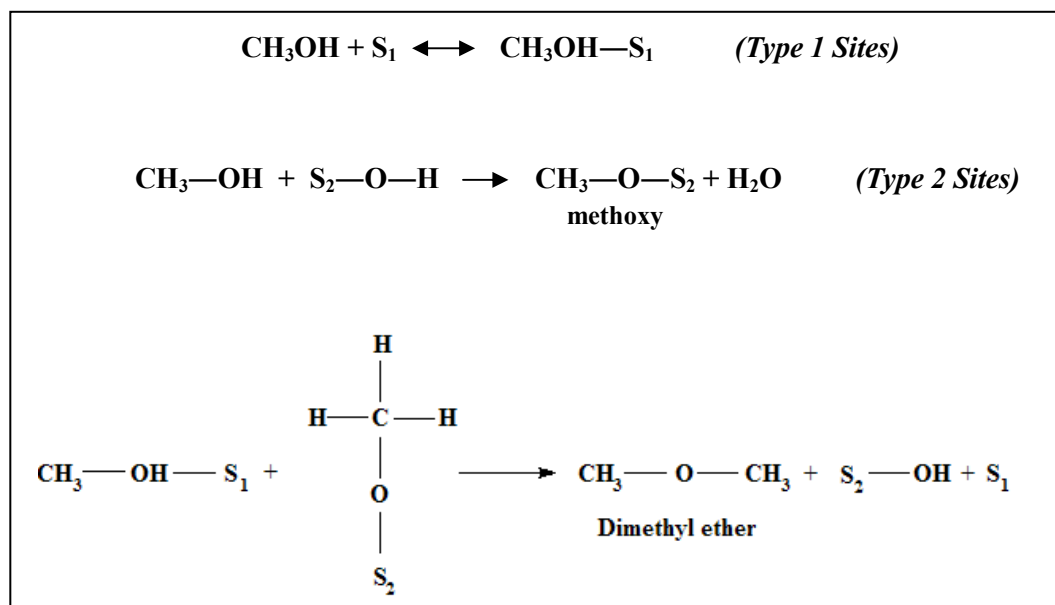


**Figure 73.** Proposed reaction mechanism for methanol dehydration

### 9.10.2. Methanol Adsorption on Nafion/Aluminosilicate Catalyst

A nafion impregnated aluminosilicate catalyst (NFMAS3) synthesized by a nafion/aluminosilicate ratio of 0.20 was tested in in situ methanol adsorption. After drying, a peak at  $1374\text{ cm}^{-1}$  appeared (Figure 87 in Appendix E), which was attributed to the undissociated sulfonic acid groups on the dehydrated nafion resin impregnated into the mesoporous aluminosilicate. The spectra of methanol adsorption and desorption with respect to temperature is shown in Figure 74. Between  $3000\text{-}3400\text{ cm}^{-1}$  OH stretch of hydrogen-bonded network of physically adsorbed methanol molecules are observed. The peaks at  $2853$ ,  $2957$  and  $2997\text{ cm}^{-1}$  are again assigned to  $\text{CH}_3\text{O-Si}$  groups. The peak at  $2923\text{ cm}^{-1}$  may be due to the methanol adsorbed on the active sites of the catalyst. The negative peak at  $1376\text{ cm}^{-1}$  signifies dissociation of sulfonic groups upon methanol adsorption and the appearance of the peaks at  $1466\text{ cm}^{-1}$  is related to the methoxy functional groups formed on the surface, which later take place in DME formation with an increase in temperature.

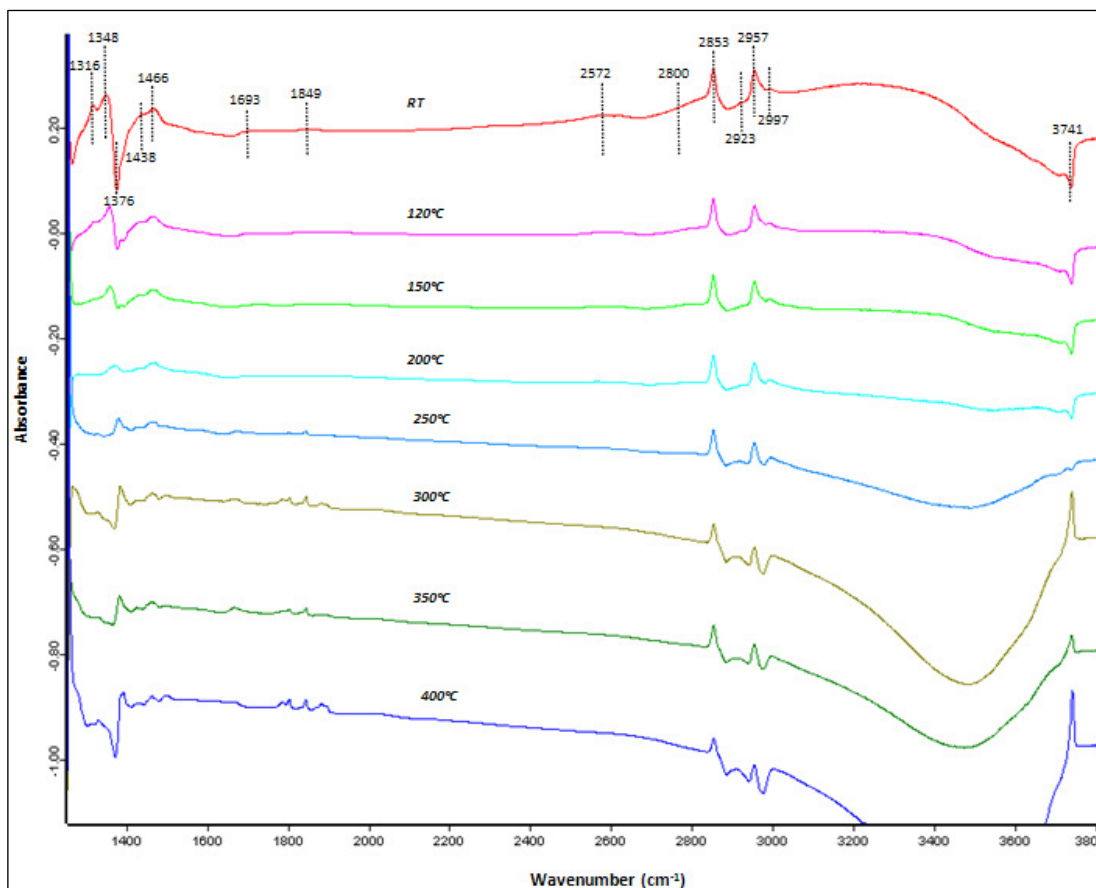


**Figure 74.** FT-IR spectra for methanol adsorption and desorption on NFMAS3 catalyst at different temperatures : RT, 120°C, 150°C, 200°C, 250°C, 300°C, 350°C, 400°C

### 9.10.3. Methanol Adsorption on STA/Silica Catalyst

Prior to methanol exposure, the STA/Silica catalyst, TRC-75-400, was dried at 300°C for 30 minutes. The resulting spectrum is shown in Figure 88 in Appendix E. Figure 75 shows the methanol adsorption and desorption spectra of TRC-75-400 at different temperatures.

Similar to nafion incorporated catalysts, the FT-IR spectrum of methanol adsorption on TRC-75-400 shows a broad band (between 3000-3400  $\text{cm}^{-1}$ ), which is due to the OH stretch of hydrogen-bonded network of adsorbed methanol molecules.

The intensity of this broad band decreases with temperature. The sites covered by these physically adsorbed methanol molecules are identified as “type 1” sites ( $S_1$ ).

Here, in addition to the peaks at 2855, 2956 and 2995  $\text{cm}^{-1}$  which are due to the methoxide adsorbed on silica, two distinct peaks were observed at 2833 and 2932  $\text{cm}^{-1}$ . Based on the study of Fisher and Bell [75], where the additional peaks in the C-H stretching region at 2830 and 2933  $\text{cm}^{-1}$  were assigned to  $\text{CH}_3\text{O-Zr}$  for methanol adsorption on a  $\text{Cu/ZrO}_2/\text{SiO}_2$  catalyst, these peaks in the FT-IR spectra of TRC-75-400 are thought to be due to the methoxy species formed on the tungsten/tungsten oxide sites related to the silicotungstic acid units. A similar observation was also reported in the study of Kumar et al. [78], where additional peaks (at 2837  $\text{cm}^{-1}$  and 2929  $\text{cm}^{-1}$ ) observed in the C-H stretching region upon methanol adsorption on  $\text{U}_3\text{O}_8/\text{MCM-48}$  samples were assigned to methoxy groups bonded to uranium sites ( $\text{U-OCH}_3$ ). The intensities of these peaks (2833 and 2932  $\text{cm}^{-1}$ ) in Figure 75 are nearly half the intensities of the peaks belonging to methoxide on silica (2855 and 2956  $\text{cm}^{-1}$ ). This supports our suggestion since the atomic ratio of W/Si was adjusted as 0.40 in the synthesis of the STA/Silica catalysts. As temperature increased, a continuous decrease was observed in the intensities of the methoxy bands at 2833 and 2932  $\text{cm}^{-1}$ , which is probably due to the involvement of these sites in methanol dehydration reaction. Thus, these sites were identified as “type 2” sites ( $S_2$ ).

Peaks at 1437 and 1454  $\text{cm}^{-1}$ , related to the  $\text{CH}_3$  umbrella mode of methoxy species, were observed with a decreasing intensity as temperature rises. Over 250°C, where the maximum activity was observed with the STA/Silica catalysts, these peaks almost disappear due to the increasing rate of methanol dehydration reaction to form and release DME. A reaction mechanism similar to that of Nafion/Silica catalysts is possible for methanol dehydration on STA/Silica catalysts.

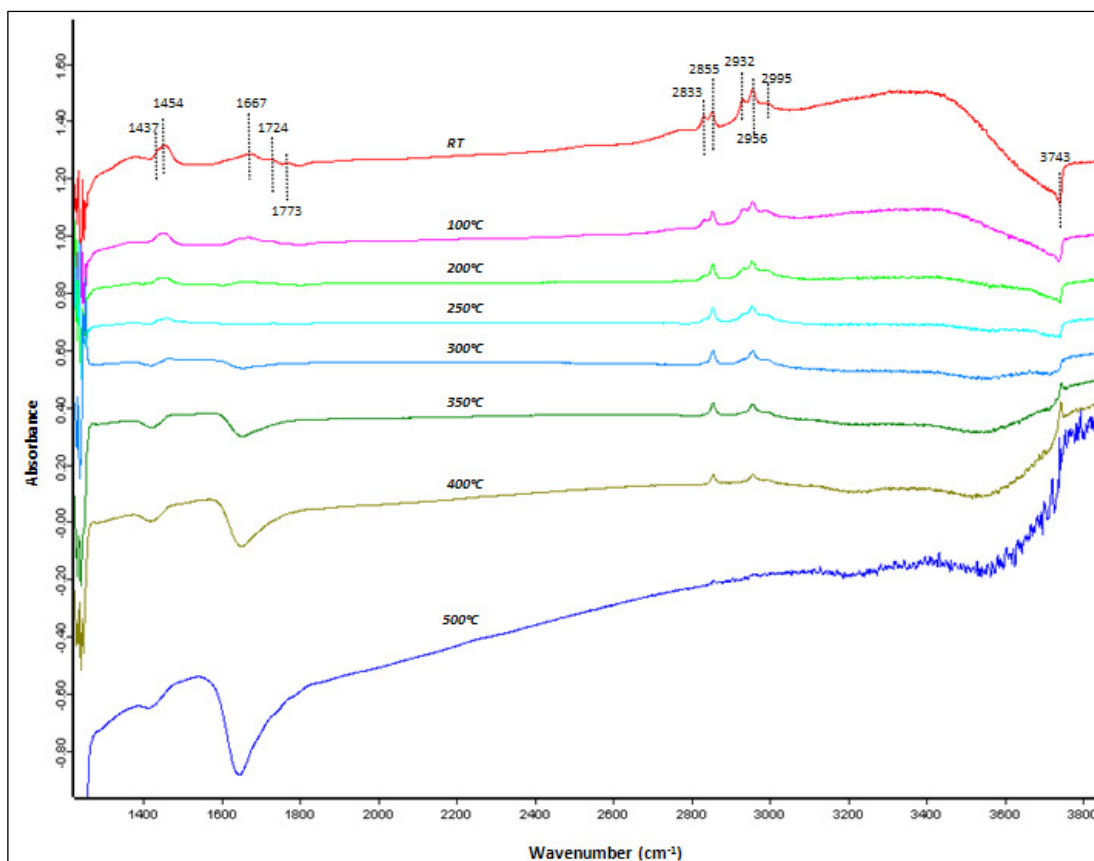


**Figure 75.** FT-IR spectra for methanol adsorption and desorption on TRC-75-400 catalyst at different temperatures : RT, 100°C, 200°C, 250°C, 300°C, 350°C, 400°C, 500°C

#### 9.10.4. Methanol Adsorption on STA/Aluminosilicate Catalyst

The STA/Aluminosilicate catalyst (STAMAS) which was found to be highly active in methanol dehydration reaction was first dried at 300°C for 30 minutes and then tested in in situ methanol adsorption and desorption studies. The FT-IR spectra obtained for STAMAS at different temperatures are given in Figure 76.

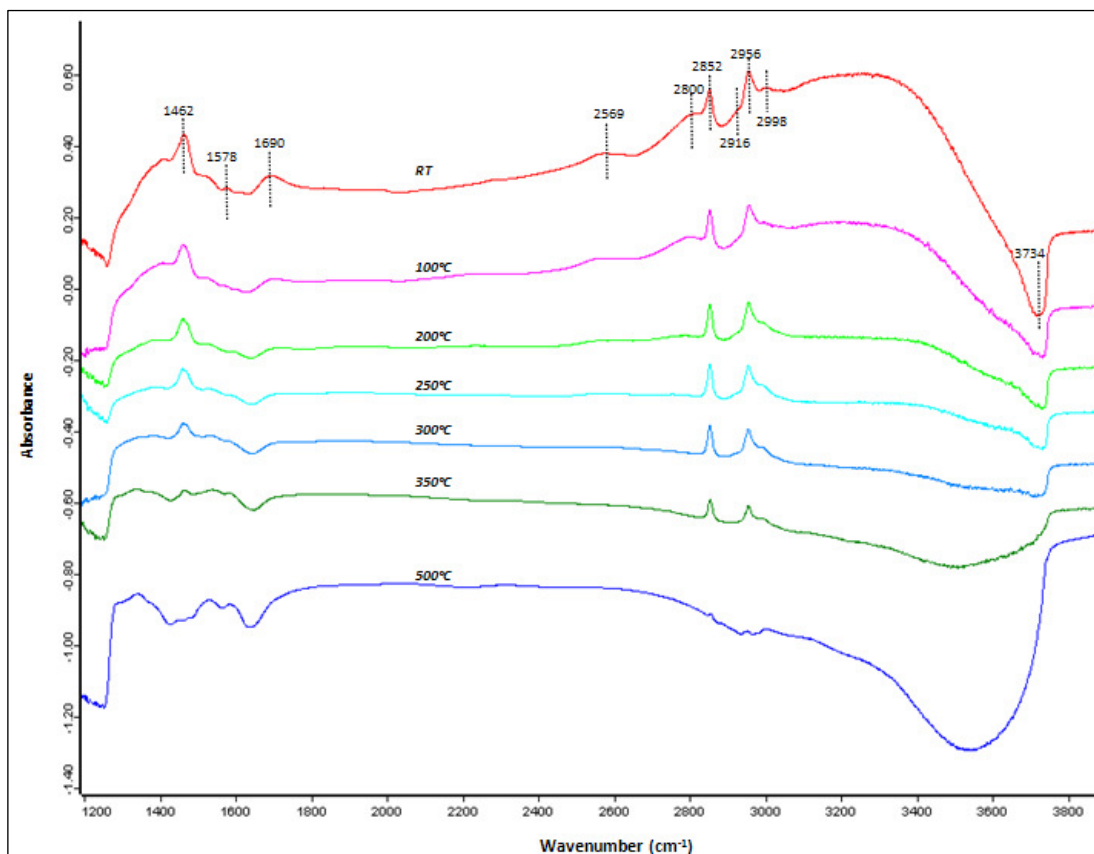


**Figure 76.** FT-IR spectra for methanol adsorption and desorption on STAMAS catalyst at different temperatures : RT, 100°C, 200°C, 250°C, 300°C, 350°C, 500°C

The spectra are quite similar to those obtained for NFMAS3. Except that, the negative peak belonging to the methanol adsorbed on the sulfonic groups are absent for the case of STAMAS. The broad band between 3000-3400  $\text{cm}^{-1}$  is due to the OH stretch of hydrogen-bonded network of adsorbed methanol molecules and the intensity of this broad band again decreases with temperature. The broad bands at 2569 and 2800  $\text{cm}^{-1}$  are identical to the bands at 2572 and 2800  $\text{cm}^{-1}$  observed for NFMAS3 (Figure 74). They are thought to be due to the aluminosilicate support. The peak at 1462  $\text{cm}^{-1}$  is much higher in intensity for STAMAS which may be explained by the much higher activity of STAMAS when compared to NFMAS3 and it again supports our idea that this band is related to the methoxy species involved in methanol dehydration reaction to form DME. Similar to the previous catalysts, the

bands in the C-H stretching region 2852, 2916, 2956 and 2998  $\text{cm}^{-1}$  are also present in the FT-IR spectra of STAMAS.

#### 9.10.5. DME Adsorption on the Nafion/Silica Catalyst

Adsorption and desorption of DME on NS4R2 was tested and the resulting spectra are shown in Figure 77.

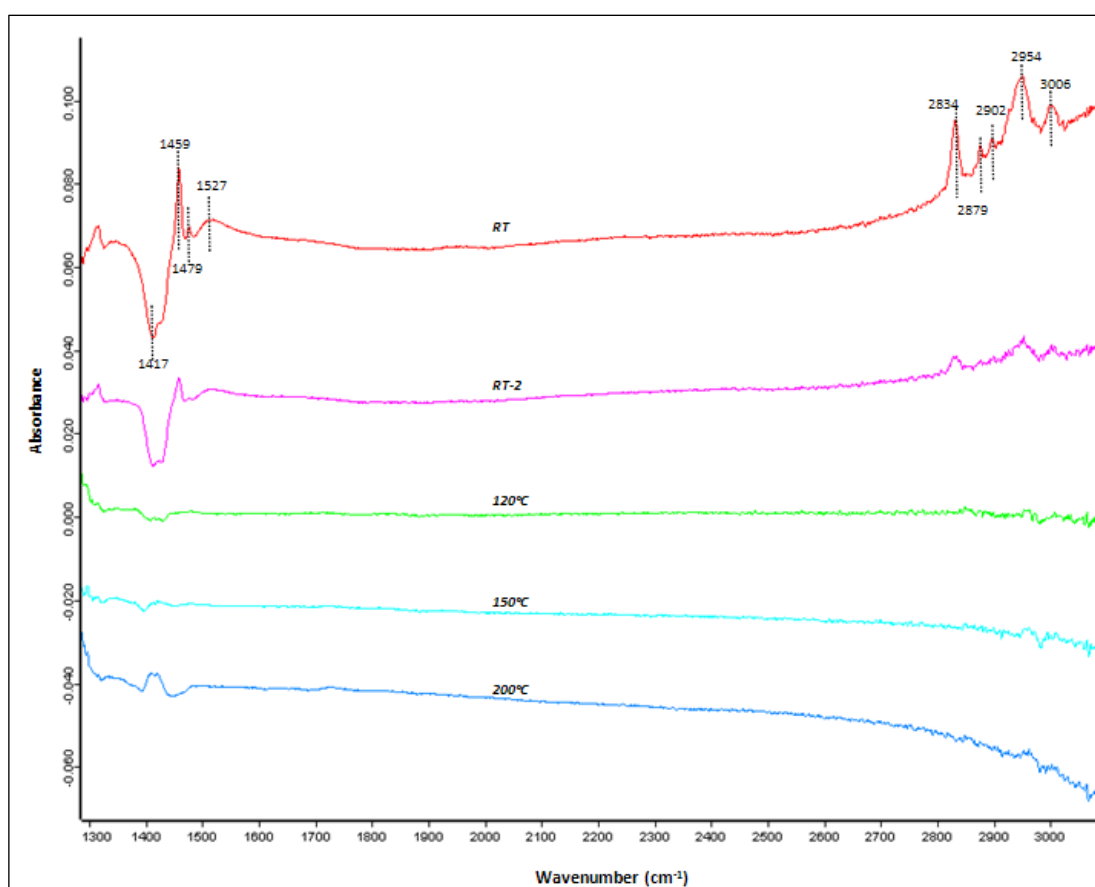


**Figure 77.** FT-IR spectra for DME adsorption and desorption on catalyst at NS4R2 different temperatures : RT, 5 min. after evacuation (RT-2), 120°C, 150°C, 200°C

DME adsorbed on the catalyst gave peaks in the C-H stretching region (2834, 2879, 2902, 2954 and 3006  $\text{cm}^{-1}$ ). The sharp peak at 1459  $\text{cm}^{-1}$  is identified. This

proves our previous conclusions derived from the methanol adsorption spectra that this peak is related to the formation of methoxy functional groups for DME synthesis. In the study of Tanaka [79] also, a band near  $1460\text{ cm}^{-1}$  was assigned to the methyl deformation vibration in  $\text{O-CH}_3$  group referring to the wavenumber of that found in dimethyl ether ( $1466\text{ cm}^{-1}$ ). An additional small peak at  $1479\text{ cm}^{-1}$  and a broad peak at  $1527\text{ cm}^{-1}$  was also observed in this region. It was observed that DME was quickly desorbed from the catalyst even at room temperature 5 minutes after evacuation (spectrum RT-2). When temperature was increased to  $120^\circ\text{C}$  or higher, the peaks in the C-H stretching region and the sharp peak at  $1459\text{ cm}^{-1}$  completely disappeared. This shows that our product, dimethyl ether, is not being adsorbed on the nafion/silica catalyst (NS4R2) synthesized.

#### **9.10.6. DME Adsorption on the STA/Silica Catalyst**

FT-IR spectra of DME adsorption on STA/Silica catalyst (TRC-75-400) is given in Figure 78. In the C-H stretching region peaks at 2840, 2877, 2956 and  $2982\text{ cm}^{-1}$  were observed. They are in agreement with the data given in literature [80] for DME adsorption on  $\text{Nb}_2\text{O}_5$  and  $\text{NbOPO}_4$ . The sharp peak at  $1459\text{ cm}^{-1}$  is again identified. With an increase in temperature complete desorption of DME takes place. Similar to our previous conclusion for the nafion/silica catalyst, for the STA/silica catalyst also we can conclude that DME is not being strongly adsorbed on the surface.

On the other hand, the temperature dependent in situ methanol desorption spectra of all the catalysts revealed that methanol was strongly adsorbed on all the catalysts synthesized and tested in this work.

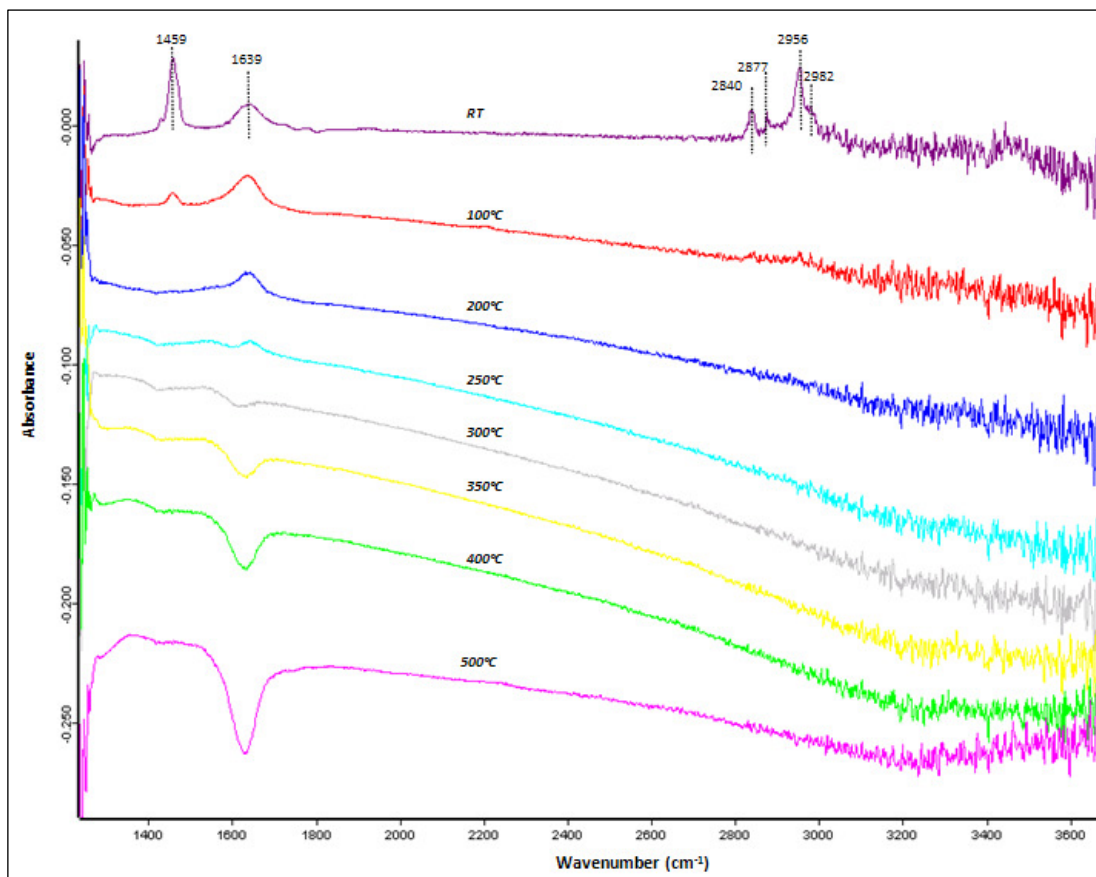


**Figure 78.** FT-IR spectra for DME adsorption and desorption on TRC-75-400 catalyst at different temperatures : RT, 100°C, 200°C, 250°C, 300°C, 350°C, 400°C, 500°C

## CHAPTER 10

### CONCLUSIONS AND RECOMMENDATIONS

In this study, novel nafion and heteropolyacids (silicotungstic acid and tungstophosphoric acid) incorporated mesoporous catalytic materials were synthesized by one-pot hydrothermal and impregnation procedures. The synthesized materials were characterized by using a variety of techniques including XRD, BET, EDS, XPS, TGA-DTA, SEM, FTIR, EDX elemental mapping and DRIFTS of pyridine adsorption. The activities of these catalysts were tested in the synthesis of diesel-fuel alternate dimethyl ether from methanol dehydration and they were compared in terms of their nafion or heteropolyacid loading, techniques and conditions applied during surfactant removal step, etc. In addition, in situ infrared studies were done by adsorbing methanol and DME on the samples and spectra was recorded to observe the desorption of them with an increase in temperature. The conclusions achieved based on these experimental studies are summarized as follows.

The synthesized STA/Silica catalysts were found to have well dispersed structures with no formation of tungsten oxide crystals different from the previously synthesized STA/Silica catalysts in literature, which is thought to be due to carrying out the hydrothermal synthesis in a fully sealed autoclave under autogeneous pressure. STA was successfully incorporated and the elemental mapping analysis of W and Si proved that these elements were perfectly dispersed in the structure of the catalyst. FTIR analyses showed that the chemical bonds belonging to the Keggin units of STA were preserved and DRIFTS of pyridine adsorption analyses showed the presence of strong Brønsted acid sites. Pure heteropolyacids are nonporous and have extremely low specific surface areas (1-5 m<sup>2</sup>/g). According to nitrogen adsorption analyses the surface areas of the novel catalysts were between 187-252

m<sup>2</sup>/g. Catalytic activity tests of these materials in methanol dehydration reaction revealed that in the presence of the STA/Silica catalyst containing a W/Si ratio of 0.33 and calcined at 350°C (TRC-75(L)), a methanol conversion of 60% and a DME selectivity of about 100% could be obtained at 250°C at a space time of 0.27 s.g.cm<sup>-3</sup>. This catalyst showed to be more active and more resistant to coke formation than the previously synthesized WO<sub>x</sub>-Silicate structured catalysts. Formaldehyde formation was observed as the main byproduct at lower temperatures. Calcination at 400°C decreased the activity due to the deactivation of STA phase at this temperature. Applying supercritical carbon dioxide extraction after washing with deionized water seemed to have no effect on the catalytic activity. Carrying out the reaction at a higher space time (0.41 s.g.cm<sup>-3</sup>) resulted in an increase in DME yield (80% at 250°C) as expected.

By synthesizing a TPA/Silica catalyst following a similar synthesis procedure with the same W/Si molar ratio of 0.40, the effect of TPA was compared as an active component. The surface area of this catalyst was found as 143 m<sup>2</sup>/g. About 30% methanol conversion was obtained at 250°C at a space time of 0.27 s.g.cm<sup>-3</sup>. The activity of TPA/Silica (TPA-75(L)) catalyst was lower than that of the STA/Silica catalyst (TRC-75(L)).

In addition, a STA/Aluminosilicate catalyst (STAMAS) prepared by impregnation procedure was tested in methanol dehydration and this catalyst was found to be quite active. 75% DME yield was obtained at 250°C when the space time was adjusted to 0.27 s.g.cm<sup>-3</sup>. Although its catalytic activity was found to be higher than TRC-75(L), STAMAS has a drawback due to its synthesis procedure. This catalyst is expected to lose impregnated STA if it is washed with polar solvents. So it cannot be used in liquid phase reactions.

The second part of this work consists of synthesizing nafion incorporated mesoporous catalysts. First, nafion/silica catalysts were prepared by one-pot hydrothermal synthesis method. Cetyltrimethylammonium bromide was used as the surfactant, TEOS was used as the silica source and two different nafion sources were used each containing 5% nafion resin. In surfactant removal step, different treatments were applied including calcination at 250°C and 350°C or washing with 1 M or 2 M of sulfuric acid solution of ethanol for 6 or 12 hours by using refluxing technique or by keeping at room temperature. The surface areas of the materials were found to

vary between 595-792 m<sup>2</sup>/g, which is quite high when compared to the surface area of pure nonporous nafion resin (0.02 m<sup>2</sup>/g). All the catalysts had pore diameters of 4.3 nm. As far as the catalytic activity of the materials were concerned, the best treatment was found to be refluxing in SAE solution for 6 hours and further refluxing in pure ethanol for another 6 hours. Optimum nafion loading on the catalyst could be achieved when the nafion/silica weight ratio in the synthesis solution was adjusted to 0.15. The highest methanol conversion obtained with the Nafion/Silica catalysts was 40% at 300°C at 0.27 s.g.cm<sup>-3</sup> achieved in the presence NS4R2 with a DME selectivity approaching to 100%. Indeed, the concentration of Brönsted acid sites in the structure of NS4R2 was found to be the highest among the Nafion/Silica catalysts synthesized. Furthermore, nafion/aluminosilicate and nafion/ $\alpha$ -alumina catalysts were prepared by following impregnation route. Their catalytic activities in methanol dehydration showed that when compared to the pure aluminosilicate and  $\alpha$ -alumina, use of these novel nafion impregnated catalysts did not result in a significant increase in methanol conversion. One-pot hydrothermal synthesis proved to be a much better method to obtain nafion incorporated porous catalysts.

Among the hydrothermally synthesized catalysts in this work, TRC-75(L) (the most active STA/Silica catalyst) showed higher activity than NS4R2 (the most active Nafion/Silica catalyst). However, in terms of stability and tolerance to coke formation, Nafion/Silica catalysts are more suitable for catalytic applications showing considerable activity even at low temperatures.

Some of the catalysts synthesized in this work (hydrothermally synthesized Nafion/Silica, STA/Silica and STA/Aluminosilicate, Nafion/Aluminosilicate by impregnation) were tested in in situ infrared methanol and DME adsorption-desorption studies. Due to methanol adsorption, several peaks were observed in the C-H stretching region in the spectra of all the catalysts, which were assigned to methoxide on silica based on the studies in literature. The in situ FT-IR spectra showed that methanol was adsorbed by the formation of methoxy species on the active sites and was also physically adsorbed in molecular form. A possible reaction mechanism was proposed based on these results. Desorption of methanol with temperature showed that methanol was strongly adsorbed on all types of catalysts used in this work through the Brönsted and Lewis sites present at the surfaces of the catalysts, existence of which were proved by DRIFTS of pyridine adsorption

analyses. Bands related to the formation and release of DME were identified and their positions were proved by adsorbing DME on the samples. By observing the desorption of DME with temperature, it was also concluded that our product, dimethyl ether was not being strongly adsorbed on the catalysts synthesized in this work.

Concerning the synthesis of nafion and heteropolyacid incorporated mesoporous catalysts, some modifications in the synthesis procedure can be done. In this work, the surfactant, silica source and the procedure in synthesizing the catalysts were based on the synthesis route of MCM-41. In the future studies, these active components may be incorporated into the structure of mesoporous SBA-15 by again following an acidic one-pot hydrothermal synthesis route and can be tested in DME synthesis from methanol. SBA-15 is known to have a thicker wall with a larger pore size and is more stable than MCM-41. Thus, solid-acid catalysts prepared by adding nafion or heteropolyacids during the one-pot synthesis of SBA-15 may lead to the formation of novel catalytic materials highly active in methanol dehydration to produce DME.

To sum up, in this work it was shown that dimethyl ether, which is a promising transportation fuel alternate for the future, can be produced at high yields in the presence of the silicotungstic acid, tungstophosphoric acid and nafion incorporated catalysts synthesized here. The mesoporous catalysts had high surface areas and pore volumes with nafion and heteropolyacids successfully incorporated into their structure. In addition to their capability of synthesizing this environmentally friendly diesel-alternate fuel from methanol, these novel catalysts may open a pathway in catalyzing many other acid-catalyzed reactions.

## REFERENCES

- [1] Dogu, T., Varisli, D., “Alcohols as Alternatives to Petroleum for Environmentally Clean Fuels and Petrochemicals”, 2007, Turkish Journal of Chemistry, 31, 551-567.
- [2] Fu, Y., Hong, T., Chen, J., Auroux, A., Shen, J., “Surface acidity and the dehydration of methanol to dimethyl ether”, *Thermochimica Acta*, 2005, 434, 22-26.
- [3] Yaripour, F., Baghaei, F., Schmidt, I., Perregaard, J., “Catalytic dehydration of methanol to dimethyl ether over solid acid catalysts”, *Catalysis Communications*, 2005, 6, 147-152.
- [4] An, W., Chuang, K. T., Sanger, A. R., “Dehydration of methanol to dimethyl ether by catalytic distillation”, *The Canadian Journal of Chemical Engineering*, 2004, 82, 948-955.
- [5] Olah, G.A., Goepfert, A., Prakash, G.K.S., “Beyond Oil and Gas: The Methanol Economy”, Wiley-VCH, 2006, Weinheim.
- [6] Wikipedia the Free Encyclopedia, [http://www.wikipedia.org/Main\\_Page](http://www.wikipedia.org/Main_Page), [http://en.wikipedia.org/wiki/Dimethyl\\_ether](http://en.wikipedia.org/wiki/Dimethyl_ether), Last Access Date: June 2009.
- [7] Nexant, ChemSystems Process Evaluation/Research Planning Program, Report Abstract, Dimethyl Ether Technology and Markets, 2008, 07/08-S3.
- [8] JFE Holdings Inc., <http://www.jfe-holdings.co.jp/en/index.html>, <http://www.jfe-holdings.co.jp/en/dme/03-yoto.html>, Last Access Date: June 2009.
- [9] International DME Association, <http://www.aboutdme.org/index.asp?sid=1>, <http://www.aboutdme.org/index.asp?bid=219#Cooking%20&%20Heating>, Last Access Date: March 2009.
- [10] Garimella, S., DME-The Next Gen Fuel, Enzen Global, 2007.

[11] Gray, C., Webster G., A Study of Dimethyl Ether (DME) as an Alternative Fuel for Diesel Engine Applications, CANMET Energy Technology Centre, Natural Resources Canada and Transportation Development Centre, Transport Canada, Advanced Engine Technology Ltd., 2001.

[12] Eberhardt, J.J., Future Fuels for Heavy-Duty Trucks, *Alternative Fuels in Trucking*, 1997, 6, 2.

[13] Bourg, H.M., “Future Prospective of DME”, 23rd World Gas Conference, 2006, Amsterdam.

[14] Vishwanathan, V., Jun, K.W., Kim, J.W., Roh, H.S., “Vapour phase dehydration of crude methanol to dimethyl ether over Na-modified H-ZSM-5 catalysts”, *Applied Catalysis A: General*, 2004, 276, 251-255.

[15] Yaripour, F., Baghaei, F., Schmidt, I., Perregaard, J., “Synthesis of dimethyl ether from methanol over aluminium phosphate and silica-titania catalysts”, *Catalysis Communications*, 2005, 6, 542-549.

[16] Fei, J., Hou, Z., Zhu, B., Lou, H., Zheng, X., “Synthesis of dimethyl ether (DME) on modified HY zeolite and modified HY zeolite-supported Cu-Mn-Zn catalysts”, *Applied Catalysis A: General*, 2006, 304, 49-54.

[17] Xu, M., Lunsford, J.H., Goodman, D.W., Bhattacharyya, A., “Synthesis of dimethyl ether (DME) from methanol over solid-acid catalysts”, *Applied Catalysis A: General*, 1997, 149, 289-301.

[18] Khom-in, J., Prasertdam, P., Panpranot, J., Mekasuwandumrong, O., “Dehydration of methanol to dimethyl ether over nanocrystalline Al<sub>2</sub>O<sub>3</sub> with mixed  $\gamma$ - and  $\chi$ - crystalline phases”, *Catalysis Communications*, 2008, 9, 1955–1958.

[19] Oye, G., Sjöblom, J., Stöcker, M., “Synthesis, characterization and potential applications of new materials in the mesoporous range”, *Advances in Colloid and Interface Science*, 2001, 89-90, 439-466.

[20] Sayari, A., Liu, P., “Non-silica periodic mesostructured materials: recent progress”, *Microporous Materials*, 1997, 12, 149-177.

[21] Taguchi, A., Schuth, F., "Ordered mesoporous materials in catalysis", *Microporous and Mesoporous Materials*, 2005, 77, 1-45.

[22] Roth, W.J. and Vartuli, J.C., "Synthesis of mesoporous molecular sieves", *Studies in Surface Science and Catalysis*, 2005, 157, 91-110.

[23] Alfredsson, V., Keung, M., Monnier, A., Stucky, G.D., Ungerb, K.K., Schuth, F., "High-resolution Transmission Electron Microscopy of Mesoporous MCM-41 Type Materials", *J. Chem. Soc., Chem. Commun.*, 1994, 921-922.

[24] Beck, J.S., Vartuli, J.C., Roth, W. J., Leonowicz, M. E., Kresge, C. T., Schmitt, K. D., Chu, C. T.W., Olson, D. H., Sheppard, E. W., McKullen, S.B., Higgins, J.B., Schlenker, J.L., "A new family of mesoporous molecular sieves prepared with liquid crystal templates", *J. Am. Chem. Soc.*, 1992, 114, 10834-10843.

[25] Varisli, D., "Kinetic Studies for Dimethyl ether and Diethyl ether Production", Ph.D. Thesis, Middle East Technical University, Ankara, Turkey, September 2007.

[26] Terasaki, O., "Mesoporous Crystals and Related Nano-Structured Materials", *Studies in Surface Science and Catalysis*, 2004, 148.

[27] Gucbilmez, Y., Dogu, T., Balci, S., "Ethylene and Acetaldehyde Production by Selective Oxidation of Ethanol Using Mesoporous V-MCM-41 Catalysts", *Ind. Eng. Chem. Res.*, 2006, 45, 3496-3502.

[28] Ozdogan, E., Dogu, T., Dogu, G., "Ni-MCM-41 type mesoporous catalysts synthesized by one-pot hydrothermal procedure for steam reforming of ethanol", *Int. J. Chem. Reactor Eng.*, 2008, 5, A111.

[29] Sener, C., Dogu, T., Dogu, G., "Effects of synthesis conditions on the structure of Pd incorporated MCM-41 type mesoporous nanocomposite catalytic materials with high Pd/Si ratios", *Microporous and Mesoporous Materials*, 2006, 94, 89-98.

[30] Wikipedia the Free Encyclopedia, [http://www.wikipedia.org/Main\\_Page](http://www.wikipedia.org/Main_Page), <http://en.wikipedia.org/wiki/Heteropolyacid>, Last Access Date: July 2009.

[31] Cavani, F., "Heteropolycompound-based catalysts: A blend of acid and oxidizing properties", *Catalysis Today*, 1998, 41, 73-86.

- [32] Okuhara, T., Mizuno, N., Misono, M., “Catalysis by heteropoly compounds-recent developments”, *Applied Catalysis A: General*, 2001, 222, 63–77.
- [33] Kozhevnikov, I.V., “Fine organic synthesis with the aid of heteropolycompounds”, *Russian Chemical Reviews*, 1993, 62 (5), 473-491.
- [34] Okuhara, T., Nishimura, T., Misono, M., “Novel Microporous Solid "Superacids":CsxH3-x PW12O40 (2<x<3)”, 11 th International Congress on Catalysis - 40th Anniversary, *Studies in Surface Science and Catalysis*, 1996, 101, 581-590.
- [35] Mizuno, N., Misono, M., “Heteropolyanions in catalysis”, *Journal of Molecular Catalysis*, 1994, 86, 319-342.
- [36] Misono, M., Ono, I., Koyano, G., Aoshima, A., “Heteropolyacids. Versatile green catalysts usable in a variety of reaction media”, *Pure Appl. Chem.*, 2000, 72, 7, 1305-1311.
- [37] Misono, M., Okuhara, T., Ichiki, T., Arai, T., Kanda, Y., “Pseudoliquid Behavior of Heteropoly Compound Catalysts. Unusual Pressure Dependencies of the Rate and Selectivity for Ethanol Dehydration”, *J. Am. Chem.Soc.*, 1987, 109 (18), 5535-5536.
- [38] Misono, M., “Acid catalysts for clean production. Green aspects of heteropolyacid catalysts”, *C. R. Acad. Sci. Paris, Série IIc, Chimie/Chemistry*, 2000, 3, 471–475.
- [39] Varisli, D., Dogu, T., Dogu, G., “Ethylene and diethyl-ether production by dehydration reaction of ethanol over different heteropolyacid catalysts”, *Chemical Engineering Science*, 2007, 62, 5349-5352.
- [40] Herrera, J.E., Kwak, J.H., Hu, J.Z., Wang, Y., Peden, C.H.F., “Effects of novel supports on the physical and catalytic properties of tungstophosphoric-acid for alcohol dehydration reactions”, *Top. Catal.*, 2008, 49, 259-267.
- [41] Haber, J., Pamin, K., Matachowski, L., Napruszewska, B., Poltowicz, J., “Potassium and Silver Salts of Tungstophosphoric Acid as Catalysts in Dehydration of Ethanol and Hydration of Ethylene”, *Journal of Catalysis*, 2002, 207, 296–306.

[42] Soled, S., Miseo, S., McVicker, G., Gates, W.E., Gutierrez, A., Paes, J., "Preparation of bulk and supported heteropolyacid salts", *Catalysis Today*, 1997, 36, 441-450.

[43] Allaoui, L.A., Aoussi, A., "Effect of the Brønsted acidity on the behavior of CO<sub>2</sub> methanol reaction", *Journal of Molecular Catalysis A: Chemical*, 2006, 259, 281-285.

[44] Taguchi, A., Abe, T., Iwamoto, M., "Non-silica-based mesostructured material. 2 Synthesis of hexagonal superstructure consisting of 11 -tungstophosphate anions and dodecyltrimethylammonium cations", *Microporous and Mesoporous Materials*, 1998, 21, 387-393.

[45] Nowinska, K., Fórmaniak, R., Kaleta, W., Waclaw, A., "Heteropoly compounds incorporated into mesoporous material structure", *Applied Catalysis A: General*, 2003, 256 115-123.

[46] Said, A.E.A., El-Wahab, M.M.A., Alian, A.M., "Perspective catalytic performance of Brønsted acid sites during esterification of acetic acid with ethyl alcohol over phosphotungstic acid supported on silica", *J Chem Technol Biotechnol*, 2007, 82, 513-523.

[47] Vazquez, P., Pizzio, L., Caceres, C., Blanco, M., Thomas, H., Alesso, E., Finkielstein, L., Lantano, B., Moltrasio, G., Aguirre, J., "Silica-supported heteropolyacids as catalysts in alcohol dehydration reactions", *Journal of Molecular Catalysis A: Chemical*, 2000, 161, 223-232.

[48] Varisli, D., Dogu, T., Dogu, G., "Novel Mesoporous Nanocomposite WO<sub>x</sub>-Silicate Acidic Catalysts: Ethylene and Diethylether from Ethanol", *Ind. Eng. Chem. Res.* (doi:10.1021/ie8008154, in press).

[49] Varisli, D., Dogu, T., Dogu, G., "Silicotungstic Acid Impregnated MCM-41-like Mesoporous Solid Acid Catalysts for Dehydration of Ethanol", *Ind. Eng. Chem. Res.*, 2008, 48, 4071.

[50] Harmer, M.A., Farneth, W.E., Sun, Q., "High Surface Area Nafion Resin/Silica Nanocomposites: A New Class of Solid Acid Catalyst", *J. Am. Chem. Soc.*, 1996, 118, 7708-7715.

[51] Harmer, M.A., Sun, Q., Vega, J.A., Farneth, W.E., Heidekum, A., Hoelderich, W.F., “Nafion resin-silica nano-composite solid acid catalysts microstructure-processing-property correlations”, The Royal Society of Chemistry, 2000, 7-14.

[52] Wang, H., Xu, B.Q., “Catalytic performance of Nafion/SiO<sub>2</sub> nanocomposites for the synthesis of  $\alpha$ -tocopherol”, Applied Catalysis A: General, 2004, 275, 247–25.

[53] Fujiwara, M., Kuraoka, K., Yazawa, T., Xu, Q., Tanaka, M., Souma, Y., “Preparation of an MCM-41/Nafion® composite material; a selective catalyst for  $\alpha$ -methylstyrene dimerization”, Chem. Commun., 2000, 1523–1524.

[54] Fujiwara, M., Shiokawa, K., Zhub, Y., “Preparation of Mesoporous Silica/Polymer Sulfonate Composite Materials,” Journal of Molecular Catalysis A: Chemical, 2007, 264, 153–161.

[55] Wang, S., Guin, J.A., “Si-MCM41 supported sulfated zirconia and nafion for ether production”, Energy&Fuels, 2001, 15, 666-670.

[56] Török, B., Kiricsi, I., Molnar, A., Olah, G.A., “Acidity and Catalytic Activity of a Nafion-H/Silica Nanocomposite Catalyst Compared with a Silica-Supported Nafion Sample”, Journal of Catalysis, 2000, 193, 132–138.

[57] Bringué, R., Tejero, J., Iborra, M., Izquierdo, J.F., Fité, C., Cunill, F., “Supported Nafion catalyst for 1-pentanol dehydration reaction in liquid phase”, Chemical Engineering Journal, 2008, 145, 135–141.

[58] Alvaro, M., Corma, A., Das, D., Fornés, V., García, H., “Nafion”-functionalized mesoporous MCM-41 silica shows high activity and selectivity for carboxylic acid esterification and Friedel–Crafts acylation reactions”, Journal of Catalysis, 2005, 231, 48–55.

[59] Alvaro, M., Corma, A., Das, D., Fornés, V., García, H., “Single-step preparation and catalytic activity of mesoporous MCM-41 and SBA-15 silicas functionalized with perfluoroalkylsulfonic acid groups analogous to Nafion”, Chem.Comm., 2004, 956–957.

[60] Martinez, F., Morales, G., Martin, A., van Grieken, R. “Perfluorinated Nafion-modified SBA-15 materials for catalytic acylation of anisole”, Applied Catalysis A: General, 2008, 347, 169–178.

- [61] Sun, Q., Harmer, M.A., Farneth, W.E., “An Extremely Active Solid Acid Catalyst, Nafion Resin/Silica Composite, for the Friedel-Crafts Benzylation of Benzene and p-Xylene with Benzyl Alcohol”, *Ind. Eng. Chem. Res.*, 1997, 36, 5541-5544.
- [62] Botella, P., Corma, A., Lopez-Nieto, J.M., “The Influence of Textural and Compositional Characteristics of Nafion/Silica Composites on Isobutane/2-Butene Alkylation”, *Journal of Catalysis*, 1999, 185, 371–377.
- [63] Laufer, M.C., Hausmann, H., Hölderich, W.F., “Synthesis of 7-hydroxycoumarins by Pechmann reaction using Nafion resin/silica nanocomposites as catalysts”, *Journal of Catalysis*, 2003, 218, 315–320.
- [64] Wang, H., Xu, B.Q., Han, M.H., Xu, C., Min, E.Z., “Nafion/SiO<sub>2</sub> Nanocomposites: High Potential Catalysts for Alkylation of Benzene with Linear C<sub>9</sub>-C<sub>13</sub> Alkenes”, *Chinese Chemical Letters*, 2002, 13, 11, 1121 – 1124.
- [65] Sarsani, V.S.R., Lyon, C.J., Hutchenson, K.W., Harmer, M.A., Subramaniam, B., “Continuous acylation of anisole by acetic anhydride in mesoporous solid acid catalysts: Reaction media effects on catalyst deactivation”, *Journal of Catalysis*, 2007, 245 184–190.
- [66] Varisli, D., Dogu, T., “Production of Clean Transportation Fuel Dimethylether by Dehydration of Methanol Over Nafion Catalyst”, *G.U. Journal of Science*, 2008, 21(2), 37-41.
- [67] Kawi, S., Lai, M.W., “Supercritical fluid extraction of surfactant template from MCM-41”, *Chem. Commun.*, 1998, 1407-1408.
- [68] Wachs, I.E., Fitzpatrick, L.E., “Characterization of Catalytic Materials”, Manning Publications Co., 1992, Greenwich.
- [69] Damyanova, S., Fierro, J.L., Sobrados, I., Sanz, J., “Surface Behavior of Supported 12-Heteropoly Acid As Revealed by Nuclear Magnetic Resonance, X-ray Photoelectron Spectroscopy, and Fourier Transform Infrared Techniques”, *Langmuir*, 1999, 15(2), 469-476.
- [70] Hogarth, W.H.J., Costa, J.C.D., Drennan, J., Lu, G.Q., “Proton conductivity of mesoporous sol-gel zirconium phosphates for fuel cell applications”, *J. Mater. Chem.*, 2004, DOI: 10.1039/b413413n.

[71] Varisli, D., Tokay, K.C., Ciftci, A., Dogu, T., Dogu, G., "Methanol Dehydration Reaction to Produce Clean Diesel Alternative Dimethylether over Mesoporous Aluminosilicate-Based Catalysts", Turkish Journal of Chemistry, 2009, 33, 355-366.

[72] Tokay, K.C. "Dimethyl Ether (DME) Synthesis over Novel Mesoporous Catalysts", M.Sc. Thesis, Middle East Technical University, Ankara, Turkey, August 2008.

[73] Ostrowska, J., Narebska, A., "Infrared study of hydration and association of functional groups in a perfluorinated Nafion membrane", Part 1, Colloid&Polymer Sci., 1983, 261,93-98.

[74] Smith B., "Infrared Spectral Interpretation, A Systematic Approach", CRC Press, 1999, Boca Raton.

[75] Fisher, I.A., Bell, A.T., "A mechanistic study of methanol decomposition over Cu/SiO<sub>2</sub>, ZrO<sub>2</sub>/SiO<sub>2</sub>, and Cu/ZrO<sub>2</sub>/SiO<sub>2</sub>", Journal of Catalysis, 1999, 184, 357-376.

[76] Dogu, T., Boz, N., Aydın, E., Oktar, N., Murtezaoglu, K., Dogu, G., "DRIFT Studies for the Reaction and Adsorption of Alcohols and Isobutylene on Acidic Resin Catalysts and the Mechanism of ETBE and MTBE Synthesis", Ind. Eng. Chem. Res., 2001, 40, 5044-5051.

[77] Thornton, R., Gates, B.C., "Catalysis by Matrix-Bound Sulfonic Acid Groups: Olefin and Paraffin Formation from Butyl Alcohols", Journal of Catalysis, 1974, 34, 275-287.

[78] Kumar D., Varma S., Kamble V.S., Gupta N.M., "The selective adsorption/desorption of methanol over nanosize uranium oxide crystallites dispersed in MCM-48: FT-IR and TPD studies" Journal of Molecular Catalysis A:Chemical, 2004, 223, 251-257.

[79] Tanaka T., "The Infrared Spectra of Methoxy-, Methylmethoxy- and Methoxy Endblocked Dimethyl-polysiloxanes", Bulletin of the Chemical Society of Japan, 1958, 31, 762-766.

[80] Sun, Q., Fu, Y., Yang, H., Auroux, A., Shen, J., "Dehydration of methanol to dimethyl ether over Nb<sub>2</sub>O<sub>5</sub> and NbOPO<sub>4</sub> catalysts: Microcalorimetric and FT-IR studies", Journal of Molecular Catalysis A: Chemical, 2007, 275, 183-193.

## APPENDIX A

### PARAMETERS FOR THE REACTION SYSTEM

#### A.1. GC CALIBRATION FACTORS AND RETENTION TIMES OF THE SPECIES

Gas chromatograph calibration factors and the retention times of the species involved in the methanol dehydration reaction are given in Table 25.

**Table 25.** GC calibration factors and retention times

Species	Calibration Factors	Retention Times
Dimethyl ether	0.76	5.0
Water	2.53	6.9
Formaldehyde	1.33	7.4
Methanol	1.00	7.8

#### A.2. CALCULATION OF FLOW RATES

Liquid methanol is injected at a flow rate of 2.1 mL/hr. Flow rate of methanol in gas phase is calculated as follows.

$$\rho = \frac{PM}{RT} = \frac{1\text{bar} \times 32.04\text{g/mol}}{83.14\text{cm}^3\text{bar/molK} \times 298\text{K}} = 0.0012932\text{g/cm}^3$$

$$\frac{\rho_{liq}}{\rho_{vap}} = \frac{0.79180}{0.0012932} = 612$$

$$2.1ml/hr \times 1cm^3/mL \times 1hr/60min = 0.035cm^3/min$$

$$612 \times 0.035cm^3/min = 21.42cm^3/min = 21.42ml/min$$

By measuring with a soap flow meter, flow rate of helium is adjusted to 10mL / 26sec.

$$\frac{10ml}{26sec} \times 60sec/min = 23.00ml/min$$

The total flow rate in the system is calculated as follows.

$$Q_{MeOH} + Q_{He} = 21.42ml/min + 23.00ml/min = 44.42ml/min$$

The ratio of the flow rate of methanol to the total flow rate is found as 0.48 as shown below.

$$\frac{Q_{MeOH}}{Q_{MeOH} + Q_{He}} = \frac{21.42ml/min}{44.42ml/min} = 0.48$$

### **A.3. EQUATIONS FOR METHANOL CONVERSION, DME YIELD AND DME SELECTIVITY**

$$n_{T,o} = n_{Formaldehyde} + n_{methanol} + 2 \cdot n_{DME}$$

$$x_{methanol} = \frac{n_{T,o} - n_{methanol}}{n_{T,o}}$$

$$S_{DME} = \frac{2 \cdot n_{DME}}{n_{T,o} - n_{methanol}}$$

$$S_{FA} = \frac{n_{FA}}{n_{T,o} - n_{methanol}}$$

$$Y_{DME} = X_{methanol} \times S_{DME}$$

$$Y_{FA} = X_{methanol} \times S_{FA}$$

## APPENDIX B

### SEM IMAGES OF THE MATERIALS

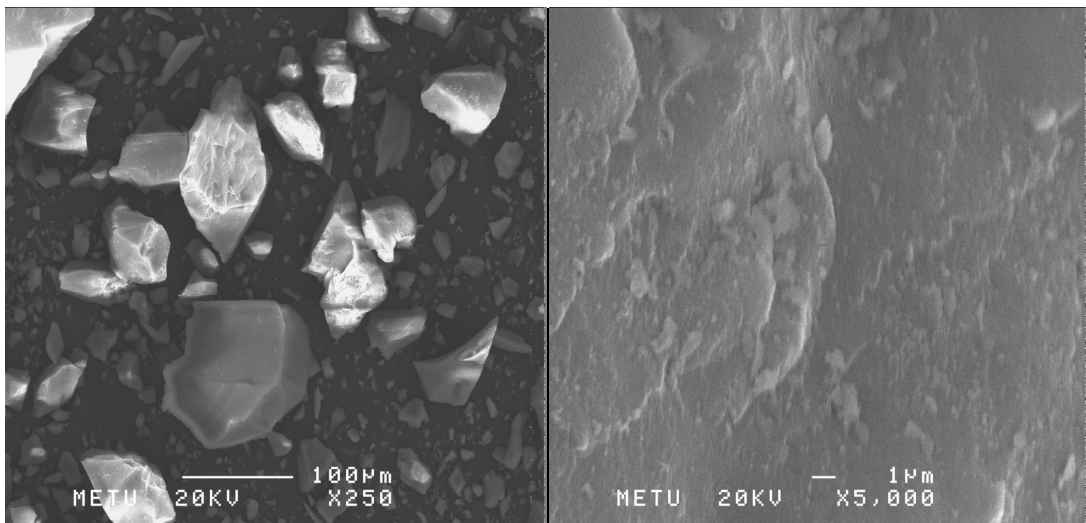


**Figure 79.** SEM images of the nafion/silica catalyst (NS1R)

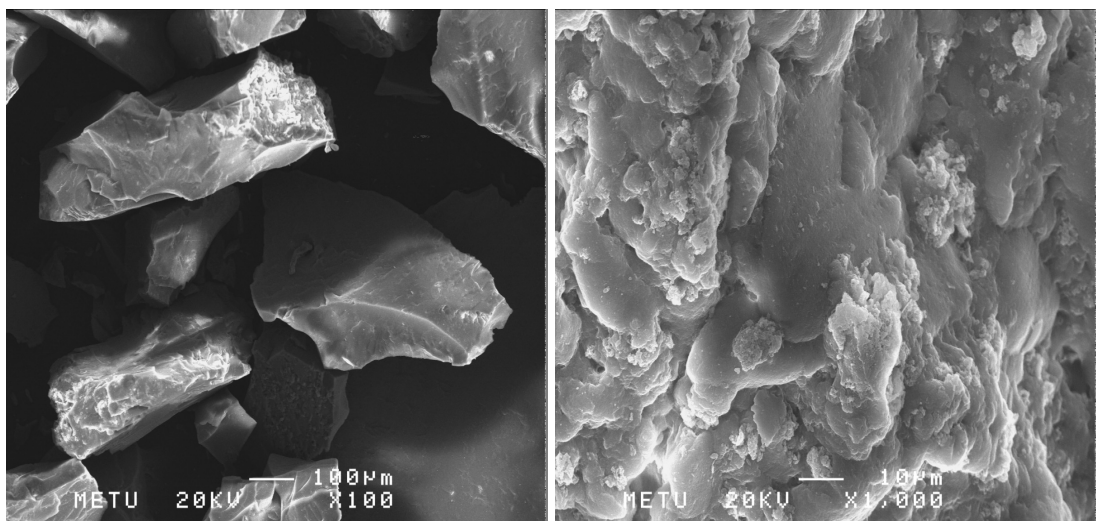


**Figure 80.** SEM images of the nafion/silica catalyst (NS3A)

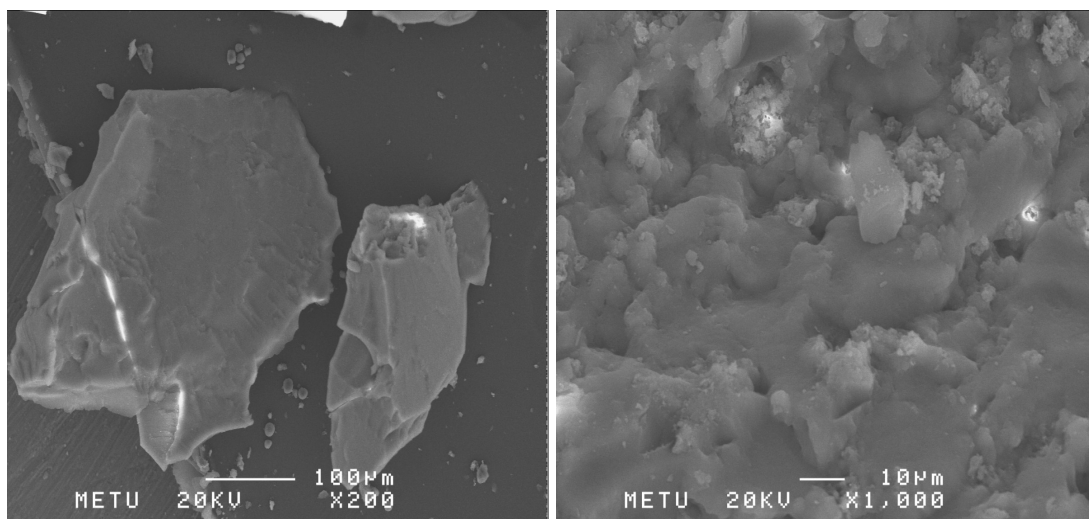


**Figure 81.** SEM images of the nafion/silica catalyst (NS3R2)

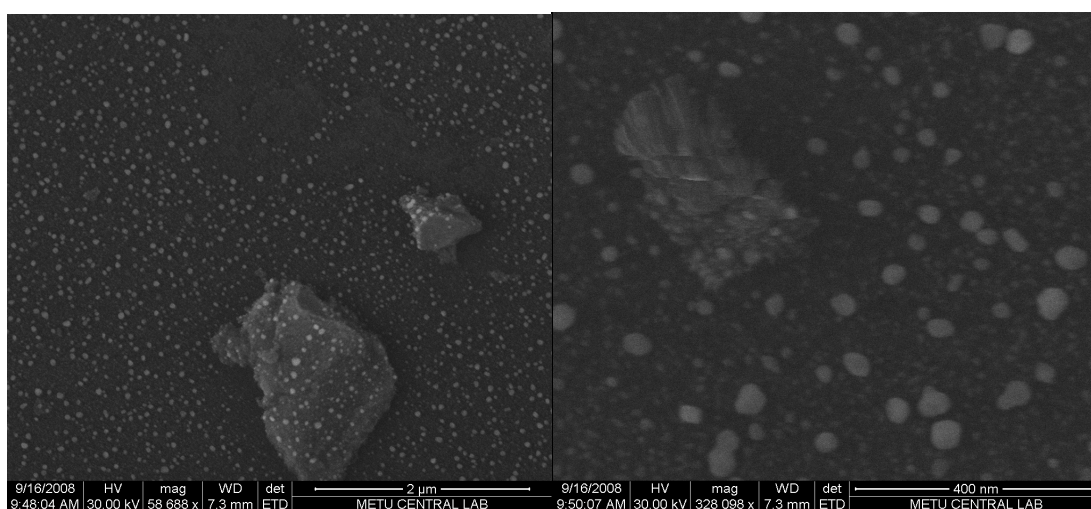


**Figure 82.** SEM images of the nafion/silica catalyst (NS1)

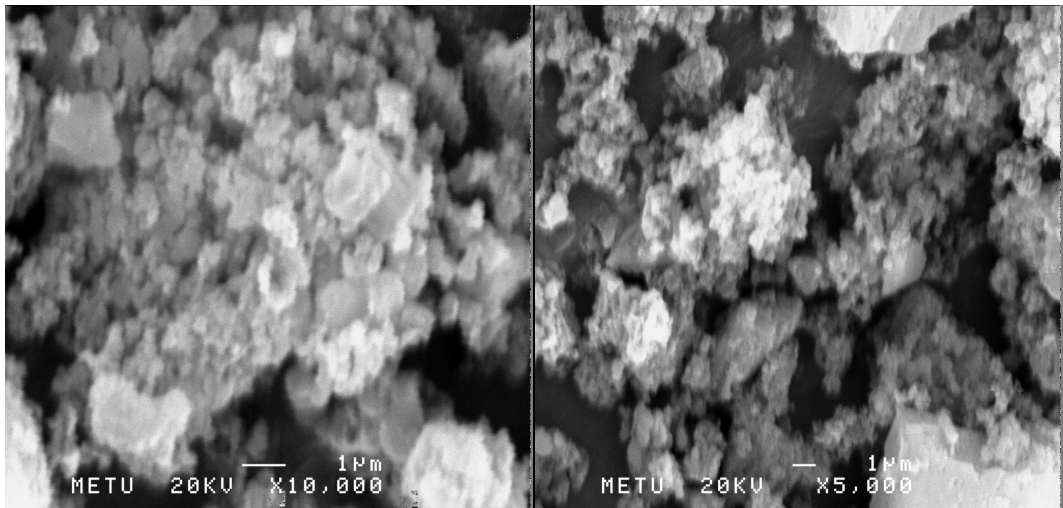


**Figure 83.** SEM images of the nafion/aluminosilicate catalyst (NFMAS2)

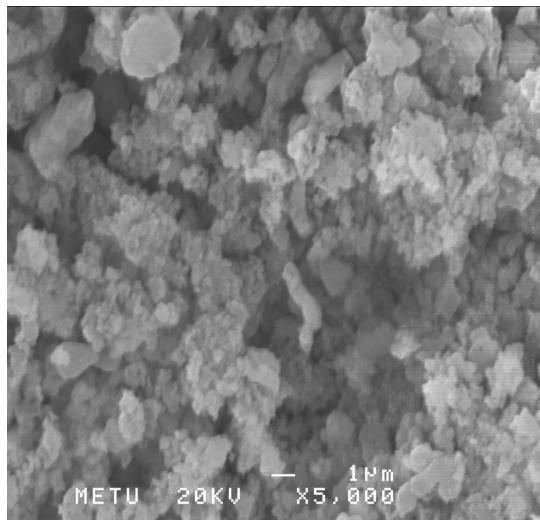


**Figure 84.** SEM image of the nafion/aluminosilicate catalyst (NFMAS3)

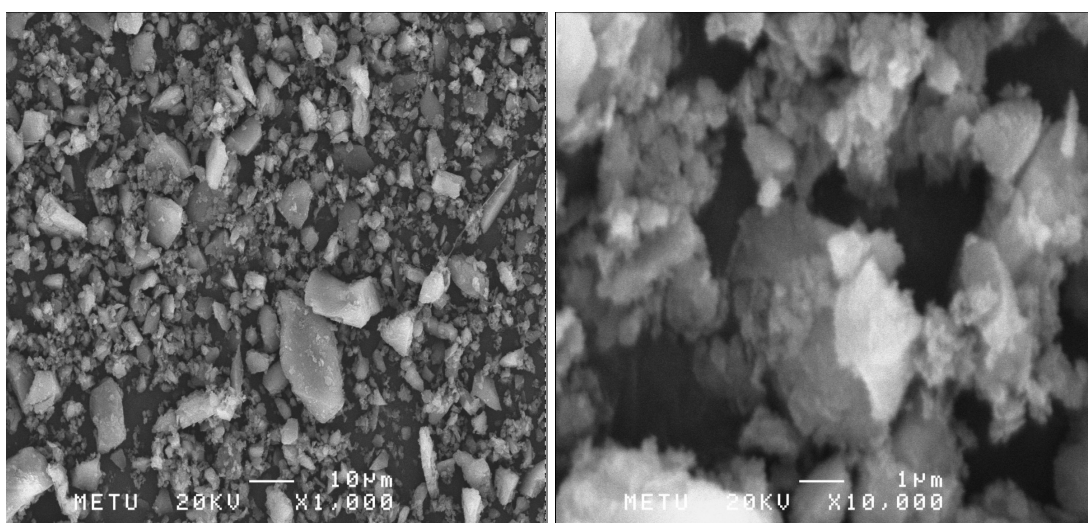


**Figure 85.** SEM images of the nafion/ $\alpha$ -alumina catalyst (NFALFA1)

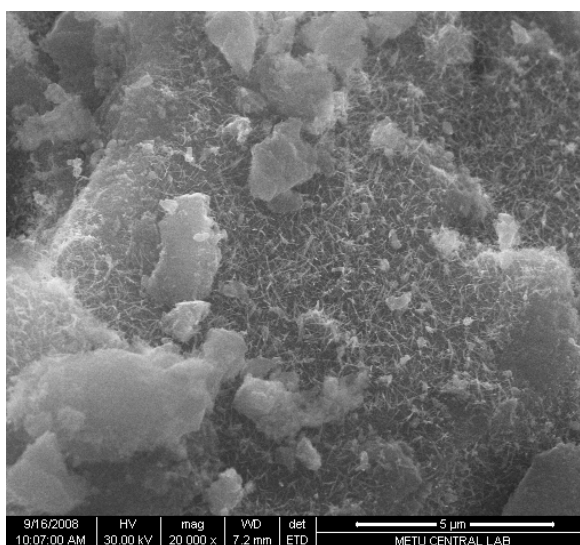
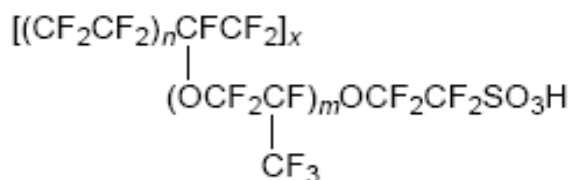


**Figure 86.** SEM image of the STA/Silica catalyst (TRC-75-400)

## APPENDIX C

### CALCULATION OF THE EXPECTED F/Si RATIOS FOR NAFION/SILICA CATALYSTS

The chemical structure of the nafion resin is given as illustrated below.



where  $m = 1, 2, \text{ or } 3$ ;  $n$  is about 6-7 and  $x$  is about 1000. By taking  $m$  as 2,  $n$  as 6.5 and  $x$  as 1000, the molecular weight of the resin was calculated as 731460 g/mol.

While synthesizing the NS1 group, to adjust the nafion/silica weight ratio to 0.05, 4.24 g from the 5% nafion containing solution was added to the synthesis mixture. So, 0.212 g nafion was present in the synthesis solution.

$$0.212 / 731460 = 2.9 \times 10^{-7} \text{ mole nafion was added.}$$

By again taking  $m$  as 2,  $n$  as 6.5 and  $x$  as 1000, moles of F in 1 mole of nafion resin was calculated as 29103.

$$2.9 \times 10^{-7} \times 29103 = 8.4 \times 10^{-3} \text{ mol F was added to the synthesis mixture.}$$

15.64 mL TEOS (0.07058 mol of Si) was added as the silica source.

$$8.4 \times 10^{-3} / 0.07058 = 0.12 \text{ is the expected F/Si ratio for the NS1 group.}$$

## APPENDIX D

### SINGLE POINT SURFACE AREAS OF THE CATALYSTS

**Table 26.** Single point surface areas of some of the catalysts

Catalyst	Single Point Surface Areas (m <sup>2</sup> /g)
TRC-75(L)	171.0
TRC-75-400	304.8
TRC-75(L)-CO <sub>2</sub>	178.4
NS1	345.7
NS2	276.2
NS4R2	637.6
NS5R2	587.6

## APPENDIX E

### FT-IR SPECTRA OF DEHYDRATED CATALYSTS

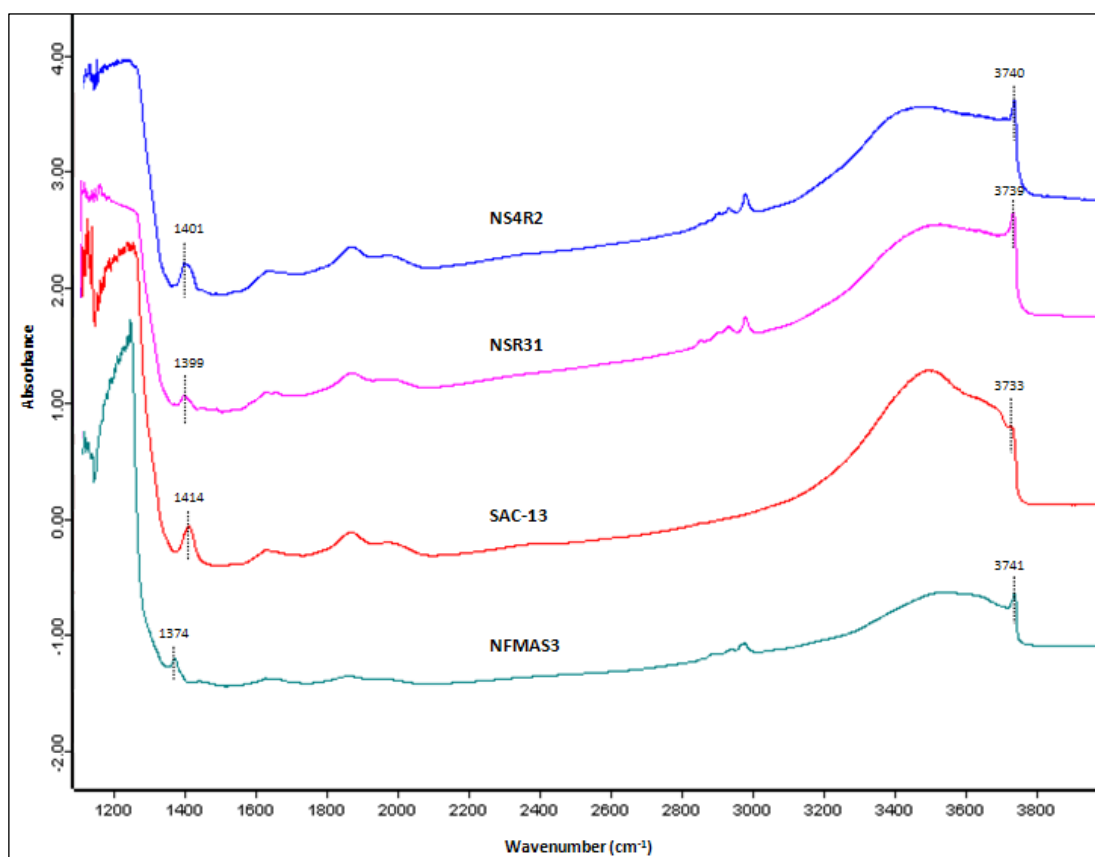


**Figure 87.** FT-IR spectra of dehydrated Nafion incorporated catalysts

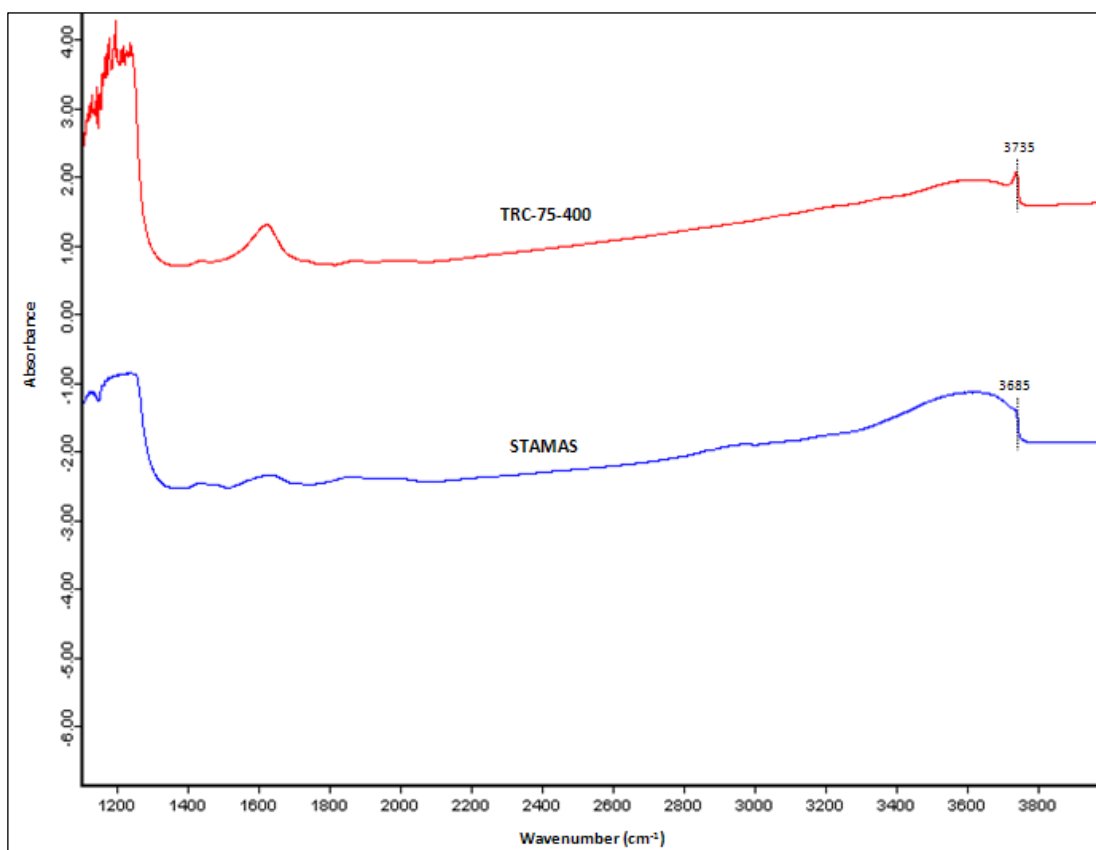


**Figure 88.** FT-IR spectra of dehydrated STA incorporated catalysts